HIDRAULICA

HYDRAULICS-PNEUMATICS-TRIBOLOGY-ECOLOGY-SENSORICS-MECHATRONICS

2023
June
No. 2

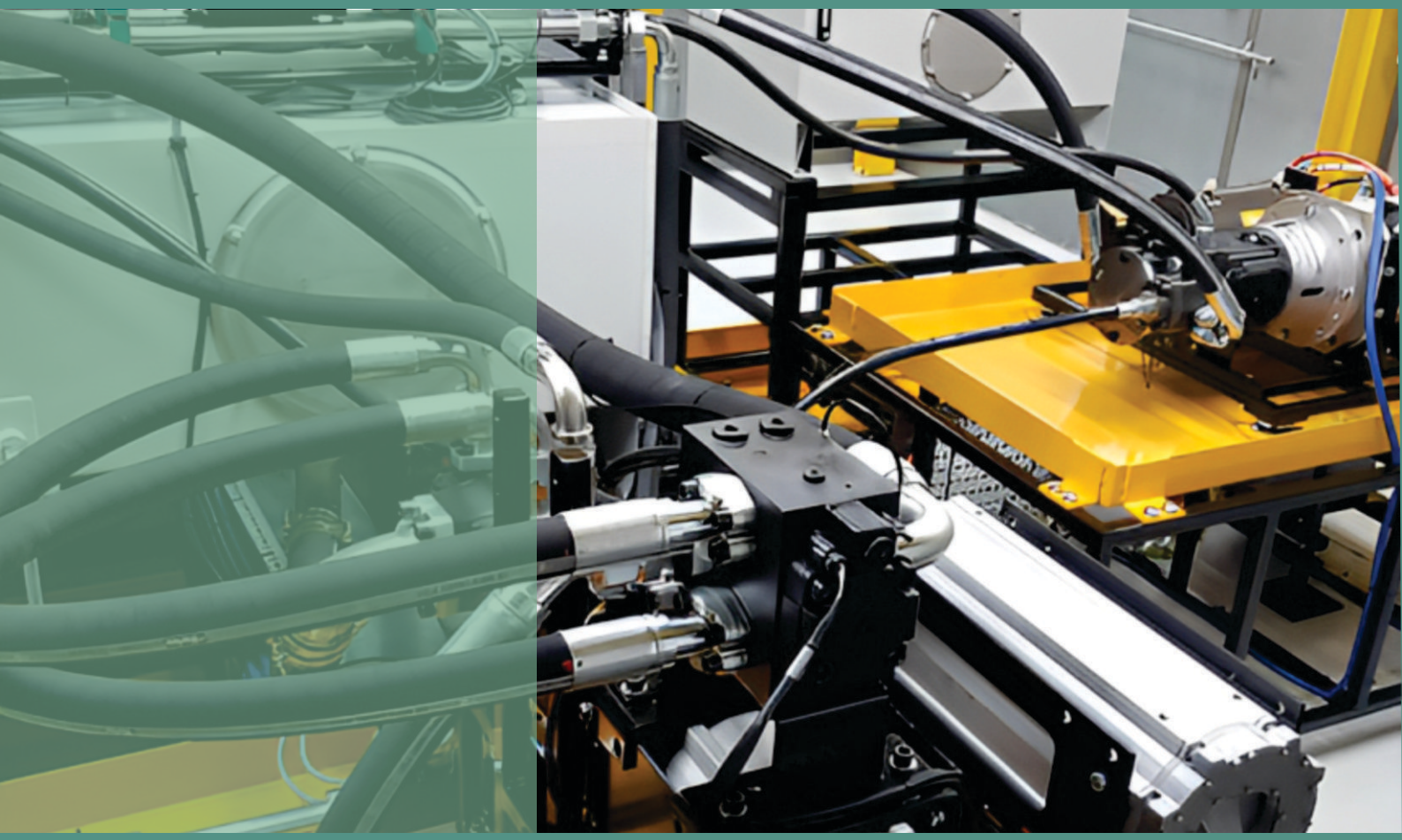

ISSN 1453 - 7303
ISSN-L 1453 - 7303

https://hidraulica.fluidas.ro

CONTENTS

Published by:
Hydraulics and Pneumatics Research Institute, Bucharest-Romania
Address: 14 Cuţitul de Argint, district 4, Bucharest, 040558, Romania
Phone: +40 21 336 39 91; Fax: +40 21 337 30 40; e-Mail: ihp@fluidas.ro; Web: www.ihp.ro
with support from:
National Professional Association of Hydraulics and Pneumatics in Romania - FLUIDAS
e-Mail: fluidas@fluidas.ro; Web: www.fluidas.ro

HIDRAULICA Magazine is indexed by international databases

ISSN 1453 – 7303; ISSN – L 1453 – 7303

EDITORIAL

Tinerii cercetători și rolul lor vital în dezvoltarea domeniilor inteligente din România

Dr. Ing. Gabriela Matache
REDACTOR ȘEF

Cercetarea științifică și tehnologică reprezintă coloana vertebrală a progresului societății noastre moderne. În România, tinerii cercetători au devenit un motor important al inovației și dezvoltării în domeniile de specializare inteligentă, aducând contribuții semnificative la evoluția acestora. Ei reprezintă o sursă de talent și energie creativă, care nu doar că transformă mediul academic, dar și contribuie la dezvoltarea economică și socială a țării. În acest editorial, voi arata importanța tinerilor cercetători în dezvoltarea domeniilor inteligente din România și impactul lor asupra societății.

România a realizat progrese semnificative în ceea ce privește crearea unui mediu propice pentru cercetare și inovare. Tinerii cercetători beneficiază de o infrastructură modernă, programe de finanțare și susținere instituțională, care îi încurajează să-și urmeze pasiunea și să-și dezvolte abilitățile în domeniile de specializare inteligentă. Acest lucru le oferă oportunități unice de a-și transforma ideile în realitate și de a contribui la progresul științific și tehnologic al țării.

Un domeniu-cheie în care tinerii cercetători din România și-au adus contribuția este inteligența artificială (IA). Prin abordarea domeniului IA, aceștia au dezvoltat algoritmi avansați de învățare automată, au aplicat tehnici de învățare profundă și au explorat aplicațiile practice ale IA în diverse sectoare, cum ar fi sănătatea, transportul și securitatea. Astfel, tinerii cercetători au pus România pe harta inovației în domeniul IA și au contribuit la creșterea competitivității țării noastre în economia globală.

Un alt domeniu deosebit de important în care tinerii cercetători din România s-au remarcat este biotehnologia. Ei au aplicat cunoștințele pe care le dețineau în biologie, chimie și inginerie pentru a dezvolta soluții inovatoare în medicină, agricultură și protecția mediului. Prin intermediul cercetărilor lor, aceștia au contribuit la îmbunătățirea calității vieții și la rezolvarea problemelor complexe cu care se confruntă societatea românească în aceste domenii.

Contribuțiile tinerilor cercetători în dezvoltarea domeniilor inteligente au un impact semnificativ asupra societății și economiei. Prin inovația lor, aceștia generează noi idei și soluții care pot îmbunătăți calitatea vieții oamenilor, pot crea locuri de muncă și pot stimula creșterea economică. Mai mult decât atât, acești tineri cercetători devin modele și inspirație pentru generațiile următoare, atrăgând și motivând alți tineri să se implice în cercetare și inovare.

În concluzie, ceea ce trebuie să stim este că tinerii cercetători reprezintă o resursă valoroasă pentru dezvoltarea domeniilor inteligente din România. Talentul și pasiunea lor, combinate cu sprijinul instituțional și infrastructura modernă, contribuie la avansul științific și tehnologic al țării noastre. Prin inovațiile lor în domeniul inteligenței artificiale, biotehnologiei și altele, acești tineri cercetători au un impact pozitiv asupra societății și economiei, deschizând noi perspective și posibilități pentru România. Este esențial să continuăm să îi susținem și să îi încurajăm pe tinerii cercetători, pentru a asigura un viitor promițător pentru domeniile de specializare inteligentă în țara noastră.

EDITORIAL

Young researchers and their vital role in the development of intelligent domains in Romania

Ph.D.Eng. Gabriela Matache
EDITOR-IN-CHIEF

Scientific and technological research is the backbone of the progress of our modern society. In Romania, young researchers have become an important engine of innovation and development in the fields of intelligent specialization, making significant contributions to their evolution. They represent a source of talent and creative energy, which not only transforms the academic environment, but also contributes to the economic and social development of the country. In this editorial, I will talk about the importance of young researchers in the development of intelligent domains in Romania and their impact on society.

Romania has made significant progress in creating an environment conducive to research and innovation. Young researchers benefit from modern infrastructure, funding programs and institutional support that encourage them to follow their passion and develop their skills in areas of smart specialization. This gives them unique opportunities to turn their ideas into reality and contribute to the scientific and technological progress of the country.

A key field in which young researchers from Romania have made their contribution is artificial intelligence (AI). By approaching the field of AI, they have developed advanced machine learning algorithms, applied deep learning techniques, and explored the practical applications of AI in various sectors such as health, transportation, and security. Thus, the young researchers put Romania on the map of innovation in the field of AI and contributed to increasing the competitiveness of our country within the global economy.

Another particularly important field in which young researchers from Romania have stood out is biotechnology. They applied their knowledge in biology, chemistry and engineering to develop innovative solutions in medicine, agriculture and environmental protection. Through their research, they have contributed to improving the quality of life and solving the complex problems faced by Romanian society in these sectors.

The contributions of young researchers in the development of smart fields have a significant impact on society and the economy. Through their innovation, they generate new ideas and solutions that can improve people's quality of life, create jobs and stimulate economic growth. Moreover, these young researchers become role models and inspiration for the next generations, attracting and motivating other young people to get involved in research and innovation.

In conclusion, what we need to know is that young researchers represent a valuable resource for the development of intelligent domains in Romania. Their talent and passion, combined with institutional support and modern infrastructure, contribute to the scientific and technological advancement of our country. Through their innovations in the field of artificial intelligence, biotechnology and others, these young researchers have a positive impact on society and the economy, opening new perspectives and possibilities for Romania. It is essential that we continue to support and encourage young researchers in order to ensure a promising future for the fields of smart specialization in our country.

Hydraulic System of Return Backlash Takeover with Pressure Bearing and without Rotary Fitting

Prof. PhD Eng. **Anca BUCUREȘTEANU**[1,*]

[1] University POLITEHNICA of Bucharest

* ancabucuresteanu@gmail.com

Abstract: *This paper makes a brief presentation of the systems of return backlash takeover currently used in the kinematic chains for circular feed in machine tools but also of a new system patented by the authors. This system is uncomplicated, effective and simplifies the kinematic chains of the machine tools. It can be applied to vertical lathes that can make milling operations too because it allows the overlapping of the kinematic chain for turning operations with the circular feed kinematic chain for boring or drilling operations. The system comes as a result of minimum modifications of the final pinion and can be used for all machines remanufactured but for the brand-new machines too. With minor constructive modifications, this system can be also applied in the feed and positioning kinematic chains for linear feed movements that use rack and pinion mechanisms.*

Keywords: *Machine tools, hydraulic system for backlash takeover*

1. Introduction. Influence of the return backlash on the accuracy of the kinematic chain for positioning/feed [1]

Figure 1 shows the crown and pinion mechanism used in most vertical lathes and rotary tables as the final mechanism of the kinematic chain for feed/positioning (C axis).

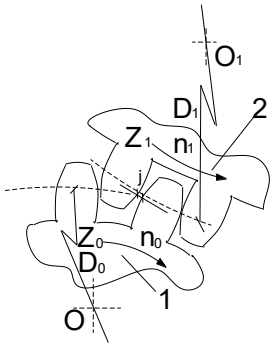

Fig. 1. Return backlash of the crown and pinion mechanism

Pinion 1, with center O, teeth Z_0 and rolling diameter D_0 engages crown 2, according to the sense in the figure above. The crown has the center O_1, teeth Z_1 and rolling diameter D_1. If the transfer ratio of the mechanism is i we can write down:

$$\frac{n_1}{n_0} = \frac{D_0}{D_1} = \frac{Z_0}{Z_1} = i \tag{1}$$

The flank clearance for this gearing is j. Because of this clearance, when the rotation sense at pinion 1 is changed, there is a delay between the return control moment and the effective performance of this one. If this clearance j is not constant, it cannot be compensated by the electronic equipment [2]; this situation affects the machining and positioning accuracy.
The error ε that will occur depends on the position of the machined surface related to the rotation center O'.
Many vertical lathes that have the table diameter in the range from 1200 to 4000 mm use the backlash takeover systems with two pinions having the same axis.
Figure 2 shows how they operate.

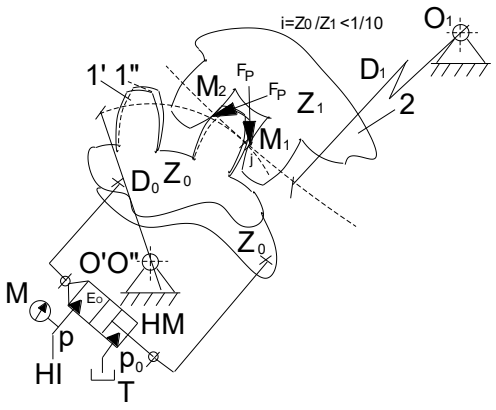

Fig. 2. System of backlash taking over with two coaxial pinions with hydraulic tensioning

Pinions 1' and 1" are identical; they have the same number of teeth Z_0 and the rolling diameters D_o. They turn in the same sense related to the center O' = O" but they are tensioned relatively through the agency of the hydraulic motor HM and they are gearing with crown 2, having teeth Z_1 and the rolling diameter D_1, on opposite flanks, in the points M_1 and M_2. Due to pressure p of the hydraulic motor, the gearing is made in the points M_1 and M_2, simultaneously but on opposite flanks. In these conditions, even if there is the backlash j, when the rotation sense changes at the two pinions, the contact between the crown and the pinions system is permanent. The hydraulic unit HI provides the pressure p that causes the apparition of the opposite forces F_p.
The construction of the system is compact and is schematically shown in Figure 3.

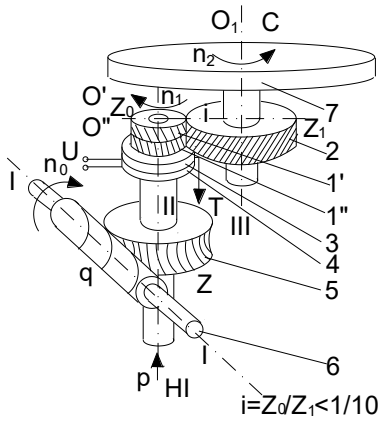

Fig. 3. Construction of circular feed box

Pinions 1' and 1" turn the crown 2 that is secured to table 7. Movement is brought from the electric motor to the duplex worm 6 that engages with the wormed gear 5. On the shaft III there is also located the vane-type hydraulic motor 3 and the electric clutch 4. When table 7 is rotated by the main kinematic chain (not shown in the figure above) the hydraulic unit is stopped and the coupling 4 is not actuated. If one wants to use the kinematic chain for circular feed, it is necessary to start the hydraulic unit and to actuate the clutch 4. Pinions 1' and 1" are tensioned and positioned on the opposite flanks of crown gear 2. Oil is supplied by the lower part of the construction by means of a rotary fitting.
By disabling the electric clutch 4, the pinions 1' and 1" start to rotate freely during the turning operations; in this case, crown 2 takes over the movement from another pinion, not shown in figure, from the main kinematic chain. Such a feed box is shown in Figure 4. Notations are the same as in the previous figure.

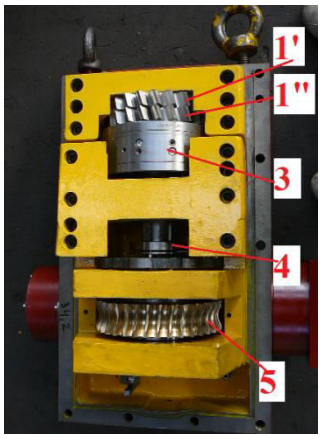

Fig. 4. Circular feed box with backlash taking over by relative tensioning with a vane-type hydraulic motor

The gear box and the circular feed box can be included in a small construction such as in Figure 5. Gear box is provided with a backlash takeover system and is used for a CNC vertical lathe with the table of 5600 mm. During turning operations, the tensioning hydraulic system is not actuated. The movement gets to pinions 1' and 1", which have parallel shafts [1], directly from the main motor via the gear box GB. In order to use the circular feed system, it is necessary to disconnect the main motor, to actuate the backlash takeover system and to couple the feed motor. This one brings the movement to the crown gear 2 by means of the toothed belt GB transmission.

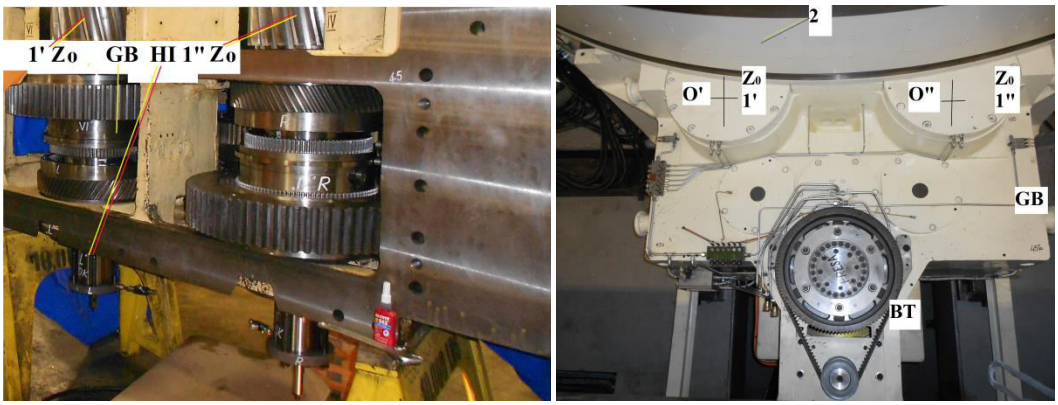

a. b.

Fig. 5. Backlash takeover system with parallel shafts pinions integrated in the gear box

Among the disadvantages of the systems above it can be mentioned:
- the need for two motors, one for driving the main kinematic chain and one for the feed kinematic chain;
- existence of an electromagnetic coupling that is activated only when using the feed kinematic chain;
- use of a rotary distributing coupling (fitting).

2. Backlash takeover system provided with two pinions, hydraulic piston, pressure bearing and without rotary coupling [3, 4, 5, 6]

In the case of the vertical lathes, the main kinematic chain is ended by a pinion as shown in Figure 6, which engages with the gear clamped on the table.
Pinion 1 is supported on the bearings 3 related to bed 2. The pinion drives the gear on teeth flanks corresponding to the direction of rotation. When stopping or reversing the direction, the contact flanks are changed because of the functional backlashes, resulting in positioning errors.

Starting from the construction of the pinion presented in Figure 4, it is possible to achieve a variant that allows to take over the return backlash only when necessary, thus for accurate positioning and milling operations.

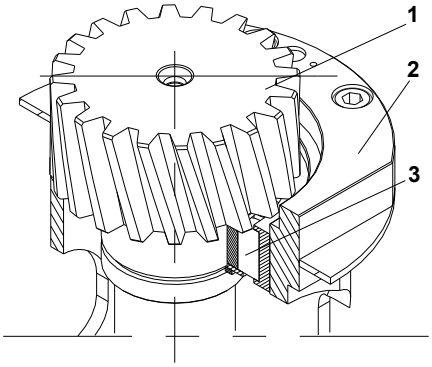

Fig. 6. Pinion that engages with the toothed gear in vertical lathes

In terms of vertical lathes, the crown and pinion mechanism belongs to the main kinematic chain in the case of turning operations and to the circular feed kinematic chain for the milling operations. Figure 7 shows schematically the new variant patented by the authors and how it operates.

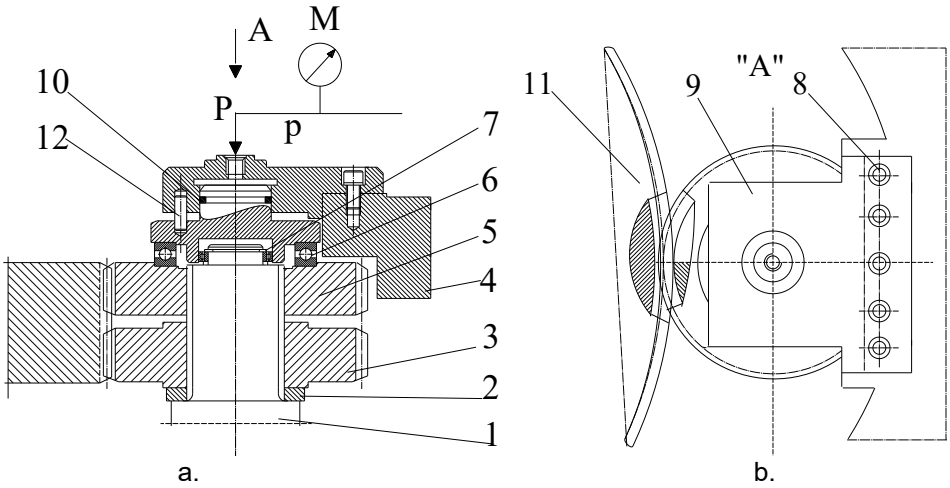

Fig. 7. New system of backlash takeover without rotary fitting

The main pinion 3 and the secondary pinion 5, which are identical in terms of teeth geometry, receive the rotation movement from the spline shaft 1. This one is supported on bearings related to bed 4 and receives the movement from the main kinematic chain, identical in this case with the circular feed chain of the machine. Support 9 is clamped to the bed by means of the screws 8. Piston 10 operates axially related to support 9 when it is supplied with oil at pressure p on the path P. The value of the supply pressure is displayed on manometer M. The axial positioning of pinion 3 is performed by means of the distance plate 2. By means of the pressure bearing (axial) 6, piston 10 presses pinion 5. The construction is centered by the radial bearing 7. The pins 12 prevent the rotation of piston 10.

During the turning operations, pinions 3 and 5 operate on the same flank of the crown 11; in this case, the system is not supplied with oil. For the milling operations, oil at pressure p will be brought on P path. The oil under pressure drives the piston 10, of diameter D, pushing it downward. The two pinions 3 and 5 have inclined teeth [7, 8, 9] same as the driven crown 11. For this reason, pinions will operate on different flanks at driven crown 11, taking over the backlash. Any losses are recovered in the bed of the machine that is also the oil tank of this one.

If the angle of inclination of teeth related to the vertical is β, the following equations can be taken into consideration:

$$F = p \cdot \frac{\pi \cdot D^2}{4} \tag{2}$$

$$F_N = \frac{F_A}{\sin \beta} \tag{3}$$

$$F_T = F_A \cdot ctg\beta \tag{4}$$

In the equations (2) ÷ (4) it was noted: F - axial force, F_N - normal force at teeth, F_T - tangential force.
Force F is dimensioned so as to ensure the permanent takeover of the backlash regardless of the instantaneous value of the torque reduced at pinion level.
Figure 8 shows the kinematic diagram of this construction, keeping the same notations above.

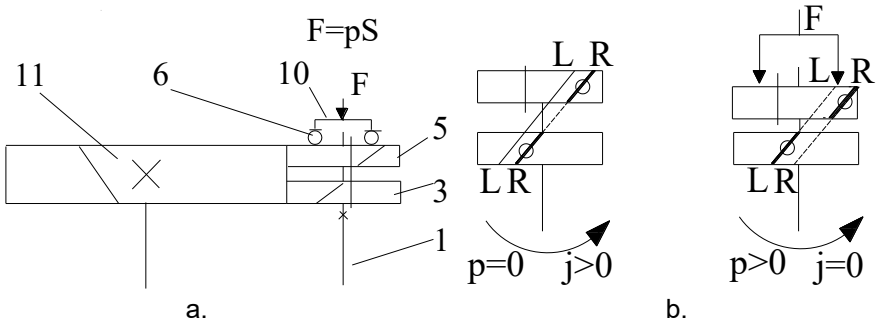

Fig. 8. Kinematic diagram of the backlash takeover system without rotary fitting

In the absence of pressure p, the two pinions are not tensioned (p = 0, F = 0). If we take into account the direction of rotation shown in the figure above, we notice that the meshing is performed only on the right side flanks (R) of the pinions. If the system is supplied with oil at pressure p, for the same direction of rotation, the two pinions are placed on the opposite flanks of the crown gear. The upper one transmits the movement on the right flank (R) and the lower one on the left one (L).
Specific to this system [6] is that the backlash is taken over because of the axial relative movement of two pinions with inclined teeth. The relative pushing down is made by means of a pressure bearing (axial) [10], which reduces the frictions and allows the elimination of the rotary fitting [5]. The pressure with which is taken over the backlash is introduced directly in the assembly mounted and not in other motor (linear or rotary) as in other versions; the same mechanism is used for turning operations (deactivated) and for milling operations (activated). Compared to the solutions presented above but also to a system previously patented [5] the new system has the advantage that it does not require a rotary fitting.
This solution allows the use of a single electric drive motor for both turning and milling operations and of a single coupling with the crown gear. In terms of kinematics, the new and modern machines that use such systems are much simpler.
Figure 9 shows the kinematic diagram of a vertical lathe equipped with a classic system for backlash takeover provided with two drive motors.
In Figure 9 there were noted: 1 - machine bed, 2 - electric motor for the main kinematic chain (M1), 3 - gear box for turning operations, 4 - crown and pinion mechanism without backlash takeover for the main kinematic chain, 5 - machine table, 6 - backlash takeover system with two tensioned pinions with vane-type hydraulic motor (with big losses) for the feed kinematic chain, 7 - feed box (constructively complicated and expensive), 8 - rotary fitting, 9 - electric motor (M2) for actuation of feed kinematic chain, P - pressure intake port, at the rotary fitting level.
Motors M1 and M2 are driven successively, depending on the operations performed: M1 for turning, M2 for milling, drilling or positioning.

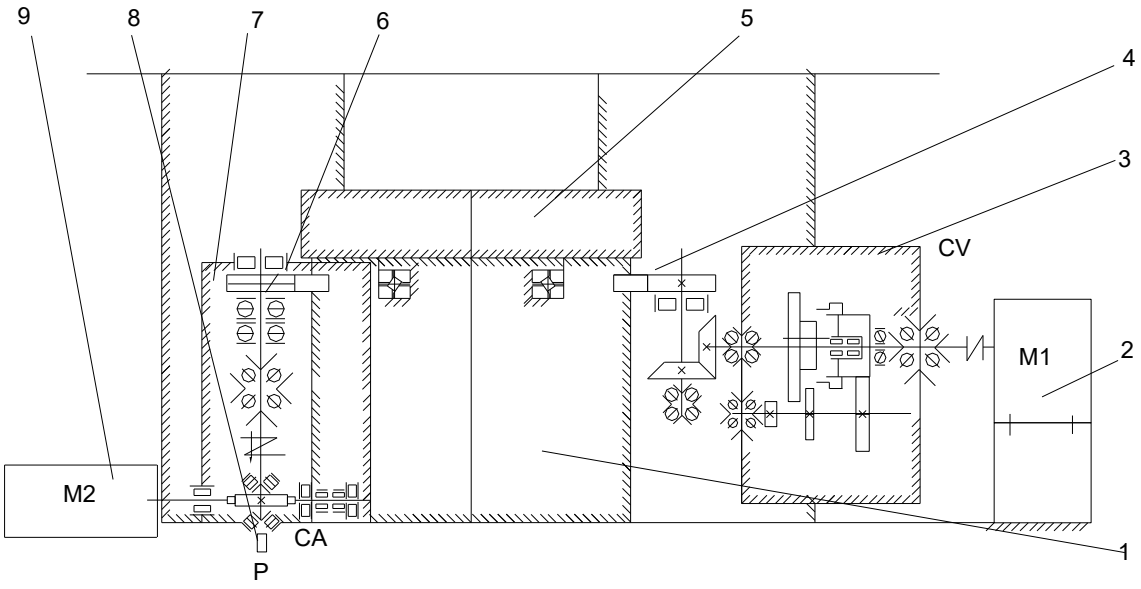

Fig. 9. Kinematic diagram of the main kinematic chain and of the circular feed chain in a vertical lathe equipped with a standard gear box and a circular feed box

The return backlash takeover system with pressure bearing and without rotary fitting, if used for modern machine-tools, equipped with two speed gear box [2, 7], leads to the simplification of the kinematic diagram as shown in Figure 10.

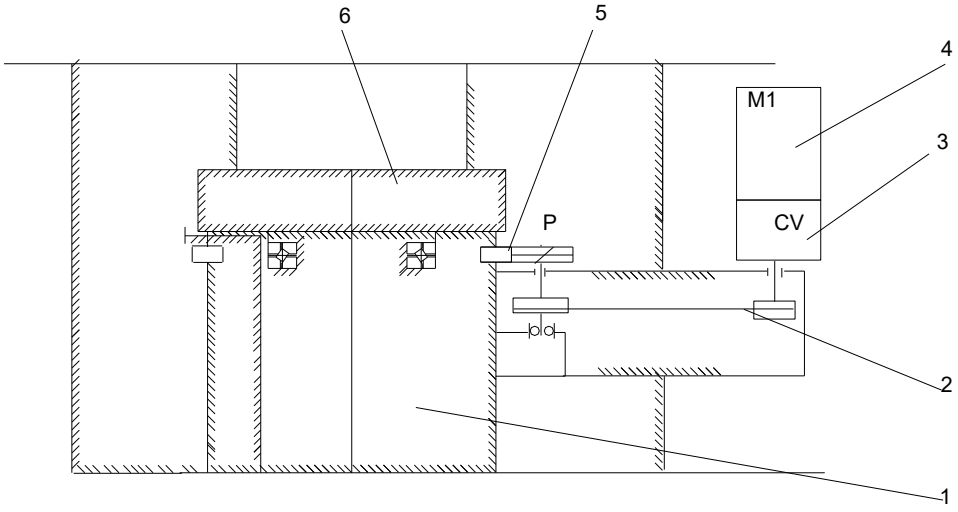

Fig. 10. Kinematic diagram of the main kinematic chain and of the circular feed chain in a vertical lathe equipped with hydraulic system for return backlash takeover system with pressure bearing and without rotary fitting

In Figure 10 there were noted: 1 - bed of the machine, 2 - toothed belt transmission, 3 - feed and gear box, 4 – ONLY ONE electric motor for turning and milling (M1), 5 - the new system for backlash takeover without rotary fitting, including the two pinions pushed down by the pressure bearing, that meshes with the crown gear, 6 - table, P - pressure intake port that does not require a rotary fitting.
Both speed steps are used for the turning operations (usually i_1 = 1/1 and i_2 = 1/4 [2, 7]). For positioning or machining operations that require C axis it shall be used only the second step of the gear box. In this case, the circular feed speed is adjusted by means of the variator of motor M1 [2].

The hydraulic unit that supplies the backlash taking over system shall include a pump of lower flow than in the case of the system shown in Figures 3 and 4 because, unlike the cane-type hydraulic motor, the patented system has no losses. The unit shall be equipped with a pressure regulating valve and elements for monitoring this one. In Figure 11, the basic hydraulic diagram is shown.

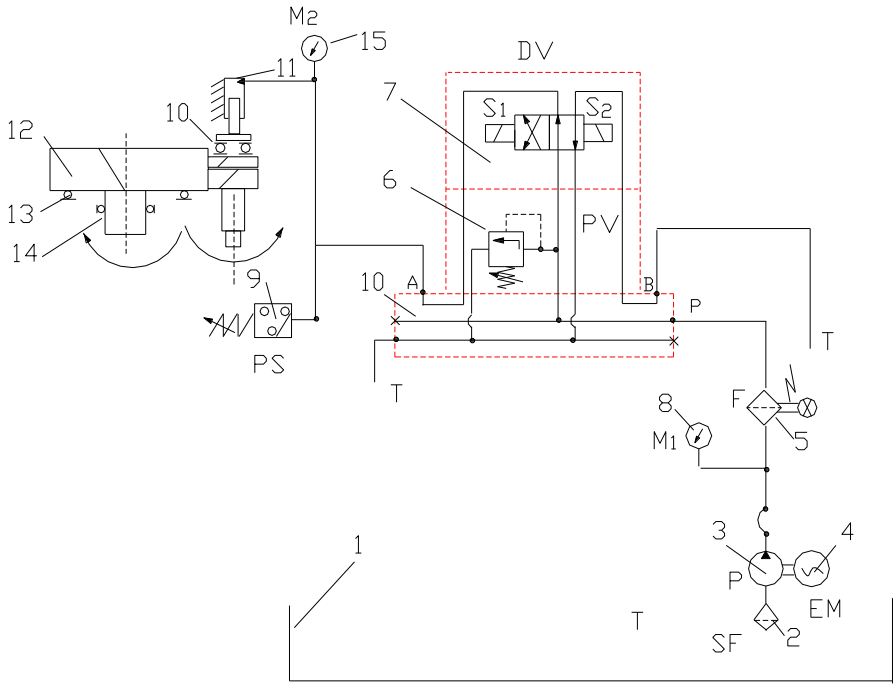

Fig. 11. Hydraulic diagram of backlash takeover system

The electric motor (EM) 4 drives the constant flow pump (P) 3. This one sucks in oil from the tank (T) 1 through the strainer (SF) 2. The oil pureness is ensured by the pressure filter (F). This one is provided with an electric indicator of clogging. The oil coming out of the filter supplies the plate 10 on which are located the pressure valve (PV) 6 and the distributor (DV) 7. Path A of the plate supplies the cylinder for backlash takeover 11. This one presses relatively the two semi-pinions via the pressure bearing 10. Path B of the plate 11 is directly connected to the tank. To view the general pressure and the pressure in the backlash takeover cylinder one shall use the manometers (M_1 and M_2) 8 and 15 respectively. The electric confirmation of existence of the required pressure is performed by the pressure relay (PS) 9. In the figure above there are also noted: 12 – crown gear, 13, 14 – table supporting on bearings. If the electromagnet S_1 is actuated, the system is uncoupled and the turning operation is made. In this case the electric motor (EM) 4 can be stopped too. If positioning or milling operations must be made (with interpolation of axes [7, 9, 11]) it is necessary to actuate the electromagnet S_2. Usually the pressure adjusted at the pressure valve (PV) 6 does not exceed 60 bar. In order to achieve turning operations exclusively, the electric motor is stopped. To achieve only milling operations, the motor is started and the electromagnet S_2 is actuated about 10 - 15 s; afterwards the voltage is cut off. If turning and milling operations are performed alternatively, for short time, the electromotor does not stop; only the electromagnets S_1 and S_2 shall be actuated, depending on needs.
The backlash takeover system presented hereby can be applied to brand-new machines or remanufactured ones, with the table up to 5000 mm. For larger size vertical lathes it is recommended to use the electric takeover of return backlash [1, 12].

3. Conclusions

In the case of positioning and machining operations with interpolation of axes performed on vertical lathes it is necessary to have systems of return backlash taking over included in the circular feed kinematic chain.

Usually, to enable fast and easy setup, these systems are driven hydraulically.
On most machines CNC type, the main kinematic chains and the circular feed kinematic chains have different motors. They are operated depending on the type of operation that is performed.
By using the patented backlash takeover system, in some cases, these two kinematic chains can be driven by a single motor.
With the patented system, the backlash takeover is made by a piston and not by vanes as in some existing variants. The system with piston has no losses, which reduces the required flow to the pump and thus the driving motor power. The possible losses must not be recovered by special elements, as they have direct access to the machine oil tank, located in the bed of the machine.
The coupling and uncoupling of this system is easy, without requiring other elements operated hydraulically or electrically.
The system can be applied to the vertical lathes with table in the range of 1200 ÷ 4000 mm.

References

[1] Prodan, Dan, Misu Petre, George Constantin and Anca Bucureșteanu. "Eliminating the Backlash of Circular Feed Drives of CNC Vertical Lathes." *Proceedings in Manufacturing Systems* 11*,* no. 1 (2016): 27–34.
[2] ***. GE Fanuc, Siemens, Pietro Carnaghi, ZF, REDEX and Baruffaldi Catalogues and leaflets.
[3] Prodan, Dan, Anca Bucureşteanu and Emilia Balan. "Hydraulic System for Taking Over the Clearance for Vertical Lathe with Milling Unit." *U.P.B. Scientific Bulletin, Series D* 71, no. 2 (2009): 53-62.
[4] Prodan, Dan, Adrian Motomancea and Anca Bucureşteanu. "Clearance Compensation Hydraulic System for Vertical Lathes with Milling Unit.*"* Paper presented at the 20th International DAAAM Symposium, Vienna, Austria, November 25-28, 2009.
[5] Prodan, Dan and Adrian Motomancea. "Hydraulic System Taking Over the Play for Vertical Lathes with Milling Unit." Patent Number(s): RO125837-A2; RO125837-B1, International Patent Classification: B23Q-005/22; B23Q-005/52; F16H-055/17.
[6] Prodan, Dan, Adrian Motomancea and Anca Bucureşteanu. "Hydraulic System of Return Backlash Takeover with Pressure Bearing and without Rotary Fitting." Patent Number: RO132040-B1, International Patent Classification: B23B-3/10; B23Q-3/08.
[7] Prodan, Dan. *Heavy machine tools. Mechanical and Hydraulic Systems/Maşini-unelte grele. Sisteme mecanice si hidraulice*. Bucharest, Printech Publishing House, 2010.
[8] Perovic, Bozina. *Machine-Tools Handbook/Handbuch Werkzeug-Maschinen*. Munchen, Carl Hanser Verlag, 2006.
[9] Joshi, P. H. *Machine-Tools Handbook*. New Delhi, McGraw-Hill Publishing House, 2007.
[10] Teixido, C., J-C. Jouanne, B. Bauwe, P. Chambraud, G. Ignatio and C. Guerin*. Mechanical Construction Guide/Guide de Construction Mecanique*. Paris, Delagrave Edition, 2000.
[11] Catrina, Dumitru, Adrian Totu, Sorin Croitoru, George Carutasu, Nicoleta Carutasu and Alexandru Dorin. *Flexible Systems of Machining by Cutting Operations/Sisteme flexibile de prelucrare prin aschiere*. Bucharest, MatrixROM Publishing House, 2005.
[12] Gornic, Corneliu. "How to choose a machine tool (III)." *T&T Technique and Technology*, no. 5 (2015): 31-35.

Opinions Regarding the Assessment of Pressure Drop in Tangential Feed Cyclones for Cleaning Industrial Dry Gases

Ph.D. Candid. **Melania CORLECIUC (MITUCĂ)[1,*],** Professor Emeritus Ph.D. Eng. **Radu I. IATAN[2],** Assoc. Prof. PhD. Eng. **Ion DURBACĂ[2],** Lecturer PhD. Eng. **Georgiana Luminiţa ENĂCHESCU[2],** Lecturer PhD. Eng. **Anca Mădălina DUMITRESCU[2],** Assist. Prof. PhD. Eng. **Gheorghe Cosmin ClOCOIU[2]**

[1] National Agency for Environmental Protection, Romania

[2] POLITEHNICA University of Bucharest, Romania

* melaniaco171@gmail.com

Abstract: *Cyclones are used to remove solid particles larger than 5 μm from impure industrial gases. They are simple constructions, without moving parts and easy to maintain. In the use of such equipment, main interest is to evaluate the pressure drop in the cyclone and the efficiency of separation. Ensuring a high value of the pressure drop involves high energy consumption, aiming to increase the separation efficiency. Many studies, exposed in the content of this work, have been carried out, in the sense of the above topic, for pressure loss assessment. The results of the empirical formulas, proposed over time, were compared, in the specialized literature, with those offered by the experimental results, obviously for practical cases of great interest.*

Keywords: *Cyclones with tangential feed, pressure drop*

1. Introduction

Cyclones are among the simplest systems used for dedusting dry gases in various industrial sectors. Among these, the ones with tangential feed of impurified gas stood out.
The design of the cyclones considers their geometry, the flowrate of the impurified gas and the number of revolutions/rotations in the downward movement. The theory developed [1] proved to be useful in the practical design of cyclones. This theory refers to the fact that the velocity profile in a cyclone does not strictly adhere to the ideal, uniform shape. Any design method is based on theories that depend on the accuracy of the evaluation of the collection efficiency and the pressure drop in the cyclone. The two characteristics represent two major criteria regarding the performance of a cyclone. Both are dependent on the dimensions of the cyclone, the height and width of the entrance ($a \cdot b$ – Figure 1), the diameter of the gas outlet D_e, the length of the outlet pipe S, the height of the cylindrical area h the height of the cyclone H and the diameter of the collected dust outlet pipe B.
Over the time, several simplified models and empirical correlations have been proposed for the design and evaluation of cyclones, the essential requirement being that of correlation with the concrete characteristics of each equipment [3]. The reference to the performance of a cyclone considered as a "*landmark*" leads, in the end, to a faulty design, since each cyclone has a specific behavior, according to the unique physical properties of the impurified gas flow [4]. The Computational Fluid Dynamics (CFD) method has become a powerful instrument in the design and evaluation of cyclones due to the rapid advances in computer technology [42]. This technique provides a great potential to predict the characteristics of the fluid flow, the trajectory of the particles and the pressure drop in the cyclone [3]. The accuracy of the numerical modeling of a turbulent flow depends primarily on the selection the appropriate turbulence model [3]. The long analysis time and therefore the high computational cost has been a major obstacle in the simulation of cyclones. In the present, thanks to the increased processing performance of computers, at a relatively low cost, it has become possible to simulate cyclones with greater precision [5, 6].

The capacity of a cyclone is determined by the value of the area of the feed pipe ($a \cdot b$ – Figure 1), and the inlet velocity of the gas to be cleaned. This is, mainly, in agreement with the connection between the main dimensions of the cyclone and its pressure drop.
Note: The first studies on the characterization of cyclones were carried out between 1930 and 1950 (***Alexander R. McK*** – 1949, ***Ter Linden A. J.*** – 1949) [16].

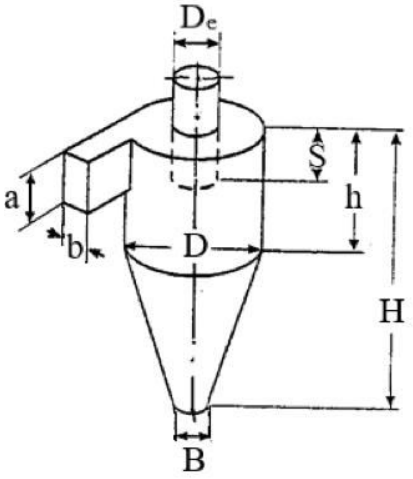

Fig. 1. Construction and characteristics of a cyclone [2]

2. Expressions for the height of the impure gas column

This characteristic (a major criterion regarding the performance of a cyclone [10]) varies with the square of the inlet gas velocity and is conveniently expressed by the height of the gas column [2]:

$$\Delta H = 2 \cdot \Delta p \Big/ \left(\rho_g \cdot v_i^2 \right), \tag{1}$$

where Δp is the pressure drop between the gas inlet and outlet of the cyclone, ρ_g - gas density, and v_i - the gas velocity at the cyclone inlet (the optimal input speed recommended by ***Abdel – Hadi M. A.*** – 2014 [41] is $18.5\, m/s$, respectively $18.0\, m/s$ - ***Chuah T. G., Gimbun J., Choong Y. S. T***. – 2003 [41]); the inlet velocity of the impure gas is primordial – ***Schnell K. B, Brown A. C.*** – 2002 [41].
Note: In paper [11], the density of the mixture of gas and particles ρ_{p-g} is used instead of the gas density ρ_p, a suggestion belonging to the authors ***Shepherd C. B., Lapple C. E*** (1951).

Note: In papers [13 - 16], the following relationships are indicated for the calculation of the parameter Δ H:

$$\Delta H = K \cdot a \cdot b / D_e^2 \text{ - } \textbf{Shepherd C B.} \text{ and } \textbf{Lapple C. E.} \text{ (1939)} \tag{2}$$

Note: The values of K are: $K = 16$ for cyclones with standard tangential inlet [11]; $K = 7.5$ for cyclones that have a vane at the entrance to change the geometry of the impure gas inlet section [16, 17]; $K = 12 \ldots 18,$ for cyclones with tangential entry [15].

$$\Delta H = 11.3 \cdot \left(a \cdot b / D_e^2 \right)^2 + 3.33 \text{ - } \textbf{Casal J.} \text{ and } \textbf{Martinez – Benet J. M.} \text{ (1983);} \tag{2}_1$$

$$\Delta H = 9.47 \cdot a \cdot b / D_e^2 \text{ - } \textbf{Coker J. K.} \text{ (1993),} \tag{2}_2$$

configurations specified in the paper [13].

2. 1. The theory of *STAIRMAND C. J.* (1949)

According to this theory, the height of the gas column is calculated with [2, 9, 17, 21, 22]:

$$\Delta H = 1 + 2 \cdot \Phi^2 \cdot \left[2 \cdot (D - b) / D_e - 1 \right] + 2.548 \cdot \left(a \cdot b / D_e^2 \right)^2, \quad (3)$$

where Φ is the ratio of the tangential velocities:

$$\Phi = \frac{\sqrt{D_e / \left[2 \cdot (D - b) \right] + 4 \cdot f \cdot A / (a \cdot b)} - \sqrt{D_e / \left[2 \cdot (D - b) \right]}}{2 \cdot f \cdot A / (a \cdot b)}, \quad (4)$$

where f is the friction coefficient, whose value, established by ***Stairmand C. J.*** (1949), is 0.005, and A is the area of the internal surface of the cyclone exposed to the spin movement of the gas [22]:

$$A = 0.785 \cdot \left(D^2 - D_e^2 \right) + 3.14 \cdot \left(D_e \cdot S + D \cdot h \right) +$$

$$+ 1.57 \cdot (D + B) \cdot \sqrt{(H - h)^2 + \left[(D - B) / 2 \right]^2}, \quad (5)$$

with the geometric notations specified in Figure 1.

2. 2. <u>The theory of *ALEXANDER R. McK*</u> (1949)

The same bibliographic sources [9, 16, 21] also present the expression of the parameter ΔH, attributed to ***Alexander R. McK*** (1949), written in the form:

$$\Delta H = 4.62 \cdot \left(\frac{a \cdot b}{D \cdot D_e} \right) \cdot \left\{ \left[\left(\frac{D}{D_e} \right)^{2 \cdot n} - 1 \right] \cdot \frac{1 - n}{n} + f \cdot \left(\frac{D}{D_e} \right)^{2 \cdot n} \right\}, \quad (6)$$

in which represents the friction factor having the expression:

$$f = 0.8 \cdot \left[\frac{1}{3 \cdot n \cdot (n - 1)} \cdot \left(4 - 2^{2 \cdot n} \right) - \frac{1 - n}{n} \right] + 0.2 \cdot \left[\frac{1 - n}{n} \cdot \left(2^{2 \cdot n} - 1 \right) + 1.5 \cdot 2^{2 \cdot n} \right], \quad (7)$$

in this expression n is calculated using the equations:

$$n = 0.263 \cdot R^{0,14}. \quad (8)$$

Experimentally, it was found that the exponent n can be expressed by the relation [24, 43]:

$$n = 1 - \left(1 - 0.67 \cdot D^{0,14} \right) \cdot \left(T / 283 \right)^{0,3}, \quad (9)$$

T representing the absolute temperature of the polluted gas, in K, and D - the inner diameter of the cylindrical part of the cyclone, in meters. The above relation is attributed to ***Alexander R. McK.*** (1949) [9, 11, 16, 21].

<u>Note</u>: In paper [25] a slight modification of the expression for n is presented in the form:

$$n = 1 - \left(1 - 0.50 \cdot D^{0,14} \right) \cdot \left(T / 283 \right)^{0,3}, \quad (10)$$

attributed to the authors ***Li E., Wang Y.*** (1989), where D is measured in meters; the paper [26] proposes the formula:

$$n = 1 - \left(1 - 0.016 \cdot D^{0,14} \right) \cdot \left(T / 283 \right)^{0,3}. \quad (11)$$

<u>Note</u>: In the paper [27], the equality $v_\theta \cdot R^n = v_t \cdot R^n = ct.$ is specified for the free vortex of the gas inside the cyclone, delimited by a radius a that separates it from the forced vortex ($a < r < 0.5 \cdot D = R$), D representing the inner diameter of the cyclone; for $0 < r < a$, the equality $v_t \cdot r = ct.$ is assumed. Works [16, 28, 29] present the correlation of the type $v_t = \left(R / r \right)^n \cdot v_i$, where v_i represents the velocity at de feed of the cyclone with impurified gas. ***Shephers C. B.*** and ***Lapple C. E.*** – (1939) - give the value $n = 0.5$ [28].

If the cyclone works at different temperatures, the exponent can be determined from the relationship:

$$\left(1-n_1\right)/\left(1-n_2\right)=T_1/T_2\,. \tag{12}$$

The paper [17] offers the conclusions of the authors ***Miller I., Freund J. E.*** (1965) that specifies that the results obtained for the evaluation of pressure loss using the methods ***Sheperd C. B., Lapple C. E.*** (1940), ***Staimand C. J.*** (1949), ***Barth W.*** (1956) are close to other experimental research. The values obtained by ***Alexander R. McK.*** and ***First M. W.*** are less precise.

2. 3. The theory of *FIRST W. M.* (1949, 1950**)**

In the papers [9, 21] is indicated the expression of the factor ΔH written in the form attributed to ***First W. M.*** (1949, 1950):

$$\Delta H=\left(24\cdot a\cdot b/D_e^2\right)\cdot\left\{D^2/\left[h\cdot\left(H-h\right)\right]\right\}^{1/3}. \tag{13}$$

Note: In the paper [17] the following expression is indicated:

$$\Delta H=\left[12\cdot a\cdot b/\left(Y\cdot D_e^2\right)\right]\cdot\left\{D^2/\left[h\cdot\left(H-h\right)\right]\right\}^{1/3}, \tag{14}$$

where the values for the constant Y are as follows: $Y=0.5$ - for cyclones with free entry of the impurified gas; $Y=1.0$ - for cyclones with fixed vane at the gas inlet; $Y=2.0$ - for cyclones with adjustable vane at the gas inlet in the cyclone.

2. 4. The theory of *BARTH W.* (1956)

In accordance with this theory, ΔH is calculated with the expression [2, 17, 18]:

$$\Delta H=\left(v_t/v_0\right)^2\cdot\left(1.274\cdot a\cdot b/D_e^2\right)^2\cdot\left(\varepsilon_i+\varepsilon_0\right), \tag{15}$$

where:

$$v_t/v_0=1.57\cdot\left(D_e/2\right)\cdot\left(D-b\right)/\left[a\cdot b\cdot\alpha+\pi\cdot h^{\bullet}\cdot\left(D-b\right)\cdot\lambda\right], \tag{16}$$

v_t is the tangential speed of the gas vortex, v_o - the tangential speed of the gas at the exit of the cyclone, $\alpha-$ a factor characterizing the entry into the cyclone [16, 18]:

$$\alpha=1-1.2\cdot b/D, \tag{17}$$

the expression being attributed to ***Muschelnautz E.*** (1972) [16]; $h^{\bullet}-$ the height of the vortex in the central area of the cyclone, which depends on the cyclone's dimensions [16, 18]:

$$h^{\bullet}=H-S, \text{ for } \quad D_e\le B; \tag{18}$$

$$h^{\bullet}=\left(H-h\right)\cdot\left(D-D_e\right)/\left(D-B\right)+h-S, \quad \text{if } \ D_e\rangle B; \tag{19}$$

ε_i - pressure loss factor at the cyclone inlet [17]:

$$\varepsilon_i=\left(D_e/D\right)\cdot\left\{\left[1-\left(v_t/v_0\right)\cdot\left(2/D_e\right)\cdot h^{\bullet}\cdot\lambda\right]^{-2}-1\right\}; \tag{20}$$

ε_0 - pressure loss factor at the exit of the cyclone [17]

$$\varepsilon_0=4.4\cdot\left(v_t/v_0\right)^{-2/3}+1, \tag{21}$$

and λ is the friction coefficient (estimated by ***Barth W.*** (1956) to be $\lambda=0.02$) [16, 17]:

$$\lambda=\lambda_g\cdot\left(1+2\cdot\sqrt{c_{si}}\right);\ c_{si}\langle 1.0;\quad \lambda=\lambda_g\cdot\left(1+3\cdot\sqrt{c_{si}}\right);\ c_{si}\rangle 1.0\,, \tag{22}$$

where c_{si} represents the concentration of particles in the mass of gas (mass of particles/mass of gas); $\lambda_g = 0.005$ for high values of number ***Reynolds O.*** (b. 1842 – d. 1912) [16].

2. 5. The theory of *DIRGO J. A.* (1985)

This is based on the analysis of the ratios of the characteristic dimensions of the cyclones and the experimental results obtained by ***Stairmand C. J.*** (1949, 1951 [30]), ***First M. W.*** (1949, 1950), ***Swift P.*** (1969), ***Hejma J.*** (1971) and others, using dimensional analysis with the relation [2]:

$$\Delta H = K \cdot A^x \cdot B^y \cdot C^z , \tag{23}$$

where K is a constant, A, B, C are dimensionless ratios, and $x, y, z -$ exponent calculated based on experimental data.
After processing the data, the following relationship was established [3]:

$$\Delta H = 20 \cdot \left(a \cdot b / D_e^2 \right) \cdot \sqrt[3]{\left(S / D \right) / \left(H \cdot B \cdot h / D^3 \right)} . \tag{24}$$

Paper [31] indicates the following expression for calculating ΔH (with the dimensions provided by Figure 1), after the analysis of the constructive models proposed by ***Shepherd C. B.*** and ***Lapple C. E.*** (1940), ***Alexander R. McK*** (1949), ***First M. W.*** (1949), ***Stairmand C. J.*** (1949), ***Bart. W.*** (1956):

$$\Delta H = 19.7 \cdot \left(a \cdot b / D_e^2 \right)^{0,99} \cdot \left(S / D \right)^{0,35} \cdot \left(H / D \right)^{-0,34} \cdot \left(h / D \right)^{-0,35} \cdot \left(B / D \right)^{-0,33} , \tag{25}$$

or [31, 32]:

$$\Delta H = 20 \cdot \left(a \cdot b / D_e^2 \right) \cdot \left[\left(S / D \right) / \left(H \cdot B \cdot h / D^3 \right) \right]^{1/3} , \tag{26}$$

No significant differences between the results offered by the two expressions were obtained [31].

2. 6. The theory of *HASHEMI B. S.* (2003, 2006)

The author suggests the following relationship for the evaluation of ΔH [9, 21]:

$$\Delta H = \frac{1}{D - D_e} \cdot \left(\frac{D \cdot N_1}{cos^3 \alpha_1} + \frac{\overline{D} \cdot N_2}{cos^3 \alpha_2} \right) + \frac{N_1 + N_2}{cos^3 \alpha_3} , \tag{27}$$

where $\alpha_1, \alpha_2, \alpha_3$ represents the angle of the velocity vector for the fluid flow in the cylindrical part of the cyclone, the conical part and in the outlet pipe respectively, so that:

$$tg\,\alpha_1 = 0.318 \cdot \frac{h}{D \cdot N_1} ; \;\; tg\,\alpha_2 = \left(tg\,\alpha_1 \right) \cdot \left(sin\,\beta \right) ; \;\; tg\,\alpha_3 = 0.318 \cdot \frac{H}{D \cdot \left(N_1 + N_2 \right)} , \tag{28}$$

where (using notations from Figure 1):

$$N_1 = \frac{D^2 \cdot h - D_e^2 \cdot S}{4 \cdot a \cdot b \cdot D} ; \quad N_2 = N_1 \cdot \left[\frac{\left(H - h \right) \cdot D}{h \cdot \overline{D} \cdot \left(sin^2 \beta \right)} \right] ; \quad \overline{D} = \frac{D - B}{ln\left(D / B \right)} , \tag{29}$$

β representing the slope of the cone generator with respect to the horizontal.

Note: In the paper [16] some corrections of the parameter ΔH are proposed, with an influencing factor of the concentration of solid particles C_{pi} in the impure gas fed at the cyclone inlet, $\Delta H^{\bullet} = \Delta H \cdot k_{\Delta H}$:

$$k_{\Delta H} = 1 / \left[1 + 0.0086 \cdot \left(C_{pi} \cdot \rho_g \right)^{0,5} \right] \quad \textbf{- Briggs L. W.} \text{ (1946) ;} \tag{30}$$

$$k_{\Delta H} = 1 - 0.02 \cdot \left(C_{pi} \cdot \rho_g \right)^{0,6} \quad \textbf{- Smolik J.} \text{ (1975) ;} \tag{31}$$

$k_{\Delta H} = 1 \Big/ \left(1 + 3.1 \cdot C_{pi}^{0,7}\right) + 0.67 \cdot C_{pi}$ - ***Baskakov A. P., Dolgov V. N., Goldovin Yu. M.*** (1990). (32)

Note: A detailed analysis of the total pressure loss in the cyclone structure is done in the papers [15, 33] – for 1D3D, 2D2D, 1D2D type cyclones and specific areas in the cyclone structure, respectively in the paper [22] – model ***Chen J.*** and ***Shi M.*** (2007).

3. Expressions of pressure drop

Note: Over time, many researchers, have suggested empirical formulas for cyclone pressure drop, such as: ***Shepherd C. B.*** and ***Lapple C. E.*** (1939), ***Alexander R. McK.*** and ***Stairmand C. J.*** (1949), ***First M. W.*** (1950), ***Bart W.*** (1956). ***Leith D.*** and ***Mehta D.*** (1973) compared through experiments and concluded that the best results were provided by the researchers: ***Shepherd C. B.*** and ***Lapple C. E.*** (1939), ***Stairmand C. J.*** (1949, 1951), ***Bart W.*** (1956), superior to the research of ***Alexander R. McK*** (1949) and ***First M. W.*** (1950) [7, 8]. The expressions proposed vary greatly in complexity and in the degree to which they are based on empiricism rather than theory [9].
In the work [39], using the Texas A&M Design (TCD) method - a simple design method for cyclones, based on an "*optimal*" speed - for 1D3D and 2D2D type cyclones [33], the dependence of the pressure drop on the speed of gas entry into the cyclone is presented experimentally.
The pressure drop total represents the difference between its value at the entry of the impure gas into the cyclone and the value of the pressure of the purified (clean) gas at the cyclone exit through the outlet pipe [40, 41].
For the domain *40 m<H<100 m* (m – meters of gas column), the relation between the pressure drop and the capacity of the cyclone is [2]:

$$\Delta p = K_1 \cdot Q^2 \cdot \rho_g \,/\, D^4 , \tag{33}$$

where K_1 is a factor that includes the effect of the friction coefficient, $Q-$ the capacity of the cyclone (gas flow), $D-$ the diameter of the cylindrical part of the cyclone.
If ΔH (the height of the gas column) is known, then the pressure drop in the cyclone can be determined using relation (1), after rearranging the terms, as [2, 12]:

$$\Delta p = 0.5 \cdot \rho_g \cdot v_i^2 \cdot \Delta H . \tag{34}$$

Relation (34) for the pressure drop calculation, is applicable to all cyclones, regardless of the method of determining the height of the gas column but depending on the theories developed for the pressure drop calculation.
Note: a) In the work [22] $\Delta H = Eu$ is identified with the number of ***Euler L.*** (b. 1707 – d. 1783).

3. 1. The theory of *SHEPHERD C. B., LAPPLE C. E.* (1939)

The papers [36 - 38] offers the following relationship for the calculation of the pressure drop Δp characteristic for a cyclone with tangential feed of the impurified gas:

$$\Delta p = 8 \cdot \left[\rho_g \cdot v_i^2\right] \cdot \left(a \cdot b \,/\, D_e^2\right), \tag{35}$$

in which are present: $a, b-$ the height and width of the cyclone inlet; D, D_e- the diameter of the cylindrical part of the cyclone, respectively of the purified gas discharge tube; ρ_g- the density of the impurified gas; v_i- gas velocity at the cyclone inlet, calculated with the expression $v_i = Q_v \,/\, (a \cdot b)$, where Q_v is the volumetric flowrate of the gas entering the cyclone.

3. 2. The theory of *STAIRMAND C. J.* (1949)

In the work [23] the following relationship is presented, noting that the results refer to the case of clean gases (not contaminated with dust):

$$\Delta p = \frac{\rho_g}{203} \cdot \left\{ v_i^2 \cdot \left[1 + 2 \cdot \phi^2 \cdot \left(\frac{2 \cdot r_t}{r_e} - 1 \right) \right] + 2 \cdot v_e^2 \right\}, \quad (36)$$

where: $v_i, v_e -$ gas velocity at the entrance to the cyclone, at the exit of the outlet tube respectively; $r_t, r_e -$ the radius of the central circumference at the entrance of the gas into the cyclone, respectively the radius of the gas outlet tube; $\phi -$ dimensionless pressure drop factor.

3. 3. The theory of *BARTH W.* (1956, 1964)

The papers [19, 20] present another expression for evaluating the pressure loss in a cyclone, in the form:

$$\Delta p = 0.5 \cdot \left(\xi_i + \xi_e \right) \cdot \rho_g \cdot v_i^2, \quad (37)$$

in which ξ_i reflects the contribution of pressure losses at the entrance to the cyclone and by friction, and ξ_e the pressure loss under the conditions of the evacuation of the purified gas:

$$\xi_i = f \cdot \left\{ 2 + 3 \cdot \left[u_t(R_e) / u_r(R_e) \right]^{4/3} + \left[u_t(R_e) / u_r(R_e) \right]^2 \right\}; \quad (37)_1$$

$$\xi_e = (R_e / R) \cdot \left\langle \left\{ 1 - \left[u_t(R_e) \cdot h_{eq} / u_r(R_e) \cdot R_e \right] \right\} \cdot \lambda \right\rangle \cdot \left[u_t(R_e) / u_r(R_e) \right]^2, \quad (37)_2$$

where (Figure 1):

- $u_r(R_e)$ radial velocity at the outer radius of the outlet pipe:

$$u_r(R_e) = w_r(R_e) = 0.159 \cdot Q_v / \left[R_e \cdot (H - S) \right]; \quad R_e = D_e / 2; \quad (38)$$

- $u_t(R_e)$- tangential speed at the inner radius of the cyclone:

$$u_t(R_e) = w_t(R_e) = v_\theta(R_e) = 0.318 \cdot \left(Q_v / R_e^2 \right) / \left[\alpha \cdot A_e \cdot R_e / (A \cdot R_\alpha) + \lambda \cdot h_{eq} / R_e \right]; \quad (39)$$

$$\alpha = 1 - (0.54 - 0.153 \cdot A_e / A) \cdot (b / R)^{1/3} - \textbf{ Bohnet M.} - (1984)\ [17] \quad (40)$$

$$\lambda = 0.05 + 287.4 / R_{et}; \qquad h_{eq} = 0.159 \cdot A_t / \sqrt{R / R_e}; \quad (41)$$

$$R_{et} = \left(2 \cdot R \cdot \rho_g / \mu_g \right) \cdot Q_v / \left\{ a \cdot b \cdot \left[0.089 - 0.204 \cdot (b / R) \right] \right\}; \quad R = D / 2, \quad (42)$$

where: $\alpha -$ correction factor; $\lambda -$ friction coefficient, depending on the geometry of the impurified gas inlet and the inlet flow rate (***Muschelnautz E., Brunner K.*** – 1967 [19]); $h_{eq} -$ the equivalent height of the cyclone; A_{tot}, $A_e = a \cdot b, A = 3.14 \cdot R_e^2 -$ the internal area of the cyclone, the cross-sectional area of the gas section in the cyclone, the cross-sectional area of the gas outlet; $R_\alpha = R - 0.5 \cdot b -$ the average length from the gas inlet to the center of the cyclone.

Note: Another formulation of the pressure drop calculation is presented in the paper [37].

3. 4. Cumulative pressure drop rating

In the works [15, 33, 44] adequate details are given for the evaluation of the total pressure drop. In this sense, the corresponding sequential values are estimated for the obvious areas: the entry of the impure gas into the cyclone, the drop of kinetic energy along the descending spiral, the ascending spiral (up to the portion of the impure dust discharge tube located in the cyclone and the one up to the exit from the cyclone), as well as the pressure drop through friction between the particles and the inner surface of the cyclone. Cyclones with recognized geometry (1D3D, 2D2D, 1D2D) are considered in the respective study.

4. Conclusions

This paper presents the opinions of different researchers, elaborated over time, referring to the evaluation of the pressure loss and the efficiency of cyclones with tangential, unilateral feeding. Known as a "*dust separator*", over a hundred years ago, current cyclones have found a well-

deserved place in the field of dry dedusting of impure industrial gases. In some analyses, the density of the gas is neglected compared to that of the particles, in others it is not. Therewith, the influence of the geometry of the inlet of the impure gas in the cyclone, of the speed corresponding to the case, but also the influence of the speed at the exit through the outlet of the purified gas are specified. In the study of the kinematics of the vortex of the mixture inside the cyclone, the hypothesis of solid particles with smooth surfaces is accepted. The influence of friction with the inner surface of the cyclone is also considered, as well as the influence of temperature by means of appropriate parameters.

Article [45] recommends an interesting constructive solution, namely the presence of rectangular "evasés", respectively conical caps over the exhaust tube (radial outlet of pure gas). Such constructions can reduce the value of the total pressure drop and protect the inside of the cyclone from the effects of the weather. These structures will be of particular scientific interest for future, experimental and theoretical works.

The results of the previously specified researches can lead to new analyses, both theoretical and experimental, in possible bachelor's, master's or doctoral theses.

References

[1] Leith, D., and W. Licht. "The collection efficiency of cyclone type particle collectors - A new theoretical approach." *AIChE Symposium Series* 68, no. 126 (1972): 196 – 206.

[2] Birsan, I. G., and D. Panturu. *Equipment for gas purification* / *Utilaje pentru purificarea gazelor*. Vol. I. Braila, Evrika Publishing House, 1997.

[3] Griffiths, W. D., and F. Boysan. "Computational fluid dynamics (CFD) and empirical modeling of the performance of a number of cyclone samplers." *Journal of Aerosol Science* 27, no. 2 (1996): 281–304.

[4] Shukla, K. S., P. Shukla, and P. Ghosh. "The effect of modeling of velocity fluctuations on prediction of collections efficiency of cyclone separators." *Applied Mathematical Modelling* 37, no. 8 (2013): 5774–5789.

[5] Shukla, S. K., P. Shukla, and P. Ghosh. "Evaluation of numerical schemes using different simulation methods for the continuous phase modeling of cyclone separators." *Advanced Powder Technology* 22, no. 2, (2011): 209–219.

[6] Shukla, S. K., P. Shukla, and P. Ghosh. "Evaluation of numerical schemes for dispersed phase modeling of cyclone separators." *Engineering Applications of Computational Fluid Mechanics* 5, no. 2 (2011): 235–246.

[7] Behrouzi, P. *Performance of multicell, axial-entry cyclones for industrial gas cleaning*. Doctoral Thesis. Department of Mechanical Engineering, Imperial College of Science, Technology and Medicine, London, U.K., 1988.

[8] Kuo, Y.K., and J. Ch. Tsai. "On the theory of particle cutoff of diameter and collection efficiency of cyclones." *Aerosol and Air Quality Research* 1, no. 1 (June 2001): 47–56.

[9] Hashemi, S. B. "A mathematical model to compare the efficiency of cyclones." *Chemical Engineering & Technology* 29, no. 12 (2006): 1444–1454.

[10] Drobota, V. *Recent ventilation and air conditioning systems* / *Sisteme recente de ventilare şi de condiţionare a aerului*. Bucharest, Technical Publishing House, 1960.

[11] De Paula, A. C. O., J. R. Henriquez, and F. A. B. Figueiredo. "Validation of a procedure for dimensioning a cyclone separator for circulating fluidized bed gasifier." Paper presented at the 13th International Conference on Heat Transfer, Fluid Mechanics and Thermodynamics, July 17 – 19, 2017, Portorož, Slovenia.

[12] Failaka, M. F. *Superstructure optimization of multiple cyclone arrangements using integer nonlinear programming*. Master's Thesis. University of Waterloo, Ontario, Canada, 2015.

[13] Ibhadode, O. O., E. O. B. Ogedengbe, and M. A. Rosen. "Performance characterization of gas – solid cyclone for separation of particle from syngas produced from food waste gasifier plant." *European Journal of Sustainable Development Research* 1, no. 2 (June 2017): 13.

[14] Pandya, D. *A low cost micro scale cyclone separator - Design and computational fluid dynamics analysis.* Master's Thesis. The University of Texas at Arlington, USA, 2010.

[15] Wang, L., B. C. Parnell, W. B. Shaw, and E. R. Lacey. "A theoretical approach for predicting number of turns and cyclone pressure drop." *Transactions of the ASABE* 49, no. 2 (2006): 491–503.

[16] Cortés, Cr., and A. Gil. "Modeling the gas and particle flow inside cyclone separators." *Progress in Energy and Combustion Science* 33, no. 5 (October 2007): 409–452.

[17] Leith, D., and D. S. Mehta. "Cyclone performance and design." *Atmospheric Environment* 7 (1973): 527–549.

[18] Dirgo, J. A., and D. Leith. "Performance of theoretically optimized cyclones." *Filtration & Separation* 22, no. 2 (1985): 119–125.
[19] Altmeyer, S., V. Mathieu, S. Jullemier, P. Contal, N. Midoux, S. Rode, and P. J. Leclerc. "Comparison of different models of cyclone prediction performance for various operating conditions using a general software." *Chemical Engineering and Processing* 43 (2004): 511–521.
[20] Bohnet, M., and Th. Lorenz. "Separation efficiency and pressure drop of cyclones at high temperatures." Chapter, pp. 17 – 23. Clift, R., and J. P. K. Seville (Eds.). *Gas Cleaning at High Temperatures*. Dordrecht, Springer, 1993.
[21] Hashemi, B. S. "Development and validation of new equations for prediction of the performance of tangential cyclones." *IJE Transactions A: Basics* 16, no. 2 (June 2003): 109–124.
[22] Nabil, K. *Study of aerodynamics and particle filtration in a cyclone separator* / *Étude de l'aérodynamique et de la filtration de particules dans un cyclone separateur*. Doctoral thesis. Mentouri Constantine University, People's Democratic Republic of Algeria, 2007.
[23] ***. "Separation equipments: General design considerations of cyclone separators, centrifuges, separation equipments." *National Programme Technology Enhanced Learning (NPTEL) – Chemical Engineering – Chemical Engineering Design II*. Accessed March 30, 2023. https://archive.nptel.ac.in/content/storage2/courses/103103027/pdf/mod5.pdf.
[24] Silva, E. L. *Air pollution control in the sugar industry* / *Controle da poluição do ar na indústria açucareira*. Society of Sugar Technicians of Brazil / Sociedade dos Técnicos Açucareiros do Brasil – STAB, 2000.
[25] Gimbun, J., T.S.Y. Choong, A. Fakhru'l-Razi, and G. T. Chuah. "Prediction of the effect of dimension, particle density, temperature, and inlet velocity of cyclone collection efficiency." *Jurnal Teknologi* 40, no. 1 (June 2004): 37–50.
[26] Betoşkin, A. G. *Dust cleaning processes and apparatus* / *Protsessy i apparaty pyleochistki*. Schoolbook. Penza State University, Penza, Russian Federation, 2005. Accessed March 31, 2023. http://echemistry.ru/assets/files/books/ekologiya/skrubbery.pdf.
[27] Fredriksson, Ch. *Exploratory experimental and theoretical studies of cyclone gasification of wood power*. Doctoral thesis. Lulea University of Technology, Sweden, 1999.
[28] Wang, L., C. B. Parnell, B. W. Shaw, and R. E. Lacey. "Analysis of cyclone collection efficiency." An ASAE Meeting Presentation. Paper Number: 034114. Paper presented at the 2003 ASAE Annual International Meeting, Las Vegas, Nevada, USA, July 27- 30, 2003.
[29] Brunnmair, E. *Development and modeling of a new high-performance cyclone for separating solid/gas mixtures* / *Entwicklung und modellierung eines neuer hochleistungszyklons zur trennung von feststoff/gas-gemischen*. Dissertation. Mintanuniversität Leoben, Austria, 2010.
[30] Stairmand, C. J. "The design and performance of cyclone separators." *Chemical Engineering Transactions* 29 (1951): 15–44.
[31] Ramachandran, G., D. Leith, J. A. Dirgo, and H. Feldman. "Cyclone optimization based on a new empirical model for pressure drop." *Aerosol Science and Technology* 15, no. 2 (1991): 135–148.
[32] Mauricio, P., P. Silva, A. Fonseca, and P. Duarte. "An algorithm for cyclone sizing" / "Um algoritmo para dimensionamento de ciclones." *Catálogo Bibliográfico* | *Universidade Fernando Pessoa*. Accessed April 3, 2023. https://bdigital.ufp.pt/bitstream/10284/539/1/40-51FCT2006-4.pdf.
[33] Wang, L. *Theoretical study of cyclone design*. Doctoral thesis. Texas A&M University, College Station, Texas, USA, 2004.
[34] Failaka, F. M., and A. Elkamel. "Superstructure optimization of multiple gas – solid cyclone arrangements." Paper presented at the 2016 International Conference on Industrial Engineering and Operations Management, Kuala Lumpur, Malaysia, March 8–10, 2016.
[35] ***. "Polluting effluents treatment plants – Course syllabus - Lesson 8. Cyclones, centrifuges" / "Impianti di trattamento degli effluenti inquinanti – Programma – Lez. 8. Cicloni, centrifughe" Accessed April 3, 2023. http://wpage.unina.it/antcaval/pdffilesitei/lez8.pdf.
[36] Dhodapkar, Sh. V., and W. L. Heumann. "Harnessing the power of a cyclone." *Chemical Engineering* 118, no. 5 (May 2011): 34-43.
[37] Bododage, G. S., and T. Y. A. Leung. "Cyclone separator theories to predict performance and flow characteristics." *Journal of Particle Science & Technology* 7, no. 2 (October 2021): 83-98.
[38] Fassani, L. F., and L. Goldstein Jr. "A study of the effect of high inlet solids loading on a cyclone separator pressure drop and collection efficiency." *Powder Technology* 107 (2000): 60–65.
[39] Faulkner, B. W., and W. B. Shaw. "Efficiency and pressure drop of cyclones across a range of inlet velocities." *Applied Engineering in Agriculture* 22, no. 1 (2006): 155–161.
[40] Chen, J., and M. Shi. "A universal model to calculate cyclone pressure drop." *Powder Technology* 171, no. 3 (February 2007): 184–191.
[41] Sabbah, F. M., A. M. Abdel - Hadi, M. S. Radwan, and S. A. El-Sayed. "Effect of design and predicted pressure drop in cyclone." *MISR Journal of Agricultural Engineering (MJAE)* 36, no. 4 (2019): 1227–1248.

[42] Karadeniz, A., C. Ayvaz, S. Demir, M. Aksel, and A. Saral. “Experimental and numerical investigation of the effects of vortex finder geometry on cyclone performance.” *Sigma Journal of Engineering and Natural Sciences* 38, no. 4 (2020): 1811–1823.
[43] García Sánchez, J. A. *Effects of varying vortex seeker sizing on the performance of a cyclone separator / Efectos de la variacion del dimensionamiento del buscador de vortices en el desempeño de un separador ciclonico*. Master's Thesis. National Polytechnic Institute, Mexico City, Distrito Federal, Mexico, 2008.
[44] Wang, L., C. B. Parnell, and B. W. Shaw. “Analysis of cyclone pressure drop.” *Proceedings of the Beltwide Cotton Conference* 2 (2001): 1325–1329.
[45] Funk, P. A. “Reducing cyclone pressure drop with evasés.” *Powder Technology* 272 (March 2015): 276–281.

Generation of Non-Linear Equations to Approximate the Normalized Annual Agricultural Production Curve, Using Drought Indexes

Eng. **Valdemar TORRES ESPINOSA**[1], PhD. **Maritza Liliana ARGANIZ JUÁREZ**[2,3,*]

[1] Escuela Superior de Ingeniería y Arquitectura, Instituto Politécnico Nacional. Gustavo A. Madero. C. P. 07738. Ciudad de México, CDMX., México

[2] Instituto de Ingeniería, Universidad Nacional Autónoma de México. Ciudad Universitaria. C. P. 04510. Ciudad de México, CDMX., México

[3] Facultad de Ingeniería, Universidad Nacional Autónoma de México. Ciudad Universitaria. C. P. 04510. Ciudad de México, CDMX., México

* Corresponding author's e-mail address: marganisj@iingen.unam.mx

Abstract: *Extreme droughts are one of the biggest problems for agricultural and livestock activities throughout Mexico. These events have caused a decrease in income for producers due to the increase in input costs, which in turn causes an increase in the price of products and food for the poorest populations. In this research equations that allow us to estimate a normalized value of agricultural production in each state of Mexico were obtained. The equations were generated with optimization of their parameters using genetic algorithms and were taken as data from agricultural production records and drought indexes registered in the country. These, in turn, depend on the return period of drought events. These models can be used to estimate agricultural production given a drought with a given return period, which will help to take preventive actions against this problem.*

Keywords: *Drought, genetic algorithm, agricultural production, regionalization, economic losses, drought indexes*

1. Introduction

Drought is a meteorological event that is defined as the decrease or absence of rainfall compared to the annual rate [1]. This climatological phenomenon is present all over the world and is occurring with increasing frequency. Unlike other climatological phenomena, drought is an event that occurs slowly and inconspicuously [2]. For this reason, it is considered one of the most devastating natural disasters worldwide due to its long-term environmental and socioeconomic impact. The direct and indirect effects caused by this phenomenon are also increasing, with negative repercussions on different sectors such as water supply systems, the natural environment, agricultural, livestock and industrial production, among others [3]. The severity of the effects depends on the level of development, population density, demand for water and other natural resources, technological development, and the political system [4].

This meteorological phenomenon is considered to cause the greatest economic damage to humanity [2]. During the last 30 years, 470 drought-related disasters have been estimated around the world [5]. In economic terms, during the last 20 years, droughts have been the cause of the loss of 5 billion USD worldwide [6]. Approximately 1.4 billion people worldwide work in the agricultural sector, and for all of them droughts mean an obstacle to achieving a life of well-being [7].

In the year 2020, in the state of California, U. S., economic losses occurred around 15 billion USD due to droughts and wildfires. In Guatemala, El Salvador, Honduras and Nicaragua about 6.4 million people lost their crops due to drought events [8]. European Commission, et al. 2020 [9] estimated in 2020 that the annual losses due to drought in the European Union and the United Kingdom are around 9 billion euros, with Spain (1.5 billion euros/year), Italy (1.4 billion euros/year), and France (1.4 billion euros/year) showing the highest losses.

Droughts can occur at any time and place; however, there are specific areas of the Earth with greater susceptibility to the phenomenon, determined by their geographic location, based on latitude [10]. Mexico has a large part of its territory in the strip of high northern latitude pressure, so

52% of its territory is classified as arid or semi-arid [1]. During the drought period from 1970 to 1978 that Mexico suffered, 30% of the Mexican territory had gone through the most severe drought period in history, and due to this event, there were deficiencies in the storage of water in several dams in the country, so there were several restrictions for sowing in irrigated areas. The economic losses of this event were estimated at 5 billion Mexican pesos [11]. These devastating events have been intensifying in recent years because of the climatological phenomenon known as "La Niña", which has spread over the last few years, with 2021 being the most severe episode of drought in the country since 2012 [12].
In nature, nothing is constant and predictable. When a natural event reaches its extreme conditions, it can be a risk for the inhabitants of a certain environment. In order to reduce the effects of any catastrophe, it is necessary to anticipate the behavior of these phenomena. In 2015, the study [13] obtained normalized equation models that allow determining the annual agricultural production in the states of Mexico for this same purpose and, like this study, generated equations using the records of drought indexes in the country and its agricultural production (but in Mexican pesos) with the genetic programming methodology. This study updates the equations obtained in [13] using more recent records of drought indexes and agricultural production (in tons), using the genetic algorithm methodology as a function of the return period.

2. Methods

2.1. Genetic Algorithm (GA)

Genetic algorithms (GA) [14] are stochastic global search methods that use a metaphor of natural biological evolution and aim to find the optimal solution to a problem by applying the principle of survival of the fittest to produce increasingly better approximations to a solution.
In each generation, a new set of approximations is created by the process of selecting individuals according to their level of fitness in the problem domain and reproducing them through operators taken from natural genetics. This process leads to the evolution of populations of individuals that are better adapted to their environment than the individuals from which they were created, just as in natural adaptation.
Individuals, or current approximations, are coded as strings, or chromosomes, composed on some alphabet, so that genotypes (chromosomal values are uniquely mapped to the decision variable (phenotypic) domain. The most commonly used representation in GAs is the binary alphabet {0, 1}, although other representations can be used, e.g., ternary, integer, real-valued, to name a few.
Examining the chromosome string in isolation yields no information about the problem we are trying to solve. Only by decoding the chromosome into its phenotypic values can any meaning be applied to the representation.
Decoding the chromosome representation allows us to evaluate the performance or fitness of individual members of a population. This is done through an objective function that characterizes the performance of an individual in the problem domain. Thus, the objective function establishes the basis for the selection of pairs of individuals that will mate during reproduction.
During the reproduction phase, each individual is assigned a fitness value derived from its raw performance measure given by the objective function. This value is used in selection to bias toward fitter individuals. Highly fit individuals have a high probability of being selected for mating.
Once individuals have been assigned a fitness value, they can be chosen from the population to be crossed or mutated to generate a new population of processed individuals. Following this, the recombination operator intervenes to exchange genetic information between pairs or larger groups of individuals. After recombination, the mutation operator slightly transforms an individual, can avoid convergence and changes the search direction. Then, population replacement establishes the criteria for survivors at each generational iteration, depending on the selection and crossing methods used [15].

2.2. Data set

The data used in the study were the agricultural production records, obtained from the SIAP platform (*Servicio de Información Agroalimentaria y Pesquera*) [16], and the records of the drought

indexes were obtained from the Meteorological Drought Monitor platform of CONAGUA (*Comisión Nacional del Agua*) [1] and from the study of [13].

3. Results and Discussion

The drought indexes were obtained from the Mexican Drought Monitor (MSM) of the National Meteorological Service (SMN). Data for the period December 2013 and July 2022 were recorded from the platform. Data prior to December 2013 were obtained from [13]. The information obtained from the MSM indicates the biweekly drought indexes. From this record, the annual average of the data was obtained. These enveloped percentages were reordered from highest to lowest as shown in Table 1.

Table 1: Drought indexes in Mexico

No.	Without affection	D0 to D4	D1 to D4	D2 to D4	D3 to D4	D4
1	76.30	75.99	61.25	45.74	27.31	7.34
2	75.75	62.13	38.84	22.39	7.95	2.42
3	73.24	57.67	38.51	19.61	6.50	0.66
4	70.70	53.84	30.84	15.53	5.23	0.65
5	70.33	52.97	30.73	12.28	3.37	0.57
6	68.37	47.68	28.04	10.87	3.14	0.15
7	65.56	47.30	26.94	9.73	1.93	0.14
8	65.43	47.17	23.76	9.59	1.85	0.14
9	59.28	46.51	22.09	8.82	1.71	0.14
10	54.39	45.61	17.87	7.41	1.58	0.09
11	53.49	40.72	17.64	6.62	1.57	0.09
12	52.83	34.57	14.16	4.68	1.06	0.07
13	52.70	34.44	11.81	3.34	0.95	0.01
14	52.32	31.63	10.57	2.31	0.66	0.00
15	47.03	29.67	8.59	2.29	0.51	0.00
16	46.17	29.30	8.28	1.93	0.39	0.00
17	42.33	26.77	7.12	1.71	0.33	0.00
18	37.88	24.26	7.01	0.99	0.12	0.00
19	24.01	23.70	6.86	0.53	0.01	0.00

The categorization of droughts, according to CONAGUA, is as follows:

- Abnormally Dry (D0): not a drought category, but a dry condition indicating the beginning or end of a drought period. Immediate impacts ranging from delaying/limiting crop or pasture growth to the point where crops or pastures may not fully recover. There is a risk of fire.
- Moderate Drought (D1): Perceptible damage to crops and pastures, a high risk of fire, and water body levels begin to drop. A voluntary restriction of water use is suggested.
- Severe Drought (D2): Losses in agricultural production are now likely, where water is usually scarce. Water consumption restrictions should be imposed.
- Extreme Drought (D3): Losses in agricultural production are greater, the risk of forest fires is extreme and scarcity forces general reductions in consumption.
- Exceptional Drought (D4): Emergency situation due to total water shortage in reservoirs, streams and wells, agricultural production with extraordinary losses and exceptional risk of fires.

From the Statistical Yearbook of Agricultural Production of the Agrifood and Fisheries Information

Service (SIAP) the record of annual agricultural production at the state level was obtained in tons from 2003 to 2021. The production values rearranged from highest to lowest are shown in Table 2.

With the data in Table 2, the mean ($\bar{X}$), standard deviation (σ) and coefficient of variation (Cv) were obtained for each state with the same equations used in [13], which are shown below (Eqs 1 to 3).

Mean.

$$\bar{X} = \sum_{i=i}^{n} \frac{X_i}{n} \tag{1}$$

Standard deviation.

$$\sigma = \sqrt{\frac{\sum_{i=i}^{n}(X_i - \bar{X})^2}{n}} \tag{2}$$

Coefficient of variation.

$$Cv = \frac{\sigma}{\bar{X}} \tag{3}$$

Where X_i is a given agricultural production value and n is the number of agricultural production values recorded.

Six groups of states were formed according to the coefficient of variation. The intervals of the groups formed are shown in Table 3.

The agricultural production values in Table 2 were normalized by dividing each production value by the calculated mean. For example, for the state of Veracruz, the highest normalized value is: 30.073 / 26.609 = 1.13. The normalized values are shown in Table 4.

Table 2: Annual statewide agricultural production record in millions of tons

State	1	2	3	4	5	6	7	8	9	10	11
AS	2.758	2.757	2.712	2.699	2.683	2.663	2.580	2.518	2.517	2.509	2.508
BC	4.214	4.028	3.994	3.858	2.507	2.474	2.458	2.428	2.409	2.362	2.344
BS	0.744	0.705	0.679	0.659	0.644	0.632	0.612	0.591	0.591	0.561	0.523
CC	2.218	1.985	1.981	1.841	1.824	1.817	1.627	1.524	1.494	1.129	1.087
CS	14.182	13.138	12.527	12.311	12.213	12.065	11.952	11.895	11.685	11.602	10.769
CH	11.178	11.048	10.223	10.020	9.969	9.569	9.486	9.329	9.179	7.835	6.431
CL	5.896	5.806	5.781	5.729	5.708	5.689	5.650	5.584	5.570	5.568	5.512
CM	3.773	3.756	3.738	3.659	3.617	3.583	3.549	3.478	3.454	3.410	3.407
DF	0.485	0.456	0.434	0.432	0.419	0.417	0.416	0.411	0.397	0.385	0.383
DG	9.117	8.593	8.563	8.504	8.351	8.257	7.883	7.674	7.489	7.157	7.092
GT	9.953	9.947	9.944	9.874	9.816	9.671	9.388	9.078	9.065	8.990	8.979
GR	5.779	5.724	5.677	5.674	5.541	5.420	5.414	5.238	5.094	4.947	4.798
HG	7.781	7.674	7.639	7.601	7.584	7.442	7.373	7.356	7.298	7.120	7.033
JC	36.295	35.548	35.537	34.394	31.409	31.152	28.452	26.752	25.732	25.041	25.003
MC	9.122	8.864	8.648	8.631	8.516	8.435	8.331	8.271	8.249	8.133	7.783
MN	11.532	11.460	11.450	10.986	10.802	10.296	9.846	9.694	9.583	9.543	9.304
MS	3.833	3.736	3.583	3.523	3.409	3.385	3.341	3.300	3.252	3.194	3.179
NT	6.347	6.243	6.201	6.157	6.145	6.131	6.103	6.016	6.010	5.953	5.744
NL	3.943	3.567	3.547	3.520	3.461	3.293	3.253	3.146	3.124	3.040	2.977
OC	20.108	19.551	19.500	19.477	19.336	18.771	18.440	16.787	15.215	15.144	14.906
PL	7.396	7.323	7.239	7.077	7.058	7.027	6.987	6.959	6.623	6.245	5.976

QO	2.250	2.166	2.164	2.135	2.121	2.095	2.040	2.013	1.956	1.931	1.912
QR	2.226	2.180	2.168	2.070	1.982	1.871	1.871	1.856	1.829	1.819	1.723
SP	11.636	11.189	10.897	10.749	10.515	10.146	9.940	8.765	7.493	7.027	7.005
SL	13.415	12.860	12.703	12.240	12.226	12.174	11.804	11.674	11.141	11.050	11.003
SR	6.997	6.918	6.616	6.484	6.210	5.958	5.692	5.594	5.563	5.490	5.441
TC	4.008	3.859	3.777	3.584	3.459	3.367	3.293	3.275	3.198	3.171	2.960
TS	10.465	9.420	9.406	9.395	9.324	9.050	8.898	8.717	8.575	8.455	8.443
TL	1.516	1.478	1.430	1.423	1.387	1.355	1.347	1.338	1.334	1.323	1.310
VZ	30.073	29.919	29.289	29.007	28.267	28.251	27.640	27.593	27.239	25.990	25.733
YN	13.234	5.716	5.682	5.601	5.589	5.533	5.462	5.382	5.338	5.300	5.285
ZS	7.282	7.089	7.063	6.903	6.856	6.817	6.489	6.307	5.857	5.298	5.242

Table 2: Annual statewide agricultural production record in millions of tons (Continuation)

State	12	13	14	15	16	17	18	19	Mean	σ	Cv
AS	2.487	2.451	2.424	2.317	2.295	2.192	2.145	2.122	2.49	0.20	0.08
BC	2.335	2.298	2.285	2.271	2.183	2.141	1.847	1.777	2.64	0.76	0.29
BS	0.460	0.441	0.438	0.436	0.430	0.429	0.429	0.415	0.55	0.11	0.20
CC	0.988	0.973	0.956	0.915	0.859	0.822	0.791	0.679	1.34	0.49	0.37
CS	10.467	10.187	10.032	9.223	8.761	8.605	6.414	6.151	10.75	2.15	0.20
CH	6.397	6.298	5.981	5.737	5.130	5.086	4.836	4.539	7.80	2.30	0.29
CL	5.410	5.364	5.329	5.318	5.271	5.000	4.394	4.236	5.41	0.44	0.08
CM	3.339	3.211	3.150	3.020	2.967	2.906	2.299	2.258	3.29	0.44	0.13
DF	0.375	0.373	0.367	0.365	0.361	0.359	0.357	0.352	0.40	0.04	0.09
DG	7.021	6.778	6.732	6.709	5.729	5.116	4.949	4.818	7.19	1.30	0.18
GT	8.817	8.701	8.522	8.510	8.471	8.358	8.227	8.023	9.07	0.64	0.07
GR	4.788	4.563	4.506	4.271	4.227	4.080	2.914	2.860	4.82	0.87	0.18
HG	7.003	6.981	6.688	6.553	6.490	6.222	6.189	6.089	7.06	0.54	0.08
JC	24.771	23.767	23.627	22.998	22.898	22.457	21.698	21.311	27.31	5.13	0.19
MC	7.332	7.285	7.266	7.082	6.867	6.802	5.692	5.597	7.73	1.01	0.13
MN	8.962	8.880	8.842	8.775	8.399	8.395	8.237	8.205	9.64	1.14	0.12
MS	3.128	3.039	3.027	3.022	2.991	2.860	2.812	2.444	3.21	0.34	0.10
NT	5.689	5.442	5.013	4.734	4.662	3.967	3.937	3.563	5.48	0.89	0.16
NL	2.883	2.827	2.771	2.736	2.659	2.638	0.963	0.706	2.90	0.81	0.28
OC	14.569	14.388	13.880	13.662	11.273	8.113	6.510	6.477	15.06	4.38	0.29
PL	5.912	5.882	5.639	5.600	5.514	5.435	5.342	5.299	6.34	0.76	0.12
QO	1.912	1.847	1.843	1.776	1.249	1.218	1.204	1.155	1.84	0.36	0.20
QR	1.633	1.619	1.595	1.439	1.387	1.279	1.187	1.171	1.73	0.33	0.19
SP	6.948	6.812	6.427	6.425	6.248	6.222	6.172	5.741	8.23	2.08	0.25
SL	10.990	10.924	10.194	10.161	9.940	9.675	9.139	8.102	11.13	1.36	0.12
SR	5.196	5.052	4.963	4.843	4.685	3.887	3.716	3.156	5.39	1.05	0.20
TC	2.903	2.830	2.744	2.627	2.605	2.466	2.434	2.417	3.10	0.50	0.16
TS	8.344	8.332	8.217	8.147	8.056	7.964	6.192	5.715	8.48	1.09	0.13
TL	1.309	1.292	1.265	1.243	1.182	1.140	1.116	0.748	1.29	0.17	0.13

VZ	25.405	25.286	24.998	24.873	24.602	24.418	24.054	22.948	26.61	2.14	0.08
YN	5.096	5.070	4.971	4.677	4.552	4.471	0.578	0.460	5.16	2.48	0.48
ZS	3.982	3.744	3.546	3.394	3.274	3.246	2.652	2.351	5.13	1.74	0.34

Table 3: Groups of states according to the coefficient of variation Cv

Group	Cv Interval
1	0.07 - 0.10
2	0.12 - 0.16
3	0.18 - 0.20
4	0.25 - 0.29
5	0.34 - 0.37
6	0.48

An average of the 19 normalized records was determined for each group of states shown in Table 3. Table 5 shows the averages of the normalized records for each group.
Correlation plots of the normalized value of annual production vs. the different drought indexes were made for each group of states. The correlation graphs, their trend lines, their equation and the coefficients of determination of these lines were obtained with the Excel tool. This is done to identify with which type of drought a better correlation is obtained according to the group of states.
Groups 1, 2, 3 and 4 had a better correlation (a higher value in the coefficient of determination) with drought indexes from D2 to D4, group 5 had a better correlation with drought indexes from D1 to D4, and group 6 had a better correlation with drought indexes from D0 to D4. For these drought types, correlation graphs were made of the enveloping percentage of drought vs. the return period in years.
The return period was obtained with the Weibull equation (n+1)/m, where n is the size of the annual series and m is the number of ordered data.
The equations of the trend lines generated from the correlation plots were generated with the Excel tool, and the coefficients of the polynomial models were obtained with Excel Solver and AG. The equations obtained are shown below (Eqs 4 to 6).

For D0 a D4.

$$D_i = 14.222\ Ln(T_D) + 29.181 \tag{4}$$

For D1 a D4.

$$D_i = 14.88\ Ln(T_D) + 6.93 \tag{5}$$

For D2 a D4.

$$D_i = -0.1044{T_D}^2 + 3.942T_D - 1.363 \tag{6}$$

Where D_i is the drought indexes and T_D is the return period in years.

Table 4: Standardized record of agricultural production

State	1	2	3	4	5	6	7	8	9	10
AS	1.11	1.11	1.09	1.08	1.08	1.07	1.04	1.01	1.01	1.01
BC	1.59	1.52	1.51	1.46	0.95	0.94	0.93	0.92	0.91	0.89
BS	1.36	1.29	1.24	1.20	1.17	1.15	1.12	1.08	1.08	1.02
CC	1.65	1.48	1.48	1.37	1.36	1.35	1.21	1.13	1.11	0.84
CS	1.32	1.22	1.17	1.15	1.14	1.12	1.11	1.11	1.09	1.08
CH	1.43	1.42	1.31	1.28	1.28	1.23	1.22	1.20	1.18	1.00
CL	1.09	1.07	1.07	1.06	1.05	1.05	1.04	1.03	1.03	1.03
CM	1.15	1.14	1.13	1.11	1.10	1.09	1.08	1.06	1.05	1.04
DF	1.22	1.15	1.09	1.09	1.06	1.05	1.05	1.04	1.00	0.97
DG	1.27	1.20	1.19	1.18	1.16	1.15	1.10	1.07	1.04	1.00
GT	1.10	1.10	1.10	1.09	1.08	1.07	1.03	1.00	1.00	0.99
GR	1.20	1.19	1.18	1.18	1.15	1.13	1.12	1.09	1.06	1.03
HG	1.10	1.09	1.08	1.08	1.07	1.05	1.04	1.04	1.03	1.01
JC	1.33	1.30	1.30	1.26	1.15	1.14	1.04	0.98	0.94	0.92
MC	1.18	1.15	1.12	1.12	1.10	1.09	1.08	1.07	1.07	1.05
MN	1.20	1.19	1.19	1.14	1.12	1.07	1.02	1.01	0.99	0.99
MS	1.19	1.16	1.12	1.10	1.06	1.05	1.04	1.03	1.01	0.99
NT	1.16	1.14	1.13	1.12	1.12	1.12	1.11	1.10	1.10	1.09
NL	1.36	1.23	1.22	1.21	1.19	1.14	1.12	1.09	1.08	1.05
OC	1.34	1.30	1.29	1.29	1.28	1.25	1.22	1.11	1.01	1.01
PL	1.17	1.15	1.14	1.12	1.11	1.11	1.10	1.10	1.04	0.98
QO	1.22	1.18	1.18	1.16	1.15	1.14	1.11	1.09	1.06	1.05
QR	1.29	1.26	1.25	1.20	1.14	1.08	1.08	1.07	1.06	1.05
SP	1.41	1.36	1.32	1.31	1.28	1.23	1.21	1.07	0.91	0.85
SL	1.21	1.16	1.14	1.10	1.10	1.09	1.06	1.05	1.00	0.99
SR	1.30	1.28	1.23	1.20	1.15	1.10	1.06	1.04	1.03	1.02
TC	1.29	1.24	1.22	1.15	1.11	1.08	1.06	1.06	1.03	1.02
TS	1.23	1.11	1.11	1.11	1.10	1.07	1.05	1.03	1.01	1.00
TL	1.17	1.14	1.11	1.10	1.07	1.05	1.04	1.04	1.03	1.02
VZ	1.13	1.12	1.10	1.09	1.06	1.06	1.04	1.04	1.02	0.98
YN	2.57	1.11	1.10	1.09	1.08	1.07	1.06	1.04	1.03	1.03
ZS	1.42	1.38	1.38	1.35	1.34	1.33	1.27	1.23	1.14	1.03

Table 4: Standardized record of agricultural production (Continuation)

State	11	12	13	14	15	16	17	18	19
AS	1.01	1.00	0.98	0.97	0.93	0.92	0.88	0.86	0.85
BC	0.89	0.88	0.87	0.86	0.86	0.83	0.81	0.70	0.67
BS	0.95	0.84	0.80	0.80	0.79	0.78	0.78	0.78	0.76
CC	0.81	0.74	0.72	0.71	0.68	0.64	0.61	0.59	0.51
CS	1.00	0.97	0.95	0.93	0.86	0.82	0.80	0.60	0.57
CH	0.82	0.82	0.81	0.77	0.74	0.66	0.65	0.62	0.58
CL	1.02	1.00	0.99	0.98	0.98	0.97	0.92	0.81	0.78
CM	1.03	1.01	0.98	0.96	0.92	0.90	0.88	0.70	0.69
DF	0.97	0.94	0.94	0.92	0.92	0.91	0.91	0.90	0.89
DG	0.99	0.98	0.94	0.94	0.93	0.80	0.71	0.69	0.67
GT	0.99	0.97	0.96	0.94	0.94	0.93	0.92	0.91	0.88
GR	1.00	0.99	0.95	0.94	0.89	0.88	0.85	0.61	0.59
HG	1.00	0.99	0.99	0.95	0.93	0.92	0.88	0.88	0.86
JC	0.92	0.91	0.87	0.87	0.84	0.84	0.82	0.79	0.78
MC	1.01	0.95	0.94	0.94	0.92	0.89	0.88	0.74	0.72
MN	0.96	0.93	0.92	0.92	0.91	0.87	0.87	0.85	0.85
MS	0.99	0.97	0.95	0.94	0.94	0.93	0.89	0.88	0.76
NT	1.05	1.04	0.99	0.92	0.86	0.85	0.72	0.72	0.65
NL	1.03	1.00	0.98	0.96	0.94	0.92	0.91	0.33	0.24
OC	0.99	0.97	0.96	0.92	0.91	0.75	0.54	0.43	0.43
PL	0.94	0.93	0.93	0.89	0.88	0.87	0.86	0.84	0.84
QO	1.04	1.04	1.00	1.00	0.96	0.68	0.66	0.65	0.63
QR	0.99	0.94	0.93	0.92	0.83	0.80	0.74	0.69	0.68
SP	0.85	0.84	0.83	0.78	0.78	0.76	0.76	0.75	0.70
SL	0.99	0.99	0.98	0.92	0.91	0.89	0.87	0.82	0.73
SR	1.01	0.96	0.94	0.92	0.90	0.87	0.72	0.69	0.59
TC	0.95	0.94	0.91	0.88	0.85	0.84	0.79	0.78	0.78
TS	1.00	0.98	0.98	0.97	0.96	0.95	0.94	0.73	0.67
TL	1.01	1.01	1.00	0.98	0.96	0.92	0.88	0.86	0.58
VZ	0.97	0.95	0.95	0.94	0.93	0.92	0.92	0.90	0.86
YN	1.02	0.99	0.98	0.96	0.91	0.88	0.87	0.11	0.09
ZS	1.02	0.78	0.73	0.69	0.66	0.64	0.63	0.52	0.46

Table 5: Normalized registers of the groups of states

No.	GROUP 1	GROUP 2	GROUP 3	GROUP 4	GROUP 5	GROUP 6
1	1.13	1.20	1.29	1.43	1.54	2.57
2	1.11	1.16	1.24	1.37	1.43	1.11
3	1.09	1.14	1.22	1.33	1.43	1.10
4	1.08	1.12	1.19	1.31	1.36	1.09
5	1.07	1.10	1.15	1.20	1.35	1.08
6	1.06	1.09	1.13	1.16	1.34	1.07
7	1.04	1.07	1.09	1.14	1.24	1.06
8	1.03	1.06	1.07	1.08	1.18	1.04
9	1.01	1.04	1.05	1.02	1.13	1.03
10	1.00	1.02	1.02	0.96	0.94	1.03
11	0.99	0.99	0.99	0.92	0.92	1.02
12	0.97	0.98	0.95	0.90	0.76	0.99
13	0.97	0.96	0.92	0.89	0.73	0.98
14	0.95	0.93	0.92	0.86	0.70	0.96
15	0.94	0.91	0.88	0.85	0.67	0.91
16	0.93	0.89	0.81	0.78	0.64	0.88
17	0.90	0.85	0.76	0.73	0.62	0.87
18	0.88	0.78	0.69	0.57	0.56	0.11
19	0.84	0.72	0.66	0.52	0.49	0.09

With equations 4, 5 and 6, the drought index record was updated using the same T_D values that were used to initially generate the equations. New correlation graphs of the normalized value of annual production vs. the new drought indexes were made from these data. With these graphs, the equation models of the trend lines were obtained with the Excel tool. The coefficients of the equation models were obtained with the GA. It was also possible to obtain the equation models with the Solver tool, but the results of this tool always showed a lower coefficient of determination than those obtained with the genetic algorithm. The equations obtained by GA are shown below (Eqs 7 to 12).

Group 1.

$$A_P = 0.075Ln(D_{iu}) + 0.861 \quad (7)$$

Group 2.

$$A_P = 0.121Ln(D_{iu}) + 0.776 \quad (8)$$

Group 3.

$$A_P = 0.17Ln(D_{iu}) + 0.685 \quad (9)$$

Group 4.

$$A_P = 0.2399Ln(D_{iu}) + 0.555 \quad (10)$$

Group 5.

$$A_P = -7.34 \cdot 10^{-4} {D_{iu}}^2 + 0.066D_{iu} + 0.048 \quad (11)$$

Group 6.

$$A_P = -5.5 \cdot 10^{-6} {D_{iu}}^3 + 7.7 \cdot 10^{-4} {D_{iu}}^2 + 3 \cdot 10^{-5} D_{iu} \quad (12)$$

Where A_P is the normalized value of annual production and D_{iu} is the updated drought index. Equations 7, 8, 9, 10, 11 and 12 had the variable D_{iu} substituted by the equations that determine the drought indexes according to the return period. The substitution is made so that from T_D the normalized value of the annual production can be obtained.
The simplified equations are shown below (Eqs 13 to 18).

Group 1.

$$A_P = 0.075Ln(-0.1044{T_D}^2 + 3.942T_D - 1.363) + 0.861 \quad (13)$$

Group 2.

$$A_P = 0.121Ln\left(-0.1044{T_D}^2 + 3.942T_D - 1.363\right) + 0.776 \quad (14)$$

Group 3.

$$A_P = 0.17Ln\left(-0.1044{T_D}^2 + 3.942T_D - 1.363\right) + 0.685 \quad (15)$$

Group 4.

$$A_P = 0.2399Ln\left(-0.1044{T_D}^2 + 3.942T_D - 1.363\right) + 0.555 \quad (16)$$

Group 5.

$$A_P = -0.1625Ln(T_D)^2 + 0.8307Ln(T_D) + 0.4701 \quad (17)$$

Group 6.

$$A_P = -0.0158Ln(T_D)^3 + 0.0584Ln(T_D)^2 + 0.4397Ln(T_D) + 0.5199 \quad (18)$$

Where A_P is the normalized value of annual production and T_D is the return period in years.

3.1. Example of application of the obtained equations

For the explanation of the application of the equations obtained in this work, the state of Veracruz will be taken as an example. According to Table 2, Veracruz has a Cv of 0.08. Then, according to the group formation defined in Table 3, Veracruz is part of group 1, since its Cv falls within the interval of 0.07-0.1.

If Veracruz presents a drought in a 19-year return period, applying equation 13, the normalized production is expected to be 1.13 (Table 6). If historically the average production has been 26,609,785 tons, then the agricultural production will be the result of equation 13 multiplied by the historical average production. That is (26,609,785 tons)*(1.13)= 30,069,057 tons (Table 7).

Table 6: Result of eq. 13. Agricultural production in Veracruz

T_D (In years)	A_P (Registered)	A_P (Calculated)
19	1.13	1.13

Table 7: Agricultural production expected in Veracruz for a 19-year T_D drought

T_D (In years)	A_P (Registered)	A_P (Calculated)
19	1.13	1.13

4. Conclusions

Droughts are meteorological events that cannot be avoided and cannot be determined with total certainty, which makes the consequences of these events inevitable, but it is possible to control the severity of the repercussions if their effects can be foreseen. The usefulness of the equations obtained in this research is in providing an estimate of the expected value of agricultural production in the face of drought events. With this information, it is possible to take actions in the face of the economic effects that droughts can cause in the agricultural sector.
The methodology used in this study made it possible to determine a similar behavior in agricultural production in the states, and with this it was possible to develop equations for different groups of states that had similarities in their agricultural production. This same methodology can be used to determine the behavior of other meteorological events. The standardization of the information recorded for agricultural production can be substituted by records of other meteorological phenomena.

Acknowledgments

This study has benefited from the public data obtained from the CONAGUA and SIAP. The authors would like to thank the Instituto de Ingeniería for their assistance and support.

References

[1] Esparza, Miguel. "Drought and water scarcity in Mexico. Current situation and future prospects." / "La sequía y la escasez de agua en México. Situación actual y perspectivas futuras." *Secuencia*, no. 89 (2014): 195-219. http://dx.doi.org/10.18234/secuencia.v0i89.1231.
[2] CENAPRED. *Droughts Fascicles* / *Fascículos Sequías*. D.F., Ministry of the Interior / Secretaría de Gobernación (SEGOB), 2007.
[3] Vatter, Juliane. *Drought Risk. The Global Thirst for Water in the Era of Climate Crisis*. Berlin, WWF Germany, 2019.
[4] Eriyagama, Nishadi, Vladimir Smakhtin, and Nilantha Gamage. *Mapping drought patterns and impacts: a global perspective*. Colombo, International Water Management Institute, 2009.
[5] UNDRR. "Number of Climate-related Disasters Around the World (1980-2011)." *The United Nations Office for Disaster Risk Reduction*, June 13, 2012. Accessed March 22, 2023. https://www.preventionweb.net/files/20120613_ClimateDisaster1980-2011.pdf.
[6] Real-Rangel, Roberto A. "Monitoring of droughts in Mexico through multivariate indices." / "Monitoreo de sequías en México a través de índices multivariados." MSCE thesis, National Autonomous University of Mexico / Universidad Nacional Autónoma de México, CDMX, 2016.
[7] Meza, Isabel, Stefan Siebert, Petra Döll, Jürgen Kusche, Claudia Herbert, Ehsan Eyshi Rezaei, Hamideh Nouri, Helena Gerdener, Eklavyya Popat, Janna Frischen, Gustavo Naumann, Jürgen V. Vogt, Yvonne Walz, Zita Sebesvari, and Michael Hagenlocher. "Global-scale drought risk assessment for agricultural systems." *Natural Hazards and Earth System Sciences*, no. 20 (2020): 695-712. https://doi.org/10.5194/nhess-20-695-2020.
[8] UNCCD. *Drought in numbers*. New York, UNCCD, 2022.
[9] European Commission, Joint Research Centre. C. Cammalleri, G. Naumann, L. Mentaschi, G. Formetta, G. Forzieri, S. Gosling, B. Bisselink, A. De Roo, and L. Feyen. "Global warming and drought impacts in the EU." *JRC PRESETA IV project: Task 7*, (2020) https://data.europa.eu/doi/10.2760/597045.
[10] CENAPRED. *Diagnosis of hazards and identification of disaster risks in Mexico* / *Diagnóstico de peligros y identificación de riesgos de desastres en México*. D.F., Ministry of the Interior / Secretaría de Gobernación (SEGOB), 2001.
[11] Florescano Mayet, Enrique, Jaime Sancho y Cervera, and David Pérez Gavilán Arias. "Droughts in Mexico: history, characteristics and effects." / "Las sequías en México: historia, características y efectos." *Comercio Exterior* 30, no. 7 (1980): 747-757.
[12] Bank of Mexico / Banco de México. "Drought in Mexico and its potential impact on economic activity"/ "Sequía en México y su potencial impacto en la actividad económica" *Bank of Mexico Quarterly Report* / *Banxico Informe Trimestral*, (2022): 30-35.
[13] Drust-Nacarino, Ariadne Sofía, Maritza Liliana Arganis-Juaréz, Rodolfo Silva-Casarín, Edgar Gerardo Mendoza-Baldwin, and Óscar Arturo Fuentes-Mariles. "Drought and Genetic Programming to Approach Annual Agriculture Production Normalized Curves". *Revista Facultad de Ingeniería Universidad de Antioquia*, no. 77 (December 16, 2015): 63–74. https://doi.org/10.17533/udea.redin.n77a09.

[14] Goldberg, David E. *Genetic Algorithms in Search, Optimization and Machine Learning.* Massachusetts, Addison-Wesley Publishing Company, 1989.
[15] Chipperfield, Andrew, Peter Fleming, Hartmut Pohlheim, and Carlos Fonseca. *Genetic Algorithm Toolbox User´s Guide.* Sheffield, University of Sheffield, Department of Automatic Control and Systems Engineering, 1994.
[16] SIAP. “Statistical Yearbook of Agricultural Production” / "Anuario Estadístico de la Producción Agrícola." *Closure of agricultural production* / *Cierre de la producción agrícola*, June 13, 2022. Accessed August 2, 2022. https://nube.siap.gob.mx/cierreagricola/
[17] CONAGUA. "Mexico Drought Monitor”/ “Monitor de sequía de México." *Monitor de sequía de México (MSM)*, 2014. Accessed August 2, 2022. https://smn.conagua.gob.mx/es/climatologia/monitor-de-sequia/monitor-de-sequia-en-mexico.

New Trends and Developments of Additive Manufacturing in the Field of Hydraulic Drive Systems according to the Circular Economy Concept

PhD. Stud. Eng. **Alexandru-Polifron CHIRIȚĂ**[1], PhD. Eng. **Adriana Mariana BORȘ**[1], MSc. Eng. **Andrei-Alexandru BENESCU**[1,*]

[1] National Institute of Research & Development for Optoelectronics / INOE 2000 – Subsidiary Hydraulics and Pneumatics Research Institute / IHP, Bucharest, Romania

* benescu.ihp@fluidas.ro

Abstract: *Increasing the efficiency of hydraulic drive systems (HDSs) maintenance activities is a permanent concern at the global level as a result of the considerable expansion of their field of applicability. The maintenance of HDSs is part of the integrated management concept and it is a complex approach to specific activities in order to maintain HDSs performance. The development of additive manufacturing methods applicable for hydraulic components based on the principle of reverse engineering gives stability to functional characteristics and reliability in the context of the circular economy. The application of reliability-based maintenance (RBM) strategies requires the detection and exploitation of the maximum potential of HDSs operation. Through the 3D printing technology, which enables innovative performance and flexibility in on-demand production, there is the opportunity to remanufacture hydraulic components with complex geometry and specific characteristics. At the end of the article, examples of the application of additive manufacturing technologies and the adaptation of the reverse engineering principle in the field of hydraulic drive systems are presented.*

Keywords: *Hydraulic drive systems, circular economy, additive manufacturing, 3D scanning*

1. Introduction

Additive manufacturing is one of the modern technologies that has introduced a new vision of industrial activity and perspective products. The use of additive manufacturing technology is advantageous for situations in which traditional manufacturing methods do not allow obtaining forms with complex geometries in a timely and cost-effective manner, the realization of a prototype or small series production, or in situations where the required raw materials are difficult or almost impossible to process. This method allows obtaining 3D models that can be used to create custom parts individually printed on high-performance rapid prototyping equipment. The obtained 3D model can be used as digital storage for the target part or for training in the virtual environment in various fields of activity. The 3D model resulting from the scan must be processed in such a way as to obtain the part in different layers, with different properties set for each of them in the virtual reality application. The final 3D model can be used to create a virtual reality application that allows the simulation of operations specific to the field for which the part was designed, using mathematical models to create profiles in polynomial form of reconstruction or parameterized modelling. The importance of the field of 3D scanning and printing continues to grow, so the multitude of tools and hardware methods for capturing the shape of real-world parts in three dimensions is constantly expanding. New software products for converting raw 3D data into usable digital format, such as computer-aided design (CAD) models, are being developed and implemented more rapidly by a growing number of developers and manufacturers in the field. Applications for 3D scanning have steadily expanded beyond its use for dimensional metrology in the aerospace, automotive, and power generation industries. Depending on the scanner and the nature of the project, the result of the scan is often a large number of very large files. Transforming these files into efficient formats for use can be one of the most challenging and time-consuming aspects of the project. Many projects require highly specialized software, intensive computing power, and operator skills, which can take years of development and significant cost. Laser, structured light and CT scanning instruments capture an impressive amount of data. These 3D digitizers devices often have a built-in software function used to transform scanned data into geometric features in real time. Special metadata processing software tools have been developed

to bridge the gap between raw scan data and its end use, which have become integral to the use of scanners for both reverse engineering and dimensional inspection applications. The measuring instruments used for these industrial metrology applications are relatively complex and expensive. However, industrial customers have always been and still are the main source of funding for research and development of additive manufacturing (3D printing) technology. New tools such as laser and optical trackers, handheld arm (coordinated measuring machines) CMMs, and structured light scanners have helped engineers solve critical manufacturing problems, leading to increased demand and more research and development by scanner manufacturers. Parts so designed can be directly inspected, sometimes while still on a machine or in a tool fixture, using these advanced 3D measurement and analysis tools. 3D scanning technologies have seen dramatic improvement in speed, accuracy, portability and reliability. The speed and ability to go from CAD to print with close to zero set-up costs has revolutionized the market, through rapid part productions with excellent unit economy and small runs. For printing production parts, speed and price are important, but the features most often exploited are design freedom and ease of customization. In the aerospace and automotive industries, topology-optimized structures with a high strength-to-weight ratio are used for high-performance parts, and components that previously required assembly can be consolidated into a single part. In healthcare, customization is key, speed and versatility make it perfect for developing products made almost exclusively using 3D printing.

2. Development of additive manufacturing technology in the field of HDSs

The concept of additive manufacturing is used in professional and specialized environments; with techniques to create objects by adding layer after layer of material, a wide range can be used, from plastic, organic fabrics, to metals, combinations, etc. 3D printers use molten material in the extruder which then solidifies, or metal powders fused by baking, liquid or UV polymerized resins, or annealing, etc. can be used. In additive manufacturing, laser sintering or laser melting, repairs and coating are possible even for components with the highest material requirements. Laser generative manufacturing processes developed to industrial standards quickly, flexibly and cost-effectively generate complex shapes and individual metal components layer by layer such as: laser fusion of metals (based on laser melting powder) and laser deposition of metals (laser welding charging). Generative manufacturing offers complete solutions that include machines, laser radiation sources and services developed for various products, which provides a clear competitive advantage. With the help of additive manufacturing, specific solutions, customized components can be implemented simply and flexibly, even in the case of series production. The high stability of complex structures, as well as the low weight of additive manufacturing components, make this technology particularly attractive for the field of lightweight materials construction, still challenging for the desired sophisticated components and geometries. 3D printing has been designed to accelerate the development of industrial products with rapid prototyping and UV light curing in various industries such as automotive, aerospace, healthcare and consumer goods. The self-replicating 3D printer launched has caused a surge in interest in this type of technology used for a wide range of more affordable forms of custom manufacturing. Today there are companies that manufacture printers and offer all kinds of services using 3D printing technology for almost any part geometry, this being one of the strengths of 3D printing. One of the limitations of 3D printing is that most parts are inherently anisotropic, or not fully dense, meaning they typically lack the material and mechanical properties of parts made using subtractive or formative techniques. Due to fluctuations in cooling or curing conditions, different prints of the same part are prone to slight variations, which limits consistency and repeatability. Control over every aspect of the process, through this method, makes it possible to produce incredibly precise parts with high repeatability. Most designs require computer-aided manufacturing (CAM) to draw custom toolpaths and efficient material removal, which adds setup time and cost. For most models, especially parts with a complex configuration, this production method, which allows for a complex design without significant material consumption, has proven to be the most cost-effective. As such, the 3D printing method does not have the limitations imposed by subtractive manufacturing where the cutting tool must be able to touch all surfaces to remove material, which greatly limits the complexity of the design. In the Subtractive Manufacturing process, a large amount of material is wasted by removal

to produce the final geometry of the part, aspect which is insignificant in the case of the Additive Manufacturing method. Additive manufacturing enables innovative performance and unmatched flexibility in on-demand manufacturing without dedicated equipment or tools, across all industries, unlocking the design tools of engineering. 3D printing has thus triggered a change in the way products are designed for both small companies and industry giants. This is reflected in the engineering complexity of today's additive manufacturing products, and as this technology expands and matures, so does the industrial environment. 3D printing, in addition to allowing companies to quickly prototype ideas for parts or new products, contributes and to significantly reducing the costs related to the creation of products, minimizing the waste produced and the storage space required for the products obtained. The market penetration and success of this technology depends on technical-economic factors such as ease of use, the technology complexity, low operating costs, the evolution of the supply-demand market. The high efficiency in terms of energy consumption and the use in the prototyping phase of environment-friendly materials place the 3D additive manufacturing technology in the area of technologies that observe the principles of sustainable development, this aspect being a promoter of the implementation of the technology in modern engineering activities [1-3]. Among the 3D additive manufacturing technologies, FMD (Fused Material Deposition) rapid prototyping technology is the most widely used due to its simplicity and affordability. The technique adopted in this method consists in rigorous temperature control for melting the material and depositing it layer by layer, being used in modeling, prototyping, but also in production applications [4]. This accessible technology that uses a wide range of materials is also known in the specialized literature under other names: MEM (Melting Extrusion Modeling), thermoplastic extrusion TPE (Thermoplastic Extrusion), FFF (Fused Filament Fabrication) manufacturing by fused filament [5,6]. Depending on the materials used, the market needs and the complexity of the equipment, a series of 3D additive manufacturing technologies have been developed such as:

- SLA – Stereolithography;
- SLS – Selective Laser Sintering;
- SLM – Selective Laser Melting;
- DLP – Digital Light Processing;
- FDM – Fused Deposition Modeling;
- PJP – PolyJet Printing;
- 3DP – Three-dimensional inkjet printing;
- LOM – Laminated Object Manufacturing.

For the accurate materialization of the 3D model, additive manufacturing technology involves passing a plastic filament through an extruder that heats it up to the melting point, then applying it uniformly (by extrusion) layer upon layer [7]. Controlled displacement of the extruder both horizontally and vertically is achieved by a numerical control mechanism specific to the printer. As it moves, the head deposits a thin thread of extruded plastic that upon cooling hardens immediately, sticking to the previous layer to form the desired 3D pattern. To prevent deformation of parts caused by sudden cooling of the plastic, the professional 3D printer includes a closed construction chamber, heated to a high temperature. The design stage in 3D additive manufacturing technology it's a purely engineering stage, defining for the final product obtained [8]. With the help of a dedicated software application, the 3D model is designed and structured in layered cross-sections.

For simplicity, a 3D scan of complex surfaces with a suitable device can be used in obtaining a 3D model. This process transforms the object to be printed into a digital model, which is subjected to changes in size or configuration with the help of a specialized 3D design program, then it is analysed and prepared for the actual printing. To carry out a 3D scan, it is necessary to use a special equipment that works on the basis of a principle similar to that used by photo cameras (photogrammetric method). The difference between these devices is the use of a laser beam that is sent to the respective object and then reflected in a sensor, synthesizing this data into a digital model. Thus, with the help of the triangulation method, the equipment calculates the distance from

the scanner to the object from different angles, so that the scanner collects data about all the dimensions of the scanned object and can create the digital model, which can then be modified depending on the case.
For complex geometries or console models, FDM technology requires printing with support material that must later be removed manually. One of the materials used in applications is polyethylene terephthalate glycol modified (PETG). This is a type of hydrophobic filament, easy to use for 3D printing, characterized by a high degree of durability and impact resistance, with excellent thermoforming properties, flexibility and high chemical resistance, with high clarity and imperceptible odour. Also, this material has a low flammability rating and is approved in food contact applications. All these properties make PETG an excellent material that combines the advantages of PLA (polylactic acid) and ABS (acrylonitrile-butadiene-styrene) and recommends it for making protections, supports or casings for equipment in the medical or pharmaceutical industry, as well as in other applications. PLA is a biopolymer, a biodegradable material, considered to be ecological being made from renewable raw materials, such as corn starch or sugar cane. Apart from 3D printing, it is commonly used for packaging materials, plastic film, plastic cups and plastic water bottles. PLA is more fragile than ABS but has a higher surface hardness, being able to be cut, filled, sanded, painted, joined with the help of adhesives. ABS is a hard oil-based plastic material that can be used to create sturdy objects, electrical equipment, Lego pieces, etc. ABS filaments at the manufacturer's recommended temperature exhibit a superior bonding of the layers, ABS parts are more flexible, malleable than PLA parts and tend to bend rather than crack when under pressure.
A prototype obtained through 3D additive technology must identify with the CAD piece, (high fidelity prototype), and respect the dimensioning from the design stage [8]. The high degree of finishing of 3D printed products and mock-ups at the prototype level allows designers and engineers to carefully evaluate the proposed concepts, their implications, and make the best decisions in the shortest time, if changes are needed to launching a range of products on the market, based on the prototype used.
Additive manufacturing covers several techniques namely: 3D printing, rapid prototyping, digital manufacturing, layered manufacturing, additive manufacturing. The applications are therefore quite limitless, starting from rapid prototyping of production models, to product development for all types of industrial sectors (medical, aerospace, fashion, etc.). The concept of additive manufacturing is therefore, used in professional and specialized environments, with techniques to create objects by adding layer by layer of material, from plastic, organic fabrics, to metals, combinations, etc. 3D printers use material melted in the extruder which then solidifies, or metal powders fused by baking, liquids or UV polymerized resins, etc. can be used. 3D manufacturing is complex and efforts are made to optimize parameters such as: speed, geometric complexity, materials, mechanical properties, surface finish, tolerances and repeatability. Thus, additive manufacturing is the best choice, especially when speed is essential for small volumes and complex designs.

3. Reverse engineering principle applied to additive manufacturing of HDSs

The concept of reverse engineering involves working principles of a device, system or software program by analyzing its structure, function and operations. This process is applied to increase production under conditions of high product competition, thus avoiding the effort encountered in the original design. Reverse engineering originates from the analysis of various devices and systems especially for commercial or military use in order to make a new similar device or system that does not copy anything from the original. Reverse engineering is also useful for estimating the costs of the elements that make the device work. The concept of reverse engineering was approached before the development of new modern technologies, being used to copy devices or information obtained by capture in espionage operations. Hackers use this technology to remove the copy protection of software programs (cracking). Reverse engineering in programming is a technique used to analyze software to recreate and strengthen the program being applied in multiple fields: industry, electronics, software, chemical engineering, biology, etc. The reverse technique is used whenever one wants to understand the inner workings of software. The goal is to make design decisions for finished products with minimal information or knowledge of the procedures involved in

initial production. Reverse engineering is used to create three-dimensional virtual models of existing parts and subassemblies, thus bringing physical geometry into the digital environment. As reverse (reconstruction) engineering is useful to analyze the functionality of products, to analyze sub-components, it can be used to complete some documents, specifically for parts designed before the development of CAD programs. The compatible reverse engineering program can interpret the measured data and generate the 3D point cloud network [9]. Measured data, usually represented as point clouds, do not contain topological information and so are often processed as triangular network (STL) files, then modeled into a usable format, a set of surfaces - Non-uniform rational B-spline (NURBS) surfaces - or a CAD solid model. Data can be transferred to a computer screen, but the overall process is much more complex. Some companies use the reverse technique when they do not yet have similar products to create their own products. The elements that allowed the development of this process consist of three-dimensional measurement systems for palpating the surface to be scanned, permanently accompanied by an information/data processing software. This information represents digital input data for processing with CAD-type software (for the integral design of products and direct obtaining of the driving programs necessary for the manufacturing system) or CAM (computer-aided manufacturing) as driving/management equipment/ of various machines and tools. To create a fully parameterized model, an advanced CAD package, for example CATIA (Computer Aided Three-Dimensional Interactive Application) or Solidworks, is usually used to achieve the final result. There are also inherent fidelity losses that occur during the technological process of reverse engineering due to the measuring equipment but also the characteristics of the part (dimensions, tolerance, visibility, density, speed, etc.). The program can be easily interfaced with third-party programs such as Polyworks, Geomagic, and Rapidform. Network generation is very fast, the key is an innovative algorithm developed to allow fast and accurate processing with fewer points, which speeds up the network generation process. The elements that allowed the development of this concept are three-dimensional measuring machines for scanning the surface, constantly assisted by a software for processing information and digital data to obtain high-performance results in terms of simulation and modeling of the desired components.

Another reason for applying the concept of reverse engineering is to compress the time required for product development to meet the competitive demands of the market. The process involves measuring an object, then reconstructing it as a 3D model. Approaching the problem from another point of view, one can observe the rapidity of the method of reconstruction of a product that no longer has the original documentation for various reasons, whether it is destroyed, incomplete, whether it is inadequate to the new technological requirements, etc. The use of reverse engineering allows a 3D product or model to be quickly transformed into a digital form, then reshaped and prepared for rapid prototyping or even rapid manufacturing. The combination of scans performed for different profiles, directions, angles and depths, in a unitary whole of great finesse and good resolution is the most recommended application in the field of reverse engineering. Once the object exists in the database, the same features can be easily called upon, even improved by correlating with other newly received/acquired information in a multitude of files that complete the complexity of the process. The 3D data in the form of a cloud of points from the database are then transmitted through information acquisition tools in an organized, orderly system, corresponding to the real geometric position of the scanned surface, compared to a previously established reference point. The data (a multitude of points) are processed mathematically, geometrically, logically, naturally and conventionally to create a virtual image of determined surfaces. The correspondence between real and virtual will be all the greater, the greater their number, an aspect that can also affect the accuracy of the final image of the product. The combination of errors due to device, software or operator in the processing steps can be fixed by a detailed analysis and filling the appropriate sections in a rigorous manner. The analysis results can also be influenced by the variation of the method used for 3D printing, the material used, the temperature of the 3D printing environment, the sensitivity of the electronic and mechanical system. Considering the average accuracy values of the modeling process, one notices that the average accuracy rate decreases gradually as the value of the scale factor decreases. This method is based on solid and surface features [10-14] of given parts, snapping adjacent surfaces, forming radii and chamfers, and performing geometric constraints on the part.

These types of processes are gradually developing, and their variety increases with the development of technology. The choice of the part modeling strategy (mechanical or non-mechanical) is important, because the fewer elements used in the modeling process, the smaller the file size will be, and the smoothness of the part will be ensured. For complex surfaces, the measurements taken are not standardized and combinations of a limited number of hardware and software equipment can be used. Laser scanning and coordinate measurement are dimensional inspection processes widely used in industry for small-sized components or for large-sized components with high precision. The synergy between 3D measurements and scans and the advanced use of CAD/CAM/CAE software packages contribute significantly to engineering achievements in industries and fields such as automotive, aerospace, biomedical, renewable energies, but also to the introduction and foundation of digital reconstruction and reconstruction methodologies. In this context, the method of the principle of reverse engineering consists of complex and interdisciplinary applications developed within programs and projects of excellence for the creation, optimization and capitalization of digital technologies, to facilitate the manufacture of products and the development of intelligent solutions compatible with the requirements of the current economic and social environment. The specialized literature [15-17] provides details on some achievements and practical contributions, new methods and techniques in different fields of activity, contributing to the development of collaboration with innovative companies from industries with high economic potential. These trans-disciplinary developments of the virtual environment bring significant scientific advantages in areas of specialization such as industrial equipment design and simulation, reverse engineering in various interdisciplinary fields such as medicine, archeology, metrology, etc., allowing specific results to be obtained.

One of the problems with successful results was the integration of high-resolution 3D scanned models directly into virtual reality applications. Due to their complexity and the fact that the parts are made of composite material, their manufacturing is computerized, starting with the stage of designing the parts, designing the molds and making them from various materials. Measuring complex surfaces is a difficult task, in some cases sampling of the inspected surface is necessary to obtain global information about its geometry.

Dimensional and symmetry verification methods are applied in the case of parts with complex surfaces to determine geometric and symmetry deviations such as: measurement in points, in plan using 2D scanned profiles, or globally using 3D scanned surfaces. The method of checking geometric deviations and symmetry in additive manufacturing for landmarks with complex surfaces provides a three-dimensional image, developed and analyzed by measurement procedures with translation of the reference system so that the system can be materialized using surfaces and elements from the inspected landmark. After aligning the CAD model and the real one, a segmentation of the landmark to be measured is made into areas of interest. Depending on the size of these areas of interest, a representative number of points to be scanned in that area as well as the scanning strategy are determined. The nominal values extracted from the CAD model are compared to the touched coordinates by calculating the deviation on all 3 axes, and the deviation of the points is presented as a color map. The results obtained by coordinate measurements are more accurate than those obtained by using for point acquisition scanners. The methodology used to determine the initial surface area of a part involves the use of scanning with trajectories parallel to the equator to obtain sets of data in the form of concentric circles used to plot circularity diagrams. This diagram can be drawn automatically using the measuring machine software. Thus, the deviation from the local circularity (positive or negative) can be highlighted and all the points that do not fall within the tolerance limit can be removed with the help of a software such as CAD, MATLAB, etc.

The CAD software used in the methods that apply the principle of reverse engineering generally have functions that allow the automatic generation, directly from the point cloud of geometric elements (cylinder, plane, cone, sphere) without introducing additional sources of error. After scanning, the coordinates of the points are exported for each circle separately and processed to eliminate the points outside the nominal radius. The remaining points are imported generating the worn surface sphere, an area that provides a high density of points and is highlighted by a color map. The method allows the objective establishment of the points that can be used to reconstruct

the initial surface based on roughness diagrams, being a mathematically documented tool implemented in software that can be used to reconstruct certain surfaces or areas of interest.
The amount of work associated with this method is quite high because establishing the diameter and shape of the initial surface is laborious, but it provides a fairly good accuracy compared to other methodologies presented in the specialized literature.

4. Maintenance efficiency concerns for Hydraulic Drive Systems (HDSs)

Systematic analysis of production costs reflects the qualitative level of activity in the context of integrated maintenance management. Maintenance responds to mixed, very complex objectives such as: ensuring the security and reliability of the system, eliminating or reducing the risks in its operation, the stability of the functional characteristics in the life cycle of the system, the continuity of the activities of this system, economic survival and competitiveness, by controlling the expenses related to the system used. The development of maintenance procedures and the application of predictive, preventive and corrective programs of technological systems and equipment is one of the essential activities with an impact on the efficiency of HDSs, being correlated with the adaptation and optimization of the plan for re-engineering the hydraulic system. It is necessary to create a clear plan for prevention and current maintenance in order to satisfy the designed functional parameters, which allow the realization of the technology in safe and precise conditions. Improving the production integrity and the technological systems quality are specific maintenance aspects in the hydraulic drive systems that find their practical solution through the correct diagnosis of the defects that appear, depending on the observed effect. In-depth knowledge of maintenance and repair techniques, in accordance with the application of European Union directives and international standards in the field, leads to the development of industrial activity, the realization of the largest possible productions, of the best quality and with the lowest possible costs. As such, these elements can determine a certain orientation of company management and machinery and equipment experts towards the development of defining measures for HDSs. The development and increasing complexity of industrial systems has led to the modernization and updating of maintenance techniques and policies. Depending on the costs related to spare parts and materials, respectively the losses due to downtime for repairs, different maintenance policies have been developed that consist of interventions on machines that have accidentally stopped working, due to wear and tear or the appearance of malfunctions. Detecting, locating and remediating the malfunction in order to restore the normal operation of the system are actions taken to ensure the optimal operation of the installed systems. The only way in which the owners of the installed technological systems have maximum benefits in their operation is to ensure maintenance with qualified and approved personnel. The use of technology connected to powerful data analysis systems makes it possible to monitor identified problems, and downtime periods / intervals can be planned according to your own schedule. Of course, part of the problem is access to a whole series of sensors, which allow a correct observation of the phenomena, but this method of intelligent maintenance is actually another way of thinking, to anticipate potential failures and trigger actions suitable to prevent or reduce the impact of these defects on the operations performed. This type of advanced technology makes it easier to predict when problems will occur. One possible approach could be to identify equipment with high failure potential as well as costly effect of unwanted interruption: e.g., pumps, compressors, motors. By implementing real-time monitoring systems, interventions on the operating status of these components can be reduced.
The monitoring can also be extended to the other equipment with a low impact of failure, reaching in the end that the whole process enjoys the possibility of anticipating operational problems, this aspect leading to increased safety over the entire technological system. Applying temperature, pressure and vibration sensors to these engines makes it easier to alert the maintenance team in case of failure. Another aspect of maintenance consists in scheduling periodic inspections based on certain sensory information, even if the system is functional. The frequency of these scheduled inspections must be considered. Technologies for testing these systems during operation and modeling algorithms that take into account the following: vibration data, measured temperatures, determination of dissolved compounds in oil, insulation resistances, partial discharges, SF6 pressure, oil level, etc., are very important, which may lead to the reduction of the number of

inspections, or even to their elimination. Thus, depending on the necessary information obtained, the adoption of the new technology can be done. Proactive maintenance emphasizes the idea of routine detection and correction of the primary causes that lead to equipment failures, which are generally the following: abnormal noise generated by cavitation or air ingress into the oil - aerations that can lead to foaming of the hydraulic oil, the high fluid temperature and too slow operation of the system [18]. The set of technical-organizational activities ensures the achievement of maximum performance for the asset considered (equipment, installation, etc.) through the approach way based on the concept of maintenance for restoring a technical system to a specific state of operation that allows it to fulfill its functions in the future. From the point of view of the strategy of the maintenance activity, the aim is to accumulate experience in the field and obtain a high efficiency for establishing the budget, quantifying the need for specific maintenance and repair expenses, necessary for the smooth development of the production process.
The strategy of diversifying the actions carried out involves the provision of specific maintenance activities in order to reduce some funds allocated depending on the impact in order to ensure maximum reliability in the key points of the production system. The principles of limiting the study and the economy of actions are mainly used, with advantages related to the technical and technological level.

5. Reliability of HDSs in the circular economy context

In order to ensure good reliability of complex systems, rigorous verification measures are adopted in the technology development phase and in the execution stage of the essential mechanisms that ensure dimensional accuracy, geometric shape as well as compliance with assembly conditions, appropriate heat treatment and maintenance norms. Another measure to increase the reliability of HDSs consists in the monitoring and preventive replacement of subassemblies with reduced reliability or oversizing some of these elements with low reliability. In such situations, the optimization of repair and maintenance technologies is required. The correct operation of the hydraulic mechanisms is conditioned by the maintenance of the drive circuits and the verification of the execution of the links between the elements according to the drive scheme. The maintenance of HDSs is a combination of all the technical, administrative and managerial actions that are taken during a life cycle of an equipment/ machine/ part/ subassembly with the aim of maintaining or restoring its ability to perform the desired function. In this sense, the maintenance of HDSs includes activities of measurement, performance control, testing, fault detection, repair, adjustment, replacement of elements or subassemblies, and service. Therefore, service or repair activity are parts of a complex maintenance and monitoring action, given that they already exist in industrial practice with wide applications in hydraulic drives. These actions ensure the continuity of activities for as long as possible without interruptions that can cause a significant decrease in productivity, with the natural consequence of reducing the consumption of raw materials and supplies. This process (Fig. 1.) minimizes the waste of raw materials that are limited and, in some cases, are already exhausted or on the verge of extinction.

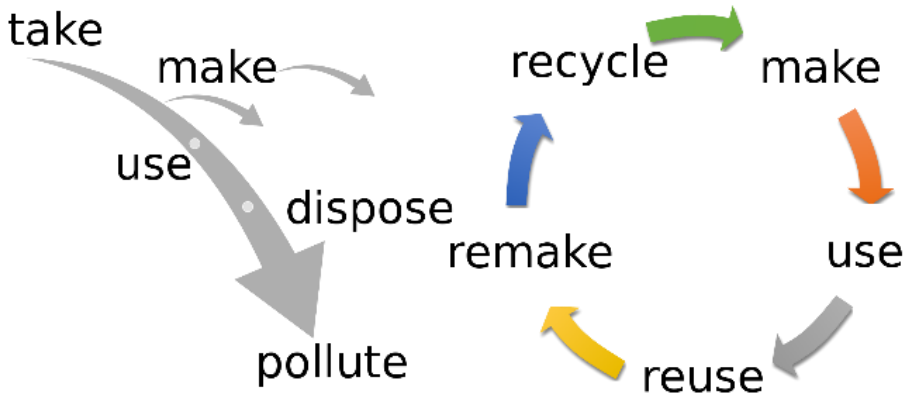

Fig. 1. An illustration showing the difference between the take-make-dispose linear economy approach, and the circular economy approach [19]

In this sense, action plans and measures are adopted at the European level for the transition to the circular economy (Fig. 2.), a transitional method for the correct management of technological waste. In the field of hydraulic drives, maintenance and manufacturing elements are items that can be included in the working methodologies of the Circular Economy concept. These aspects that should become principles of life for humanity aim reusing waste as a raw material, using objects with a long life instead of disposable ones, minimizing packaging, etc. As such, the circular economy represents a model of production and consumption that involves all stages, from design to consumption and then to recycling, ultimately resulting in only a reduced amount of waste comparable to the raw material and initial materials used. This new concept helps the economy as a result of the reduced consumption of new materials and raw materials and creates a new closed loop system that allows the reuse of existing products in a circuit from design to exhaustion. Approaching the circular economy concept aims at the impetuous need to move to a system that favours the recovery of waste materials and products, instead of favouring their destruction. Thus, a close connection between the concept of sustainable development and that of the circular economy is highlighted, supported by arguments regarding existing international trends about some ways of aligning with the requirements of technical and scientific research in the field of HDSs.

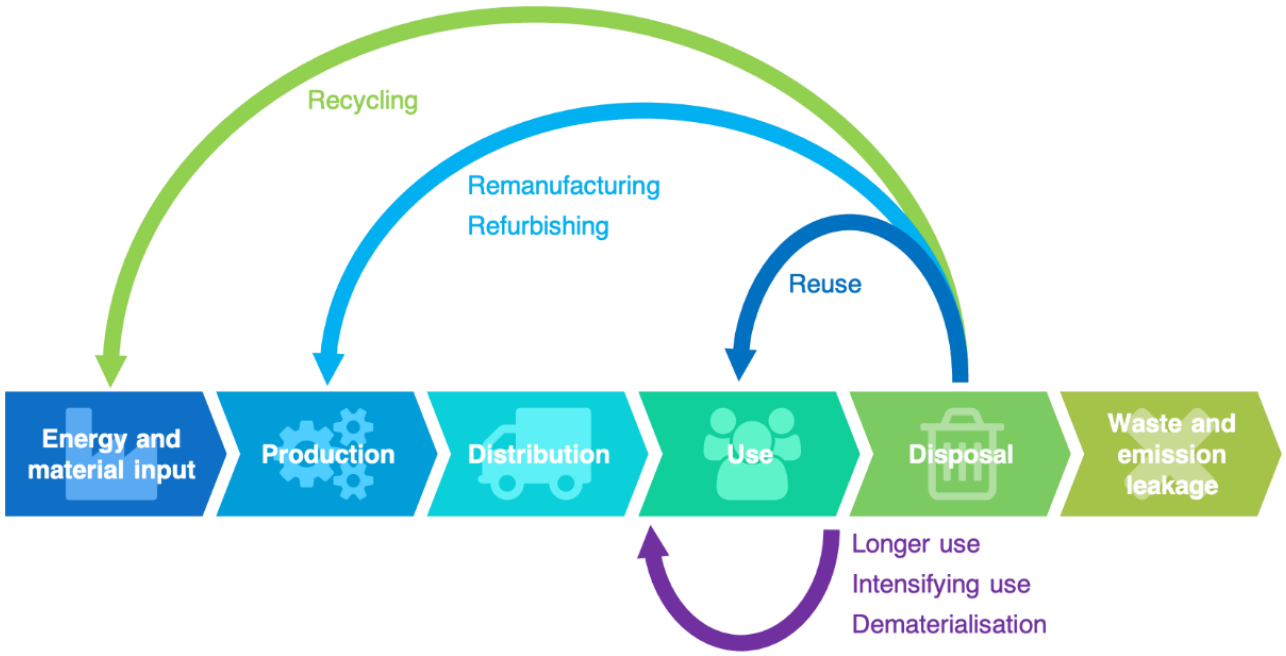

Fig. 2. An illustration of the circular economy concept [20]

6. Conclusions

In this article, the authors have explored the new trends and developments of additive manufacturing in the field of hydraulic drive systems (HDSs) according to the circular economy concept. The maintenance of HDSs is crucial for ensuring their efficient operation, especially considering the expanding range of applications for these systems. By adopting an integrated management concept and employing a complex approach to maintenance activities, the performance of HDSs can be effectively maintained.

The field of hydraulic drive systems (HDSs) has witnessed significant advancements and developments in recent years, driven by the need to enhance maintenance activities and embrace the principles of the circular economy. The integration of additive manufacturing methods and 3D scanning technologies has opened up new possibilities for improving the efficiency, reliability, and sustainability of HDSs.

Additive manufacturing, also known as 3D printing, has emerged as a transformative technology in the field of hydraulic components production. Its ability to enable on-demand production, innovative

performance, and flexibility has paved the way for the remanufacturing of hydraulic components with complex geometries and specific characteristics. This allows for the revitalization of worn-out or obsolete components, reducing waste and supporting the circular economy principles. Throughout the article, the authors have presented various examples of the application of additive manufacturing technologies and the adaptation of the reverse engineering principle in the field of hydraulic drive systems. These examples highlight the practical implementation of 3D scanning and additive manufacturing techniques for remanufacturing hydraulic components, such as pumps, valves, and cylinders, with enhanced performance and extended lifespan. The utilization of additive manufacturing methods in the production of hydraulic components based on the principles of reverse engineering offers stability to functional characteristics and enhances reliability within the context of the circular economy. Additive manufacturing, also known as 3D printing, provides innovative performance and flexibility in on-demand production, enabling the remanufacturing of hydraulic components with complex geometries and specific characteristics. This technology opens up new opportunities for optimizing the maintenance and lifecycle of HDSs.

Reliability-based maintenance (RBM) strategies play a crucial role in maximizing the potential of HDSs operation. By implementing RBM, it becomes possible to detect and exploit the maximum capabilities of hydraulic drive systems, ensuring their continuous and efficient performance. Additive manufacturing serves as a valuable tool in RBM strategies, offering the ability to quickly produce replacement parts or customized components when needed, reducing downtime and costs associated with traditional manufacturing and supply chains.

The integration of additive manufacturing methods into the maintenance practices of hydraulic drive systems brings numerous benefits, including reduced lead times, increased customization possibilities, improved resource efficiency, and minimized waste generation. By embracing these new trends and developments, industries can enhance the sustainability and circularity of their hydraulic drive systems, contributing to a more efficient and environmentally friendly approach to manufacturing and maintenance.

The principle of reverse engineering plays a crucial role in the adaptation of additive manufacturing technologies for HDSs. By utilizing 3D scanning techniques, the existing components can be accurately captured and converted into digital models. These models serve as a basis for the production of new components through additive manufacturing, ensuring stability in functional characteristics and reliability.

Overall, the combination of additive manufacturing, 3D scanning, and the circular economy concept presents a promising future for the field of hydraulic drive systems. By leveraging these technologies and principles, it is possible to achieve sustainable and efficient maintenance practices, leading to enhanced performance and reduced environmental footprint in the hydraulic industry. As the field of additive manufacturing continues to evolve, further research and development are needed to explore the full potential of this technology in the context of hydraulic drive systems. Continued collaboration between academia, industry, and policymakers is crucial to address the challenges and seize the opportunities offered by additive manufacturing, circular economy concepts, and the integration of advanced maintenance strategies.

Acknowledgments

This work was carried out through the Core Program within the National Research Development and Innovation Plan 2022-2027, carried out with the support of the Romanian Ministry of Research, Innovation and Digitalization (MCID), project no. PN 23 05. The research was financially supported by a project funded by MCID through Programme 1 – Development of the national research & development system, Sub-programme 1.2–Institutional performance–Projects financing the R&D&I excellence, Financial Agreement no. 18PFE/30.12.2021.

References

[1] Shahrubudin, N., T. C. Lee, and R. Ramlan. "An Overview on 3D Printing Technology: Technological, Materials, and Applications." *Procedia Manufacturing* 35 (2019): 1286-1296.

[2] Palmara, Gianluca, Francesca Frascella, Ignazio Roppolo, Annalisa Chiappone, and Alessandro Chiadò. ″Functional 3D printing: Approaches and bioapplications.” *Biosensors and Bioelectronics* 175 (March 2021): 112849.
[3] Derossi, A., R. Caporizzi, M.O. Oral, and C. Severini. ″Analyzing the effects of 3D printing process *per se* on the microstructure and mechanical properties of cereal food products.” *Innovative Food Science & Emerging Technologies* 66 (December 2020): 102531.
[4] Nazir, Aamer, Aashir Azhar, Usman Nazir, Yun-Feng Liu, Waqar. S. Qureshi, Jia-En Chen, and Eisa Alanazi. ″The rise of 3D Printing entangled with smart computer aided design during COVID-19 era.” *Journal of Manufacturing Systems* 60 (July 2021): 774-786.
[5] Mohan, Manu K., A.V. Rahul, Geert De Schutter, and Kim Van Tittelboom. ″Extrusion-based concrete 3D printing from a material perspective: A state-of-the-art review.” *Cement and Concrete Composites* 115 (January 2021): 103855.
[6] Prabhakar, M. Manoj, A.K. Saravanan, A. Haiter Lenin, I. Jerin leno, K. Mayandi, and P. Sethu Ramalingam. ″A short review on 3D printing methods, process parameters and materials.” *Materials Today: Proceedings* 45, Part 7 (2021): 6108-6114.
[7] Singh, Gurmeet. ″Replace wooden pattern to polymer pattern by 3D printing.” *Materials Today: Proceedings* 37, Part 2 (2021): 2453-2457.
[8] Macdonald, Eric, Rudy Salas, David Espalin, Mireya Perez, Efrain Aguilera, Dan Muse, and Ryan B. Wicker. ″3D Printing for the Rapid Prototyping of Structural Electronics.” *IEEE Access* 2 (2014): 234-242.
[9] Govindarajalu, B. *IBM PC and CLONES: Hardware, Troubleshooting and Maintenance*. 2nd edition. McGraw Hill Education, 2002.
[10] Kumar, A., P. K. Jain, and P.M. Pathak. ″Reverse engineering in product manufacturing: An Overview.” Chapter 39 in Katalinic, B., and Z. Tekic (Eds.). *DAAAM International Scientific Book*, pp. 665-678. Vienna, DAAAM International, 2013.
[11] Wang, J., D. Gu, Z. Yu, C. Tan, and L. Zhou. ″A framework for 3D model reconstruction in reverse engineering.” *Computers & Industrial Engineering* 63, no. 4 (December 2012): 1189-1200.
[12] Günpınar, E. ″Creation of a three-dimensional geometric model by reverse engineering and some applications in the shipbuilding industry” / ″Tersine mühendislik yoluyla üç boyutlu geometrik modelin oluşturulması ve gemi yapım endüstrisindeki bazı uygulamaları.” *Dokuz Eylul University Faculty of Engineering Journal of Science and Engineering* / *Dokuz Eylül Üniversitesi Mühendislik Fakültesi Fen ve Mühendislik Dergisi* 18, no. 54 (2016): 624-639.
[13] Anwer, N., and L. Mathieu. ″From reverse engineering to shape engineering in mechanical design.” *CIRP Annals* 65, no. 1 (2016): 165-168.
[14] Ke, Y., S. Fan, W. Zhu, A. Li, F. Liu, and X. Shi. ″Feature-based reverse modeling strategies.” *Computer-Aided Design* 38, no. 5 (May 2006): 485-506.
[15] Dudek, P., and A. Rapacz-Kmita. ″Rapid prototyping: Technologies, materials and advances.” *Archives of Metallurgy and Materials* 61, no. 2 (2016): 891-896.
[16] Campbell, I., D. Bourell, and I. Gibson. ″Additive manufacturing: rapid prototyping comes of age.” *Rapid Prototyping Journal* 18, no. 4 (June 2012): 255-258.
[17] Gibson, I., D. W. Rosen, and B. Stucker. *Additive Manufacturing Technologies: 3D Printing, Rapid Prototyping, and Direct Digital Manufacturing*, 2nd edition. New York , Springer, 2016.
[18] Assofluid - Italian Association of Manufacturing and Trading Companies in Fluid Power Equipment and Components. *Hydraulics in Industrial and Mobile Applications*. Brugherio (Milano), Grafiche Parole Nuove s.r.l., 2007.
[19] Wikipedia. "Linia_kontraŭ_Cirkulero.svg", Accessed July 14, 2023. https://www.wikiwand.com/en/File:Linia_kontra%C5%AD_Cirkulero.svg.
[20] Wikipedia. "The_Circular_Economy_concept.png", Accessed July 15, 2023. https://www.wikiwand.com/en/File:The_Circular_Economy_concept.png.

Evaluation of Stress States in Areas with Geometric Structure Discontinuities in the Configuration of Pressure Equipment. I. Direct Discontinuity

Professor Emeritus Ph.D. Eng. **Radu I. IATAN**[1,*],
Assist. Prof. PhD. Eng. **Gheorghe Cosmin CIOCOIU**[1],
Lecturer PhD. Eng. **Anca Mădălina DUMITRESCU**[1]

[1] *POLITEHNICA University of Bucharest, Romania*

* Corresponding author's email address: iatan.radu@gmail.com

Abstract: *The various geometric discontinuities in the structure of the pressure equipment components, existing from the initial phase or during their operation, lead to the appearance of stress states that must be evaluated with great precision. Their values can be compared with the load-bearing capacity of the structures or with that established at the time of evaluation. In this way, the future lifetime of the structure or its decommissioning can be determined.*
This article considers a geometric discontinuity between three cylindrical elements, with different thicknesses, built from the same material, with a sudden transition between them. The intermediate element is considered a short cylinder. The analysis of the continuity of the radial and angular deformations, the deduction of the connection loads and the subsequent evaluation of the developed stresses under the action of the existing external loads are accepted.

Keywords: *Structural geometric discontinuities, deformation continuity, stress states*

1. Introduction

The human requirements for obtaining the most diversified products, using both metallic and non-metallic materials, imposed the design, manufacture and use of specialized equipment, with a well-justified life span. Chemically and/or mechanically aggressive substances can lead to component damage, which is an essential reason for which theoretical, analytical, and numerical, as well as experimental, methods must be developed to estimate the current stress states. Those stated refer to static equipment under pressure: pressure vessels with geometric discontinuities or structural imperfections [1 - 16], technological pipes [17, 18], assemblies with flanges [19], jackets for heating/cooling [20]; dynamic equipment: centrifuges [21, 22]; material breakage criteria [23], holes, notches, for example.

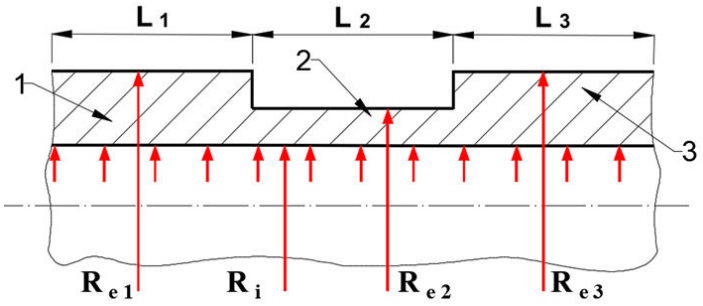

Fig. 1. The geometric structure subject to analysis

This article deals with the analytical evaluation of the stress states developed in a geometric structure composed of neighboring cylindrical areas, with different geometries, with a passage without connection between them - figure 1. As working parameters, the internal pressure and temperature are considered (the analysis of stress states is not excluded in the case of above-ground pipes, buried ones or structures required by dynamic loads).

To determine the connection loads (unitary shear forces Q_{01}, Q_{02} $[N/m]$ and unitary bending moments M_{01}, M_{02} $[N \cdot m/m]$) – figure 2 - the compatibility of the continuity equations of radial displacements and rotations of neighboring elements is used.

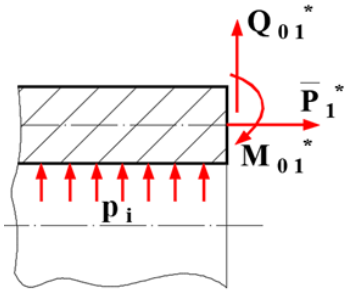

a)

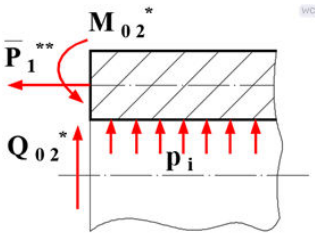

b)

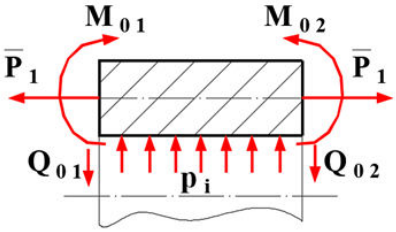

c)

Fig. 2. Discretization and loading of the analyzed geometric structure
a - structural element 1; b) – structural element 3; c) structural element 2 (short cylindrical element)

2. Working assumptions

1. The construction material of the cylindrical sections is considered homogeneous, isotropic and continuous. The load is considered to be in the elastic range. The transition between sections, with different thicknesses, is abrupt (no linear transition or curve).
2. The intermediate section has a constant thickness, less than that of the side sections. Its length falls into the category of short cylinders [24]: $L_2 < L_{sc} \approx 12.5 \cdot \sqrt{R_{m2} \cdot \delta_2}$ (length less than the characteristic half-wavelength [24])

3. Determination of connection loads

As previously mentioned, to determine the connection loads in the present case, the deformation continuity equations are written, resulting in the linear algebraic system:

$$[A] \cdot \{M_{01}, Q_{01}, M_{02}, Q_{02}\}^T = \{b_1, b_2, b_3, b_4\}^T, \quad (1)$$

where $[A]$ represents the non-zero matrix of the influence factors of the connection loads:

$$[A]=\begin{bmatrix} a_{11} & a_{12} & a_{13} & a_{14} \\ a_{21} & a_{22} & a_{23} & a_{24} \\ a_{31} & a_{32} & a_{33} & a_{34} \\ a_{41} & a_{42} & a_{43} & a_{44} \end{bmatrix}, \tag{2}$$

where:

$$a_{11}=\frac{1}{2\cdot k_1^2\cdot \Re_1}\cdot\frac{R_{m2}}{R_{m1}}+\frac{1}{2\cdot k_2^2\cdot \Re_2}\cdot f_{1m};\ a_{12}=-\frac{1}{2\cdot k_1^3\cdot \Re_1}\cdot\frac{R_{m2}}{R_{m1}}+\frac{1}{2\cdot k_2^3\cdot \Re_2}\cdot f_{1q};$$

$$a_{13}=\frac{1}{2\cdot k_2^2\cdot \Re_2}\cdot f_{md}(L_2);\ a_{14}=\frac{1}{2\cdot k_2^3\cdot \Re_2}\cdot f_{qd}(L_2);$$

$$a_{21}=\frac{1}{k_1\cdot \Re_1}\cdot\frac{R_{m2}}{R_{m1}}+\frac{1}{k_2\cdot \Re_2}\cdot f_{2m};\ a_{22}=-\frac{1}{2\cdot k_1^2\cdot \Re_1}\cdot\frac{R_{m2}}{R_{m1}}+\frac{1}{2\cdot k_2^2\cdot \Re_2}\cdot f_{23q};$$

$$a_{23}=-\frac{1}{2\cdot k_2\cdot \Re_2}\cdot f_{mr}(L_2);\ a_{24}=-\frac{1}{2\cdot k_2^2\cdot \Re_2}\cdot f_{qr}(L_2);$$

$$a_{31}=\frac{1}{2\cdot k_2^2\cdot \Re_2}\cdot f_{md}(L_2);\quad a_{32}=\frac{1}{2\cdot k_2^3\cdot \Re_2}\cdot f_{qd}(L_2); \tag{3}$$

$$a_{33}=\frac{1}{2\cdot k_3^2\cdot \Re_3}\cdot\frac{R_{m2}}{R_{m3}}+\frac{1}{2\cdot k_2^2\cdot \Re_2}\cdot f_{1m};\quad a_{34}=-\frac{1}{2\cdot k_3^3\cdot \Re_3}\cdot\frac{R_{m2}}{R_{m3}}+\frac{1}{2\cdot k_2^3\cdot \Re_2}\cdot f_{1q};$$

$$a_{41}=\frac{1}{2\cdot k_2\cdot \Re_2}\cdot f_{mr}(L_2);\ a_{42}=-\frac{1}{2\cdot k_2^2\cdot \Re_2}\cdot f_{qr}(L_2);$$

$$a_{43}=\frac{1}{k_3\cdot \Re_3}\cdot\frac{R_{m2}}{R_{m3}}+\frac{1}{k_2\cdot \Re_2}\cdot f_{2m};\ a_{44}=-\frac{1}{2\cdot k_3^2\cdot \Re_3}\cdot\frac{R_{m2}}{R_{m3}}+\frac{1}{2\cdot k_2^3\cdot \Re_2}\cdot f_{23q};$$

$\{M_{01},Q_{01},M_{02},Q_{02}\}^T$ - the transposed vector of the connection loads – figure 2;

$\{b_1,b_2,b_3,b_4\}^T$ - the transposed vector of the free terms:

$$b_1=\frac{p_i}{16}\cdot\left[\frac{R_{m2}}{k_1^4\cdot \Re_1\cdot R_{m1}}-\frac{1}{k_2^4\cdot \Re_2}-\nu\cdot R_i^2\cdot\left(\frac{1}{k_1^4\cdot \Re_1\cdot R_{m1}^2}-\frac{1}{k_2^4\cdot \Re_2\cdot R_{m2}^2}\right)\right]+$$
$$+E\cdot\alpha_T\cdot\left(\frac{\delta_1\cdot R_{m2}\cdot\Delta T_1}{k_1^4\cdot \Re_1\cdot R_{m1}^2}-\frac{\delta_2\cdot\Delta T_2}{k_2^4\cdot \Re_2\cdot R_{m2}}\right);\ b_2=0; \tag{4}$$

$$b_3=\frac{p_i}{16}\cdot\left[\frac{R_{m2}}{k_3^4\cdot \Re_3\cdot R_{m3}}-\frac{1}{k_2^4\cdot \Re_2}-\nu\cdot R_i^2\cdot\left(\frac{1}{k_3^4\cdot \Re_3\cdot R_{m3}^2}-\frac{1}{k_2^4\cdot \Re_2\cdot R_{m2}^2}\right)\right]+$$
$$+E\cdot\alpha_T\cdot\left(\frac{\delta_3\cdot R_{m2}\cdot\Delta T_3}{k_3^4\cdot \Re_3\cdot R_{m3}^2}-\frac{\delta_2\cdot\Delta T_2}{k_2^4\cdot \Re_2\cdot R_{m2}}\right);\ b_4=0. \tag{5}$$

Note:

1. The radial displacements of elements 1 and 3 have been corrected by bringing them to the values corresponding to the median surface of element 2 - figure 2.

2. In the previous analysis only the effect of an internal pressure was considered. In the situation where the structure is subjected not only to internal pressure but also to external pressure, p_e, as in the case of buried pipes, for example, the significance of p_i will be reconsidered by means of the load $p_i^{\bullet} = p_i - p_e$.

The mentioned connection tasks are established using the equality:

$$\left\{ M_{01}, Q_{01}, M_{02}, Q_{02} \right\}^T = \left[A \right]^{-1} \cdot \left\{ b_1, b_2, b_3, b_4 \right\}^T, \tag{6}$$

where $\left[A \right]^{-1}$ represents the inverse of the nonzero matrix $\left[A \right]$.

Notations used above:

- the influence factors, dimensionless, from the previous expressions, have the configuration:

$$s_h = sh\left(k_2 \cdot L_2\right) = 0{,}5 \cdot \left[exp\left(k_2 \cdot L_2\right) - exp\left(-k_2 \cdot L_2\right) \right];$$

$$c_h = ch\left(k_2 \cdot L_2\right) = 0{,}5 \cdot \left[exp\left(k_2 \cdot L_2\right) + exp\left(-k_2 \cdot L_2\right) \right];$$

$$N = N\left(k_2 \cdot L_2\right) = sh^2\left(k_2 \cdot L_2\right) - sin^2\left(k_2 \cdot L_2\right);$$

$$s = sin\left(k_2 \cdot L_2\right);\ \ c = cos\left(k_2 \cdot L_2\right);$$

$$f_{1m} = f_{1m}\left(k_2 \cdot L_2\right) = \left(s_h^2 + s^2\right) / N;\ \ f_{2m} = f_{2m}\left(k_2 \cdot L_2\right) = -\left(s \cdot c + s_h \cdot c_h\right) / N;$$

$$f_{1q} = f_{1q}\left(k_2 \cdot L_2\right) = \left(s \cdot c - s_h \cdot c_h\right) / N;\ f_{2q} = f_{2q}\left(k_2 \cdot L_2\right) = s_h^2 / N;$$

$$f_{3q} = f_{3q}\left(k_2 \cdot L_2\right) = s^2 / N;\ f_{23q} = f_{23q}\left(k_2 \cdot L_2\right) = f_{2q} + f_{3q};$$

$$f_{md} = f_{md}\left(k_2 \cdot L_2\right) = f_{1m} \cdot c \cdot c_h + f_{2m} \cdot \left(c \cdot s_h + s \cdot c_h\right) + s \cdot s_h;$$

$$f_{mr} = f_{mr}\left(k_2 \cdot L_2\right) = f_{1m} \cdot \left(c \cdot s_h - s \cdot c_h\right) + 2 \cdot f_{2m} \cdot c \cdot c_h + c \cdot s_h + s \cdot c_h;$$

$$f_{qr} = f_{qr}\left(k_2 \cdot L_2\right) = f_{1q} \cdot \left(c \cdot s_h - s \cdot c_h\right) + f_{2q} \cdot \left(c \cdot c_h - s \cdot s_h\right) + f_{3q} \cdot \left(c \cdot c_h + s \cdot s_h\right). \tag{7}$$

$k_j = \sqrt[4]{3 \cdot \left(1 - \nu^2\right)} \Big/ \sqrt{R_{mj} \cdot \delta_j}$ – attenuation factor, $\left[N / m^2 \right]$; $j = 1, 2, 3$;

p_i – internal pressure, $\left[N / m^2 \right]$;

δ_j – wall thickness of cylindrical elements, j , $j = 1, 2, 3$;

α_T – thermal deformation factor, $\left[1 / K \right]$;

E – modulus of longitudinal elasticity of the construction material, $\left[N / m^2 \right]$;

L_j – length of cylindrical elements, j $\left(j = 1, 2, 3 \right)$;

$\overline{P}_1 = 0{,}5 \cdot p_i \cdot R_i^2 / R_{m2}$; $\overline{P}_1^{\bullet} = \overline{P}_1 \cdot R_{m2} / R_{m1}$; $\overline{P}_1^{\bullet\bullet} = \overline{P}_1 \cdot R_{m2} / R_{m3}$ – unit axial forces $\left[N / m \right]$;

R_i – inner radius of the analyzed cylindrical elements, $\left[m \right]$; $R_{mj} = R_i + \delta_j / 2$ – average radius j $\left(j = 1, 2, 3 \right)$;

$\Re_j = E \cdot \delta_j^3 \Big/ \left[12 \cdot \left(1 - \nu^2\right) \right]$ – the cylindrical bending rigidity of the constructive elements, $j = 1, 2, 3$;

ΔT_j – thermal gradient characteristic of the cylindrical element $\left[K \right]$ j $\left(j = 1, 2, 3 \right)$; for constant internal temperature and different external temperatures, the thermal gradient is different for each section; in the case of constant internal temperature inside and outside, $\Delta T_1 = \Delta T_2 = \Delta T_3 = \Delta T$.

4. Stress states

4. 1. Cylindrical elements 1 and 3

The axial $\sigma_{1t}(x)$ and annular stresses $\sigma_{2t}(x)$ developed in the cylindrical elements 1 and 3, under the action of external loads - internal pressure and temperature - have the expressions:

$$\sigma_{1t}(x)=\frac{p_i\cdot R_{mt}}{2\cdot\delta_t}\pm\frac{6\cdot M_{ct}(x)}{\delta_t^2}+E\cdot\alpha_T\cdot\Delta T_t; \tag{8}$$

$$\sigma_{2t}(x)=\frac{p_i\cdot R_{mt}}{\delta_t}\pm\frac{6\cdot\nu\cdot M_{ct}(x)}{\delta_t^2}+\frac{T_t(x)}{\delta_t}+E\cdot\alpha_T\cdot\Delta T_t, \tag{9}$$

where t represents the number of the constructive element ($t=1,3-$ figure 2), respectively $M_t(x)$ - unitary radial bending moment, developed by the unitary force Q_{0t} and the unitary radial bending moment M_{0t} - figure 2:

$$M_t(x)=\left[\frac{1}{k_t}\cdot Q_{0t}\cdot s_{tex}-M_{0t}\cdot\left(c_{tex}+s_{tex}\right)\right]\cdot\frac{R_{m2}}{R_{mt}}, \tag{10}$$

$T_t(x)$ - unitary annular force:

$$T_t(x)=2\cdot\left[Q_{0t}\cdot c_{tex}-k_t\cdot M_{0t}\cdot\left(c_{tex}-s_{tex}\right)\right]\cdot k_t\cdot R_{m2}, \tag{11}$$

respectively:

$$s_{tex}=exp\left(-k_t\cdot x\right)\cdot sin\left(k_t\cdot x\right);\ c_{tex}=exp\left(-k_t\cdot x\right)\cdot cos\left(k_t\cdot x\right). \tag{12}$$

Note:

The current quota, for the cylindrical elements 1 and 3, has every time zero value in the separation plan from cylinder 2. It is measured, further, along the characteristic generator of each long cylinder 1 and 3.

4. 2. Cylindrical element 2

The expressions for the radial tension $\sigma_{12}(x)$ and for the annular tension $\sigma_{22}(x)$, corresponding to cylinder 2 (fig. 2), have the forms:

$$\sigma_{12}(x)=\frac{p_i\cdot R_{m2}}{2\cdot\delta_2}\pm\frac{6\cdot M_{2x}\left(x,\,M_{01},M_{02}\right)}{\delta_2^2}\mp\frac{6\cdot M_{2x}\left(x,\,Q_{01},Q_{02}\right)}{\delta_2^2}+E\cdot\alpha_T\cdot\Delta T_2; \tag{13}$$

$$\sigma_{22}(x)=\frac{p_i\cdot R_{m2}}{\delta_2}\pm\frac{6\cdot K_{2x}\left(x,\,M_{01},M_{02}\right)}{\delta_2^2}\mp\frac{6\cdot K_{2x}\left(x,\,Q_{01},Q_{02}\right)}{\delta_2^2}+$$

$$+\frac{T_{2x}\left(x,M_{01},M_{02}\right)}{\delta_2}+\frac{T_{2x}\left(x,Q_{01},Q_{02}\right)}{\delta_2}+E\cdot\alpha_T\cdot\Delta T_2, \tag{14}$$

where the following notations were used:

$$M_{2x}\left(x,M_{01},M_{02}\right)=M_{01}\cdot\left[\begin{array}{c}-f_{1m}\cdot s_{k_2x}\cdot s_{hk_2x}+\\+f_{2m}\cdot\left(c_{k_2x}\cdot s_{hk_2x}-s_{k_2x}\cdot c_{hk_2x}\right)+\\+\ c_{k_2x}\cdot c_{hk_2x}\end{array}\right]+$$

$$+M_{02}\cdot\left\{-f_{1m}\cdot s_{k_2L_2x}\cdot s_{hk_2L_2x}+f_{2m}\cdot\left[\begin{matrix}c_{k_2L_2x}\cdot s_{hk_2L_2x}-\\-s_{k_2L_2x}\cdot c_{hk_2L_2x}\end{matrix}\right]+c_{k_2L_2x}\cdot c_{hk_2L_2x}\right\}\ ; \tag{15}$$

$$M_{2x}\left(x,Q_{01},Q_{02}\right)=\frac{1}{k_2}\cdot Q_{01}\cdot\left(-f_{1q}\cdot s_{k_2x}\cdot s_{hk_2x}-f_{2q}\cdot s_{k_2x}\cdot c_{hk_2x}+f_{3q}\cdot c_{k_2x}\cdot s_{hk_2x}\right)+$$

$$+\frac{1}{2}\cdot Q_{02}\cdot\left[-f_{1q}\cdot s_{k_2L_2x}\cdot s_{hk_2L_2x}-f_{2q}\cdot s_{k_2L_2x}\cdot c_{hk_2L_2x}+f_{3q}\cdot c_{k_2L_2x}\cdot s_{hk_2L_2x}\right]; \tag{16}$$

$$K_{2x}\left(x,M_{01},M_{02}\right)=\nu\cdot M_{2x}\left(x,M_{01},M_{02}\right); \tag{17}$$

$$K_{2x}\left(x,Q_{01},Q_{02}\right)=\nu\cdot M_{2x}\left(x,Q_{01},Q_{02}\right); \tag{18}$$

$$+s_{k_2x}\cdot s_{hk_2x}\Big]+M_{02}\cdot\left[f_{1m}\cdot c_{k_2L_2\cdot x}\cdot c_{hk_2L_2x}+f_{2m}\cdot\left(\begin{matrix}c_{k_2L_2\cdot x}\cdot s_{hk_2L_2x}+\\+s_{k_2L_2\cdot x}\cdot c_{hk_2L_2x}\end{matrix}\right)+s_{k_2L_2\cdot x}\cdot c_{hk_2L_2x}\right]\Bigg\}; \tag{19}$$

$$T_{2x}\left(x,Q_{01},Q_{02}\right)=-2\cdot k_2\cdot R_{m2}\cdot\Big[\,Q_{01}\cdot\left(\begin{matrix}f_{1q}\cdot c_{k_2x}\cdot c_{hk_2x}+f_{2q}\cdot c_{k_2x}\cdot s_{hk_2x}+\\+f_{3q}\cdot s_{k_2x}\cdot c_{hk_2x}\end{matrix}\right)+$$

$$+Q_{02}\cdot\left(f_{1q}\cdot c_{k_2L_2x}\cdot c_{hk_2L_2x}+f_{2q}\cdot c_{k_2L_2x}\cdot s_{hk_2L_2x}+f_{3q}\cdot s_{k_2L_2x}\cdot c_{hk_2L_2x}\right)\Big]; \tag{20}$$

$$s_{k_2x}=sin\left(k_2\cdot x\right);\ c_{k_2x}=cos\left(k_2\cdot x\right);\ s_{hk_2x}=sh\left(k_2\cdot x\right);\ c_{hk_2x}=ch\left(k_2\cdot x\right); \tag{21}$$

$$s_{k_2L_2x}=sin\left[k_2\cdot\left(L_2-x\right)\right];\ \ s_{hk_2L_2x}=sh\left[k_2\cdot\left(L_2-x\right)\right]; \tag{22}$$

$$c_{k_2L_2x}=cos\left[k_2\cdot\left(L_2-x\right)\right];\ \ c_{hk_2L_2x}=ch\left[k_2\cdot\left(L_2-x\right)\right]. \tag{23}$$

Note: In equations (13) and (14) the plus sign for the radial unit bending moments $M_{2x}\left(x,M_{01},M_{02}\right)$ and $K_{2x}\left(x,M_{01},M_{02}\right)$ is characteristic of the inner surface of the cylindrical element 2. In the case of the radial unit bending moments $M_{2x}\left(x,Q_{01},Q_{02}\right)$ and $K_{2x}\left(x,Q_{01},Q_{02}\right)$ the plus sign corresponds to the outer surface of the short cylinder 2 (fig. 2). In the case of the same equalities (13) and (14), the annular unitary forces have a plus sign for $T_{2x}\left(x,M_{01},M_{02}\right)$, respectively a minus sign for $T_{2x}\left(x,Q_{01},Q_{02}\right)$, as shown by the equalities (19) and (20). The x quota has its origin in the separation plane of elements 1 and 2 and its maximum value ($x=L_2$), in the separation plane of components 2 and 3.

5. Conclusions

In this paper, the connection between two long cylindrical elements and a short, intermediate cylindrical element is considered. The continuity equations of the radial and angular deformations are established, so that based on the linear algebraic system, the expressions of the connection loads - unit bending moments and unit shear forces - are deduced. With their help, the expressions of the radial and annular stresses (plane stress state), dependent on a current quota, expressed in the context, are described. For the accepted resistance theory (usually the IV or V theory [25]), the maximum equivalent stresses are established on the internal and external surface of the analyzed constructive element Such a value is compared with the admissible resistance of the construction material, under the specific conditions of application. As a result, the bearing capacity of the construction can be appreciated, for safe operating conditions. In the case of designing structures with discontinuities, the above data allow the modification of the geometry to ensure safe

conditions of use. The previous calculation methodology can also be used if the transitions from one structure to another will be with a connection or with a linear transition.

References

[1] Iatan, I. R., C.D. Tacă, and M. Păunescu. ″Evaluation of the intensity of the state of stress in the joint area by welding two coaxial cylindrical ferrules of different diameters.″ / ″Evaluarea intensităţii stării de solicitare în zona de îmbinare prin sudare a două virole cilindrice coaxiale de diametre diferite.″ *Construcţia de Maşini* 37, no. 4 (1985): 222 – 226.

[2] Iatan, I. R., M. Păunescu, and C.D. Tacă. "On the stress concentration in the joining area of two cylindrical ferrules with shape deviations.″ / ″Asupra concentrării de tensiuni în zona de îmbinare a două virole cilindrice cu abateri de formă.″ *Buletinul Institutului Politehnic Bucureşti, Seria Mecanică* 56 – 57 (1984 – 1985): 170 -178.

[3] Păunescu, M., I. R. Iatan, and C.D. Tacă. ″Aspects regarding the lifetime of a pressure vessel, with deviations from the geometric shape.″ / ″Aspecte privind durata de viaţă a unui recipient sub presiune, cu abateri de la forma geometrică.″ *Buletinul Institutului Politehnic Bucureşti, Seria Mecanică* 49 (1987): 87 – 91.

[4] Iatan, I. R., and L. Nicolau. ″Evaluation of the influence of the connection between the frustoconical and cylindrical ferrules on the stress state.″ / ″Evaluarea influenţei racordării între virolele tronconice şi cilindrice asupra stării de tensiuni.″ *Buletinul Institutului Politehnic Bucureşti* 50 (1988): 57 – 64.

[5] Iatan, I. R., V. Marchidan, and I. Vasilescu. ″Calculation of the state of tension in the area of the circular weld with deviations from the straightness of the interior of the ammonia synthesis column.″ / ″Calculul stării de tensiune în zona sudurii circulare cu abateri de la rectilinitate a interiorului coloanei de sinteză a amoniacului.″ *Buletin de Informare Tehnică* (*B.I.T.) – I.S.C.I.R.*, no. 4 (1991): 8 – 34.

[6] Iatan, I. R. ″General calculation method of a joint of flat plate type - cylindrical shell (II).″ / ″Metodă generală de calcul al unei îmbinări de tip placă plană – înveliş cilindric (II).″ *Buletinul Universităţii Petrol - Gaze Ploieşti*, *Seria Tehnică* 52, no. 2 (2000): 171 – 173.

[7] Iatan, I. R. ″States of tension in the connection areas of the cylindrical-conical portions of the equipment under pressure.″ / ″Stări de tensiune în zonele de racordare ale porţiunilor cilindro-conice ale echipamentelor sub presiune.″ *Construcţia de Maşini* 52, no. 12 (2000): 9 – 11.

[8] Iatan, I. R. ″Study of the stress states in the areas of joining spherical shells with cylindrical shells - I. The effect of the weld bead in the joint is neglected.″ / ″Studiul stărilor de solicitare în zonele de îmbinare a învelişurilor sferice cu învelişuri cilindrice - I. Se neglijează efectul cordonului de sudură din îmbinare.″ *Revista de Chimie* 56, no. 1 (2005): 19 – 23.

[9] Iatan, I. R. ″Evaluation of stress states in spherical caps with marginal rings (I).″ / ″Evaluarea stărilor de tensiuni în capacele sferice cu inele marginale (I).″ *Buletinul Universităţii Petrol-Gaze din Ploieşti*, *Seria Tehnică* 57, no. 4 (2005): 207 – 212; ″Evaluation of stress states in spherical caps with marginal rings (II).″ / ″Evaluarea stărilor de tensiuni în capacele sferice cu inele marginale (II).″ *Buletinul Universităţii Petrol-Gaze din Ploieşti*, *Seria Tehnică* 57, no. 4 (2005): 213 – 218.

[10] Iatan, I. R., and Al. Marin. ″Evaluation method on the residual lifetime of technological equipment in petrochemical plants. II c. Case Study.″ *The Scientific Bulletin of Valahia University – Materials and Mechanics*, no. 1 (6) (year 6) (2008): 185 – 187.

[11] Iatan, I. R., and Al. Marin. ″Regarding an evaluation method of the residual life duration of technological equipment from petrochemical installations. III. Case study.″ *The Scientific Bulletin of Valahia University – Materials and Mechanics*, no. 4 (7) (year 7) (2009): 205 – 210.

[12] Iatan, I. R., and Al. Marin. ″Regarding an evaluation method of the residual life duration of technological equipment from petrochemical installations. IV. Case study.″ *Modelling And Optimization In The Machines Building Field / Modelare și Optimizare în Construcția de Mașini (MOCM)* 15, no. 3 (2009): 26 – 37.

[13] Zichil, V., R. I. Iatan, Luminiţa Bibire, Paraschiva Busuioceanu (Grigorie), and L. Şerban. ″Thermo-mechanical loading in bevelled area between two cylindrical shells with different thicknesses. Theoretical study – Connection loads.″ *Journal of Engineering Studies and Research* 20, no. 1 (2014): 87 - 100.

[14] Le, Xiaobin, and Zelong Le. ″Stress concentration factors due to typical geometric discontinuities for shaft design by numerical simulation.″ Paper presented at the 120th ASEE Annual Conference and Exhibition, Atlanta, GA, USA, June 23 – 26, 2013.

[15] Dogariu, A. I., and D. Dubina. ″Influence of imperfection and geometrical discontinuities on the behavior of the steel towers.″ Paper presented at the 5th International Conference on Structural Engineering, Mechanics and Computation SEMC 2013, Cape Town, South Africa, September 2 - 4, 2013.

[16] ***. ″Pressure Vessel Discontinuity Stresses.″ *Oil & Gas Industry Technology Updates*. Accessed May 30, 2023. http://www.industrialseparation.com/20180412_pressure-vessel-discontinuity-stresses.html

[17] Iatan, I. R., and Al. Marin. ″Some aspects regarding the evaluation of the residual life cycle of some pipelines in petrochemical equipment. II. Case study.″ *The Scientific Bulletin of Valahia University – Materials and Mechanics*, no. 4 (7) (year 7) (2009): 199 – 204.

[18] Peter, M. Cr. *Research on the influence of structural discontinuities on the lifetime of industrial technological pipelines* / *Cercetarea influenţei discontinuităţilor structurale asupra duratei de viaţă a conductelor tehnologice industriale*. Doctoral thesis. Petroleum-Gas University of Ploiești, 2022.

[19] Iatan, I. R., and C. Filimon. ″Calculation of assemblies with flanges and clamps (I).″ / ″Calculul asamblărilor cu flanşe şi cleme (I).″ *Revista de Chimie* 42, no. 1 – 3 (1991): 117 – 121; ″Calculation of assemblies with flanges and clamps (II).″ ″Calculul asamblărilor cu flanşe şi cleme (II).″ *Revista de Chimie* 42, no. 8 – 9 (1991): 443 – 448.

[20] Iatan, I. R., and Marlena Iuliana Prodea. ″States of stress in the evacuation areas of working media from containers with heating/cooling jackets (I).″/ ″Stări de solicitare în zonele de evacuare a mediilor de lucru din recipientele cu mantale de încălzire/răcire (I).″ *Tehnologia Inovativă, Revista Construcţia de maşini* 59, no. 1 (2007): 85 – 92.

[21] Iatan, I. R., E. Stoican, N. Botea, and C. Hristescu. "Calculation and construction of centrifuge drums. I. Non-stiffened cylindrical drums, with flat bottoms and covers, for sedimentation.″ / ″Calculul şi construcţia tamburelor centrifugelor. I. Tambure cilindrice nerigidizate, cu funduri şi capace plane, pentru sedimentare.″ *Revista de Chimie* 36, no. 12 (1985): 1138 – 1145.

[22] Iatan, I. R., M. Jugănaru, and M. Ştefănescu. ″Calculation and construction of centrifuge drums. II. States of deformations and stresses in flat circular bottoms.″/ ″Calculul şi construcţia tamburelor centrifugelor. II. Stări de deformaţii şi de tensiuni în fundurile circulare plane.″ *Revista de Chimie* 41, no. 1 (1990): 67 – 74.

[23] Iatan, I. R., P. Florescu, and Carmen T. Popa. ″Regarding some interactive criteria used in isotropic and quasi-isotropic materials fracture mechanics.″ *Buletinul Universităţii Petrol – Gaze din Ploieşti, Seria Tehnică* 68, no. 3 (2016): 1 – 10.

[24] Jinescu, V. V. *Calculation and construction of chemical, petrochemical and refining equipment* / *Calculul şi construcţia utilajului chimic, petrochimic şi de rafinării.* Vol. 1. Bucharest, Didactic and Pedagogical Publishing House, 1983.

[25] Buzdugan, Gh. *Material Resistance* / *Rezistenţa materialelor*. Bucharest, Publishing House of the Romanian Academy, 1986.

Surgical Robots: Current Performances and Perspectives of Development and Use

Eng. **Ana Maria BARBU**[1,*], Assoc. Prof. PhD. Eng. **Iulian Alexandru TABĂRĂ**[1], Lecturer PhD. Eng. **Iulian Sorin MUNTEANU**[1,*]

[1] POLITEHNICA University of Bucharest, Romania

* ana.maria_barbu@yahoo.com, iulian.munteanu0306@upb.ro

Abstract: *The surgical field represents a delicate and complex side of medicine and the introduction of robots has considerably improved the lives of patients and doctors. Robotic surgery has advanced astonishingly in recent decades and specialists are trying to exceed the expectations that people may have from the robots used in medicine at the present time. The technology used in these robots continues to amaze not only by the complex way in which they work, but also by the fact that soon the operations will be able to be fully automated or carried out even remotely. This paper broadly presents an evolution of robotic surgery from the first application of robots in the surgical field to the present.*

Keywords: *Robot, surgeon, robotic surgery, da Vinci Xi, Mako*

1. Introduction

Once the robots have been implemented in the surgical field, the quality of the medical act has increased considerably and this is largely due to the way of how the robots are working because they have a much higher accuracy compared to the surgeon's hand.
The robots improve the dexterity and abilities of the doctor and they offer a better visibility during interventions because they use advanced imaging systems.
Even though they have demonstrated impressive performances, a surgical robot is different from an industrial one because it does not have the same autonomy and requires assistance from doctors during surgery.
The present work aims to highlight the complexity and performances of these medical robots, while demonstrating how much robotic surgery has advanced in recent years and where it is headed. The research methodology and development of this scientific paper is based on recent experiments and specialist's demonstrations, brochures and professional journals, case studies and computer-aided design.

2. Present state

2.1 General considerations

The first application of a robot in medicine was made in the field of neurosurgery when an industrial robot, PUMA 200, was successfully used for a brain biopsy procedure in 1985.

Fig. 1. PUMA 200, the first robot used to assist human neurosurgery [2]

PUMA 200 (Programmable Universal Machine for Assembly) was, in fact, an industrial robotic arm originally created for the General Motors company. Under CT guidance, PUMA performed a brain biopsy on a 52-year-old man with a deep brain injury. This robot was able to precisely position the biopsy needle and it is considered the prototype of the robotic systems which are now used in neurosurgery [1].
Medical interventions assisted by robots represent a completely different experience from classic surgery therefore, doctors do not get to operate with them immediately and they have to go through certain stages before. The first step would be to practice in virtual programmes. In this regard, simulators for robotic surgery exist. They even have a haptic feature that helps surgeons feel the resistance of the tissues they need to sew or dissect, thus surgeons experience an environment as close as possible to reality. The next step is to operate on animals and then pass an exam that brings them accreditation in robotic surgery [1].

2.2. Surgical robots used in Romania and worldwide

There are surgical robots in 15 public and private hospitals, and only 8 robots are functional, the others not being used, mainly because of financial reasons. *Regina Maria* is the health network in Romania that has 4 surgical robots and two of them are da Vinci Xi robots - the best performing surgical system currently available [3].
The da Vinci Xi robot is an ultra-performance system, controlled by the doctor from a computerized console, through which the surgeon simultaneously manipulates the 4 robotic arms. An arm is designed to accurately handle the 3D and HD endoscope, and the other 3 arms handle the surgical instruments. The robotic arms are articulated, they have 7 degrees of freedom and perform a natural movement, but much more extensive and accurate compared to the one made by the human hand. The movements of the surgeon's hands are filtered and transformed by the system to become much more precise, without tremors. The 3D image transmitted by the robot can be magnified up to 10 times, observing even the smallest details [4].
An overview of the da Vinci Xi performing system is represented in Fig. 2, and the Fig. 3 and 4 closely show the arms of the robot and the console where the surgeon sits and through which he handles the robot. The console has two joysticks which the doctor uses for transmitting movements at the robot.

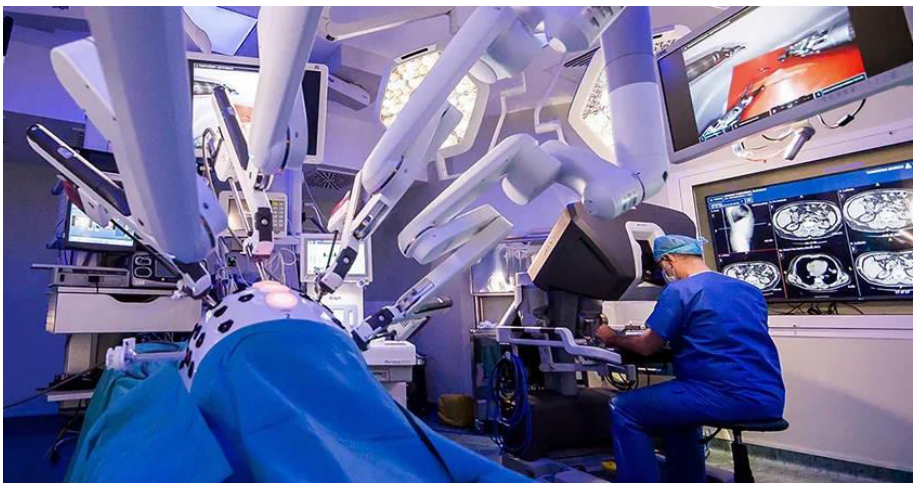

Fig. 2. The da Vinci Xi robot [4]

With the help of the da Vinci Xi robot, the surgeon manages to enter narrow anatomical spaces, thus operating millimetrically, with great accuracy. In the operating field, da Vinci Xi far exceeds the doctor also because of its superior vision, he rendering high-quality images from hard to reach areas [4].

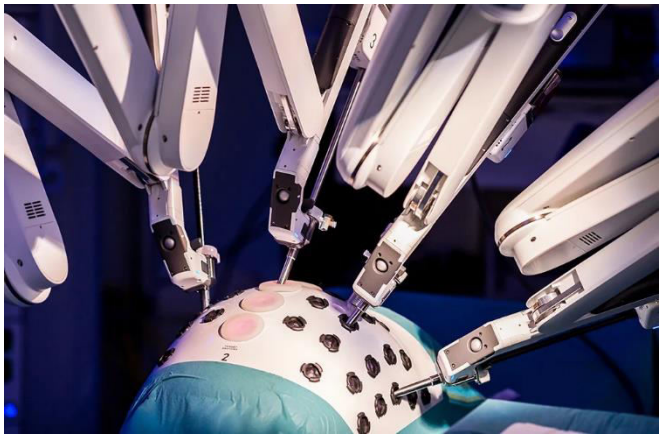

Fig. 3. The arms of the da Vinci Xi robot [3]

Fig. 4. The console through which the surgeon controls the da Vinci Xi robot [3]

The second surgical robot introduced in Romania is Mako, considered the first robot in Eastern Europe used in orthopedic hip and knee replacement surgery. Mako is rather a robotic arm that provides an excellent precision to the surgeon's hand. The robot is intended for total hip arthroplasty and total and partial knee arthroplasty. From all of the prosthesis procedures, the knee one is the most difficult to achieve because it involves an extremely complex articulation which requires high precision. The Mako robot manages to provide this precision, making the difference between the classic operation and the one where robots are integrated [3].

Fig. 5. The Mako robot handled by the surgeon [3]

Fig. 6. The Mako System [5]

Before any intervention, the problem is assessed and a customized 3D model of the prosthesis is designed according to the anatomy of each patient [3].
Also, Mako uses haptic technology ensuring that only the affected bone is sectioned. The robotic arm will emit a warning sound if the surgeon exceeds the limits created in the operative plan [5].
Following the use of the Mako robot in interventions, many things have been observed: reductions in pain and recovery time for the patient, reduced use of pain medication and reduced postoperative complications. Fig. 7 contains a graph which indicates the pain experienced by patients over a period of 90 postoperative days, both for the classic operation, performed only by the surgeon, and for the operation in which the Mako robot was involved. Throughout these 90 postoperative days, patients felt less pain in the case of interventions performed with the Mako robot [5].

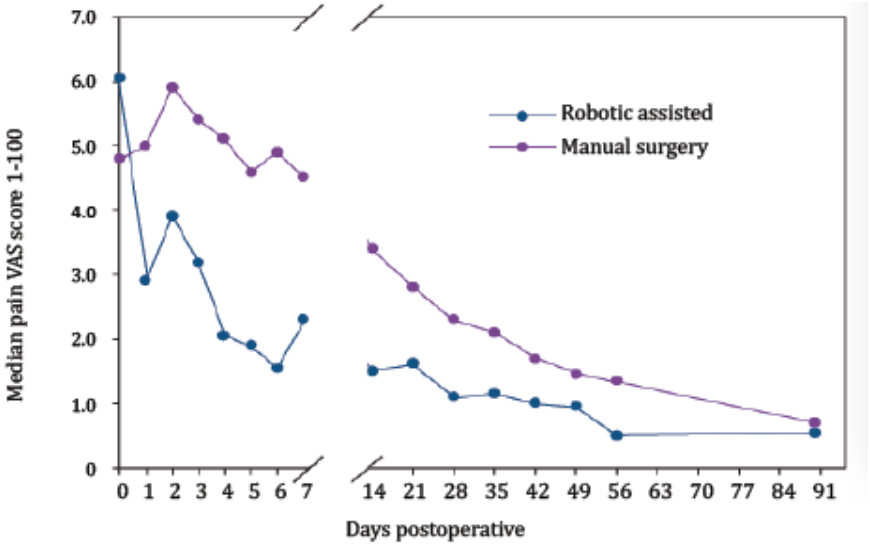

Fig. 7. Visual analog scale for 90 days after surgery [5]

According to the study conducted by Raed A. Azhara, Mohamed A. Elkoushyb and Saad Aldousarica in 2019 (article: Robot-assisted urological surgery in the Middle East: Where are we and how far can we go?), it turns out that the Middle East possesses only 1% of robotic systems da Vinci surgical systems installed worldwide (of which approximately 19 in Saudi Arabia; 6 in Qatar; 2 each in Kuwait and Lebanon; 3 in the United Arab Emirates; and only one in Egypt), while in Europe and the USA the presence of robots surgical da Vinci is much more significant, as follows: France 90 pcs., Italy 84 pcs., Germany 77 pcs., Belgium 34 pcs., Turkey 34 pcs., and 2344 pcs. installed in the USA.

2.3. Robotic automation in surgery

Robotic automation in surgical field has highly developed and it is demonstrated by current researches. A team of experts from Johns Hopkins University designed "STAR" (Smart Tissue Autonomous Robot) which was able to perform laparoscopic surgery on the soft tissue of a pig without being guided by the human hand [6].
Experts have equipped the robot with a three-dimensional endoscope and advanced imaging systems that provide more accurate views of the operating field. Because of its unpredictability, soft tissue surgery is particularly difficult for robots as they are forced to adapt quickly to deal with any unexpected obstacles in case of necessity. STAR has in its composition a new control system which can adjust the surgical plan in real time, like a surgeon would. Therefore, the robot has 3 essential functions: planning, adaptability and execution. Experiments showed that the robot produced significantly better results than doctors performing the same procedure individually. STAR is an improved version of a robot from 2016 which precisely operated on the intestines of a pig. The old version made a larger incision to access the intestine and has required more guidance from the doctors. The actual study represents a significant step in robotics for fully automated surgery on humans [6].
The robot uses artificial intelligence along with haptic and virtual sensors during surgical interventions and has been shown to outperform surgeons in certain tasks based on quantitative analysis [7].

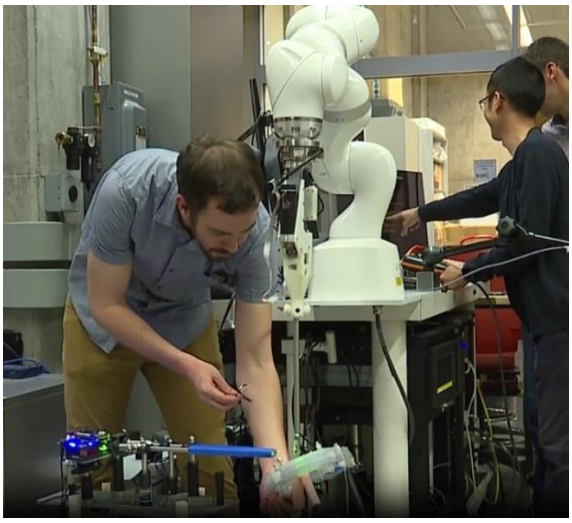

Fig. 8. The autonomous robot STAR [8]

STAR gives the surgeon a supervisor role who monitors the operation process and interferes only if it's necessary. Experts said that the robot can work for a long time ensuring the same accuracy. The team expects that in about 5 years, STAR will be in the operating rooms [8].

2.4. Remote robotic surgery

Robot-assisted surgery has advanced so far that a question of operating remotely with the help of robots arises. The most recent study in this regard was done by the Monogram Orthopedics company which is revolutionizing knee arthroplasty and orthopedic implants. Monogram demonstrated the possibility of remote operation in a recent experiment from March 2023 where it was demonstrated that it is possible to operate from a distance of approximately 1743 miles. From New York, with the help of a pedal, the surgeon guided the robot which was located in Austin, Texas. The main steps of the procedure were: detection of the femur and tibia, points control recording, actual cutting with the robot, and finally checking the articulation [9].

Fig. 9. The monogram robot in the operating room (at Austin) [9]

Fig. 10. The pedal used by the surgeon from New York to control the robot's positions [9]

The robot proves to be effective due to several characteristics such as: 7 degrees of freedom which allow a wide range of movement, closed loop control system and an actively navigated milling which is easily and accurately carried out in the idea of preparing the space for the implant. The tool used is a sagittal saw or a milling cutter. The surgeon uses the high-performance imaging system provided by the robotic system. The CT scan (Fig. 11) represents the patient's plan which is the basis of the operation. With the help of this plan, the doctor can access what he wants for analysis and surgical intervention. First, the doctor analyzes this plan, then the position is checked, the femur is examined first, then the tibia, and the control points for each one are recorded. These steps are followed by the actual cutting procedure exemplified in Fig. 12 [9].

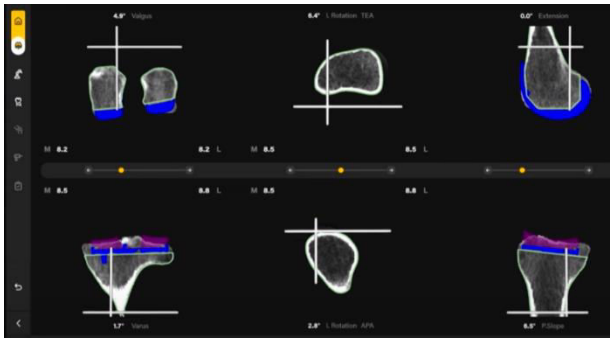

Fig. 11. The patient's CT plan [9]

Fig. 12. Incision [9]

The implants used by Monogram company also involves a different technology. Currently, cemented implants are used in over 90% of joint replacement surgeries. These can break, causing problems over the time. Monogram says it will use porous metal press-fit protheses, which allow the bone to fuse with the metal and hold it in place as naturally as possible [10].

3. Case study – Finite element analysis of a telemanipulator

The case study concerns the finite element analysis of a telemanipulator used in minimally invasive surgery to demonstrate its performance. Fig. 13 shows the 3D model of the telemanipulator made in the SolidWorks program [11].

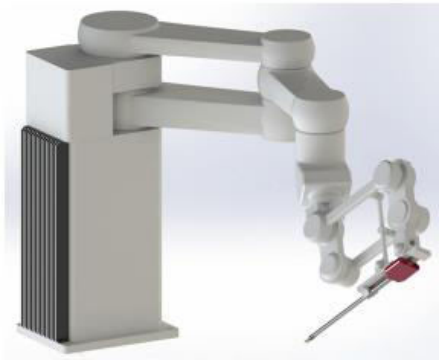

Fig. 13. The 3D model of the telemanipulator [11]

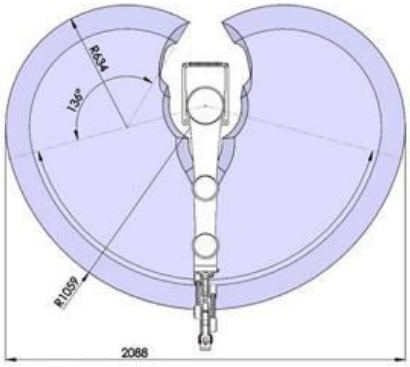

Fig. 14. The telemanipulator's workspace [11]

For the finite element analysis, two cases are represented in Fig. 15. In the first case (a) a force of 50 N was applied, and for the second case (b) one of 5 N. Images show the X-axis displacement results for the positive direction in case (a) and the negative direction in case (b).

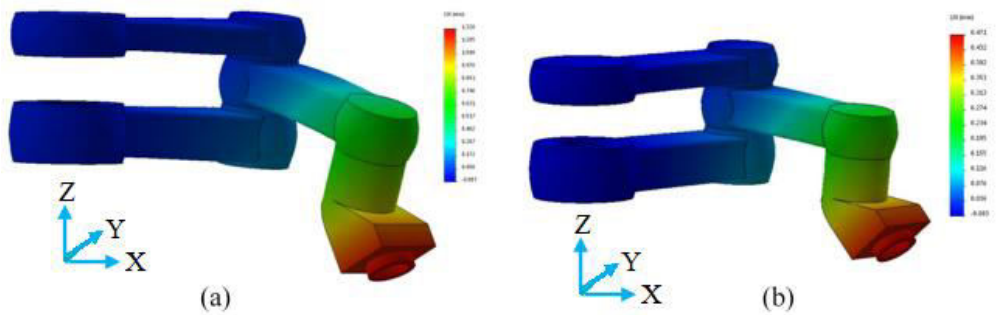

Fig. 15. Finite element analysis (after [11])

The results obtained from the finite element analysis (FEA) show that the resulting maximum displacements do not exceed 1.5 mm in all of the considered cases [11].

Thus, the resulted displacements from this analysis are very small and do not affect the performance of the robotic arm during operation.

4. Conclusions

The introduction of robots in surgical interventions offers numerous advantages such as: greater precision during the medical act, smaller incisions, therefore smaller scars, reducing the risk of infections, quick recovery, reduced length of hospital stay.
Also, with the integrability of robots in interventions, less blood was lost during surgery, so it is a less need for blood transfusions, less pain and less administration of analgesics.
Operating with robots is a completely different experience and doctors go through a training process in order to be able to operate with them. Same as patients, the doctors have seen improvements, reporting less fatigue following robot-assisted interventions and feeling a greater satisfaction for the medical procedure.
Currently, a robot used in the operating room does not have the autonomy of an industrial robot. More specifically, it does not perform an operation after receiving an order, and that is precisely why the surgical robots currently used in operations are assisted and guided by doctors. However, recent studies have shown that robotic automation in surgeries is possible, a concrete case being the STAR robot from Johns Hopkins University.
Although, at the present moment, robots assist doctors during interventions, in the future seems that they will perform the operations by themselves, and the surgeon will only supervise the process. Current studies demonstrate this possibility and reveal how powerful the technology used for medical robots is.

References

[1] Antonescu, Oana. "Robots that are changing the face of medicine. <They are an extension of the surgeon>"/ "Roboții care schimbă fața medicinei. <Sunt o extensie a chirurgului>". *Smart Living*. Accessed April 2, 2023. https://smartliving.ro/roboti-medicali-extensie-a-chirurgului/.
[2] Veneziano, Domenico, A. Tafuri, J. Gomez Rivas, A. Dourado, Z. Okhunov, B. K. Somani, N. Marino, G. Fuchs, G. Cacciamani, and ESUT-YAUWP Group. "Is remote live urologic surgery a reality? Evidences from a systematic review of the literature." *World Journal of Urology* 38, no. 10 (2020): 2367-2376, DOI: 10.1007/s00345-019-02996-0.
[3] Livadaru, Alex. "A true story of humans and robots in the operating room. Or how human intelligence and artificial intelligence help patients to be born again" / "O poveste adevărată cu oameni și roboți în sala de operație. Sau despre cum inteligența umană și inteligența artificială ajută pacienții să se nască a doua oară", January 16, 2023. *Republica*. Accessed April 3, 2023. https://republica.ro/o-poveste-adevarata-cu-oameni-si-roboti-in-sala-de-operatie-sau-despre-cum-inteligenta-umana-si-inteligenta.
[4] Regina Maria. "Center of Excellence in Robotic Surgery" / "Centru de Excelenta in Chirurgia Robotica". Accessed April 22, 2023.https://www.reginamaria.ro/ponderas/centru-de-excelenta-in-chirurgia-robotica.
[5] Stryker. "The clinical and economic value of Mako SmartRobotics™". *Mako SmartRobotics Brochure*, 2020. Accessed April 26, 2023. https://medist-imaging.ro/sites/default/files/download/products/1080-mako_smartrobotics.pdf
[6] Johns Hopkins University. "Robot performs first laparoscopic surgery without human help", January 26, 2022. *Science Daily*. Accessed April 25, 2023. https://www.sciencedaily.com/releases/2022/01/220126143954.htm.
[7] Atallah, Asa B., and Sam Atallah. "Cloud Computing for Robotics and Surgery." Atallah, Sam (Ed.). *Digital Surgery,* pp. 37-58. Cham, Springer International Publishing AG, 2020.
[8] Lewis, Nordea. "'New type of way to perform surgery': Johns Hopkins students design robots to perform surgery." *WMAR 2 News*, April 13, 2022. Accessed April 26, 2023. https://www.wmar2news.com/news/local-news/new-type-of-way-to-perform-surgery-johns-hopkins-students-design-robots-to-perform-surgery.
[9] Monogram Orthopedics. Accessed April 19, 2023. https://www.monogramorthopedics.com/.
[10] Doe, Danetha. "Is Monogram a good investment?" *Money & Mimosas Blog*, March 08, 2023. Accessed April 19, 2023. https://www.moneyandmimosas.com/growmoney/is-monogram-a-good-investment.
[11] Trochimczuk, Roman, Andrzej Łukaszewicz, Tadeusz Mikołajczyk, Francesco Aggogeri, and Alberto Borboni. "Finite element method stiffness analysis of a novel telemanipulator for minimally invasive surgery." *Simulation: Transactions of the Society for Modeling and Simulation International* 95, no. 11 (2019): 1015–1025, DOI: 10.1177/0037549719835920.

Design of Digital Control System for Line Following Robot

Dr. **Mohanad ABDULHAMID**[1,*]

[1] Al-Hikma University, Iraq

* moh1hamid@yahoo.com

Abstract: *Design of mobile robots has become an increasingly growing trend in the technology of modern times. They are very attractive engineering systems, not only because of many interesting theoretical aspects concerning kinematics, intelligent behavior and autonomy, but also because of applicability in many human activities. A typical example is the line following robot (LFR). In order for a LFR to function effectively, it must demonstrate excellent line tracking control. This is achieved by having accurate and responsive control algorithms as well as high precision color sensor systems. This paper proposes a system to show that good line tracking performance can be achieved with moderately simple digital control algorithms. The platform used is a differentially driven wheeled robot constructed using the Lego Mindstorms components. The simulation models are presented and analyzed using MATLAB Simulink. The main programming environment is the EV3 Software.*

Keywords: *Digital control, line following robot*

1. Introduction

Robotics is a branch of engineering that involves the conception, design, manufacture and operation of robots. The field overlaps with electronics, computer science, artificial intelligence, mechatronics, nanotechnology, bioengineering and control engineering. Robots are mechatronic engineering products, capable of acting autonomously while implementing assigned behaviors in various physical environments. The developed use of robots in many areas makes the fundamental understanding of them fundamental.
In recent years there has been a rapid increase in the use of digital controllers in control system. It has become routinely practicable to design very complicated digital controllers and to carry out the extensive calculations required for their design. The current adoption of digital rather than analog control in robotics is due to the genuine advantages found in working with digital signals rather than continuous time signals.
The use of analog controllers in control engineering poses problems such as limited accuracy, susceptibility to noise and drift of power supply, cost ineffectiveness and less flexibility. Digital control systems are more suitable for modern control systems because of reduced cost, noise immunity and speed.
Line following robots need to adapt accurately, faster, efficiently and cheaply to changing operating conditions. The drawbacks prominent in analog controllers reduce their suitability in robotics. Hence, the necessity for digital controllers which provide better performance capabilities. Some works on this topic can be found in literatures [1-5].

2. Design methodology

2.1 Lego Mindstorms line follower robot design

A line follower shown in Fig.1 is a mobile robot which is able to follow a visible line on a surface consisting of contrasting colours. To build and run the robot, the required hardware included; Lego EV3 brick, power supply, 2 large servo motors, a set of wheels, colour sensor, connector cables, beams, axles, bushes and pins. The EV3 brick formed part of the chassis, equipped with wheels. The servo motors are used to drive the two front wheels. Two rear small castor wheels supported the robot. The robot had a colour sensor mounted at the front end to identify the line. It is centered between the two front wheels, which are separated by a distance of 7.4 cm. It is designed to follow an oval track made of black electrical tape (18 mm wide) on a white surface.

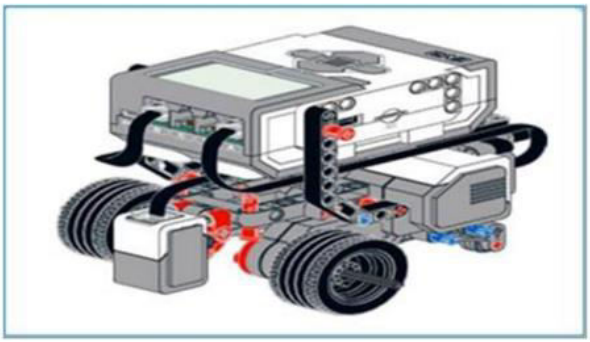

Fig. 1. Line following robot

2.2 Study of Lego Mindstorms EV3 motor

Lego Mindstorms has not published the EV3 motor's electromechanical characteristics. Table 1 shows the proposed parameters used in this paper, while, Table 2 shows the operational specifications.

Table 1: Lego Mindstorms EV3 large motor characteristics

Motor Parameter	Unit	Value
Torque constant	N.m/A	0.2
Back e.m.f. constant	V.s/rad	0.5
Armature resistance	Ω	5
Armature inductance	H	0.005
Viscous damping coefficient, B	N.m/rad.s	0.0006
Rotor inertia coefficient, J	N.m	0.001

Table 2: Operational specifications

Nominal Voltage	7.2V or 9V
Rotation Speed at no load	160 – 170 rpm
Running Torque	0.20 N-m
Stall Torque	0.40 N-m

Fig.2 shows the motor model simulated using MATLAB Simulink.

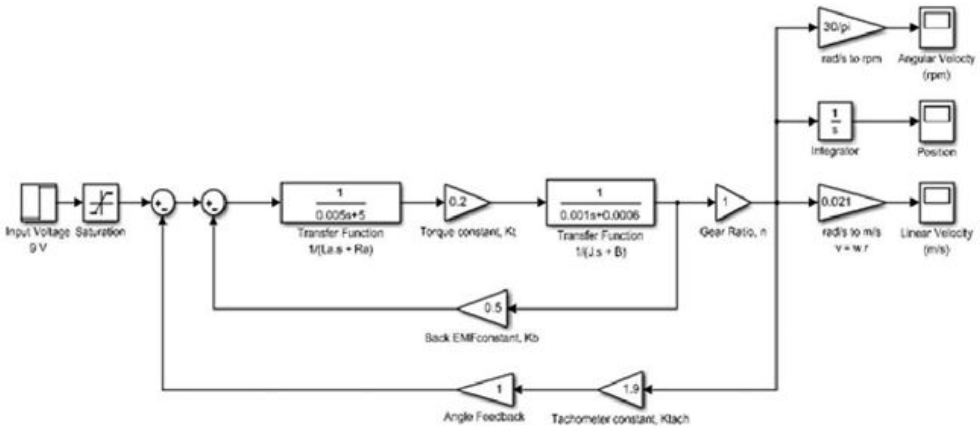

Fig. 2. Motor implementation on Simulink

2.3 Line following robot algorithms

Line following works by using the colour sensor (in reflected light intensity mode) to read the changes in the reflected light levels along the edge of a dark and light surface. The reflected light intensity is measured as a percentage from 0% (very low reflectivity) to 100% (very high reflectivity). More light is reflected from a white surface compared to the black surface. Depending on the light sensor value, the motors are directed to vary the speed.
In a program, white and black values are defined using a threshold value. Threshold is the average of the sensor value with the sensor on the black line and one found on the white area. Different measurements for black and white depend on factors such as the light level in the room, the robot's battery level, and the type of surface used.
The light sensor will read the light value. Then the robot can be programmed such that if the sensor sees black, which is when the sensor value is less than the threshold, the robot should turn right, else it should turn left. The basic line following approach is shown in Fig.3, and can be summarized as follows:
1- The robot will be started. It will then be set to move forward. It will be made to steer right until it detects the line edge.
2-Once the sensor sees black, the robot will continue to go forward while turning left gradually.
3-Whenever the sensor will see white (i.e. the robot leaving the line), the robot will turn to the right until the sensor finds black again.
4-The sequence then will be repeated in a loop, unless the robot is stopped.

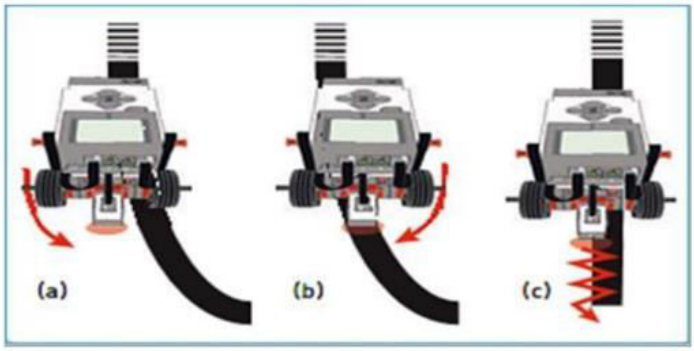

Fig. 3. Basic line following approach

2.4 Digital controller design

A robot without a controller will oscillate a lot about the line, leading to more consumption of battery power, less speed and following the line less efficiently.
When designing a line following robot, the transient response specifications are defined as:
1-Rise time: It is how fast the robot will try to get back to the line after it has drifted off.
2-Overshoot: The distance past the line edge the robot will tend to go as it is responding to an error. 3-The amount of overshoot indicates the relative stability of the system.
4-Steady-state error: The offset from the line as the robot follows a long straight line.
5-Settling time: The time the LFR will take to settle down when it encounters a turn.
The performance criteria are stipulated as follows:
1-Constant speed of 0.1m/s to be maintained despite the presence of turns.
2-Steady-state error: Less than 2%
3-Settling time of less than 0.1 seconds
4-Overshoot (%) of less than 1.0
5-Finite phase margin
The robot controller to be designed is to be modified until the transient response met is satisfactory.

2.4.1 Proposed controller design

The proposed controller is a Proportional-plus-Integral-plus-Derivative (PID) digital controller. The PID controller would control the position of the robot with quick response time and minimize the

overshoot. The proportional part would determine the magnitude of turn required to correct the error sensed. The integral part would improve the steady state error (proportional offset) which increases while the robot is not on the line. The derivative part would measure the deviation from the path and minimize overshoot. It would reduce the oscillating effect about the line. The derivative control is used to provide anticipative action.

2.5 Implementation of line following control algorithm for Lego Mindstorms EV3 hardware

Fig.4 shows the Simulink line tracking program with PID controller, while Fig.5 shows EV3 software line following program with PID controller. Sensors and motors contain blocks that interface with the EV3 hardware. Actual speed values block uses the values from each motor encoder to calculate the position and velocity of the robot. Desired velocity takes the user-provided velocity (m/s) and converts it into the desired state values for the velocity controller. Desired light takes the color sensor's white and black values to choose an appropriate reference value for the light. Velocity control has the PID controller implementation to control the forward velocity. Line tracking controller has the PID controller implementation to control the turning.
However, to download and run a line tracking Simulink model on the Lego Mindstorms EV3 robot, EV3 Wi-Fi Dongle or USB Ethernet Adaptor, and Wi-Fi Router are required to set up a network connection between EV3 brick and host computer.
The line following program is then written in EV3 software programming language. The black and white light intensity values are calibrated accordingly for the robot and the track. Using the provided USB cable, the program is downloaded and run on the robot. PID parameters (K_p, K_i, and K_d) tuning is done experimentally to achieve smoother line tracking.

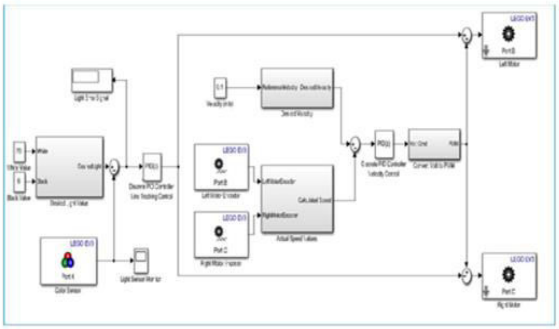

Fig. 4. Simulink line tracking program with PID controller

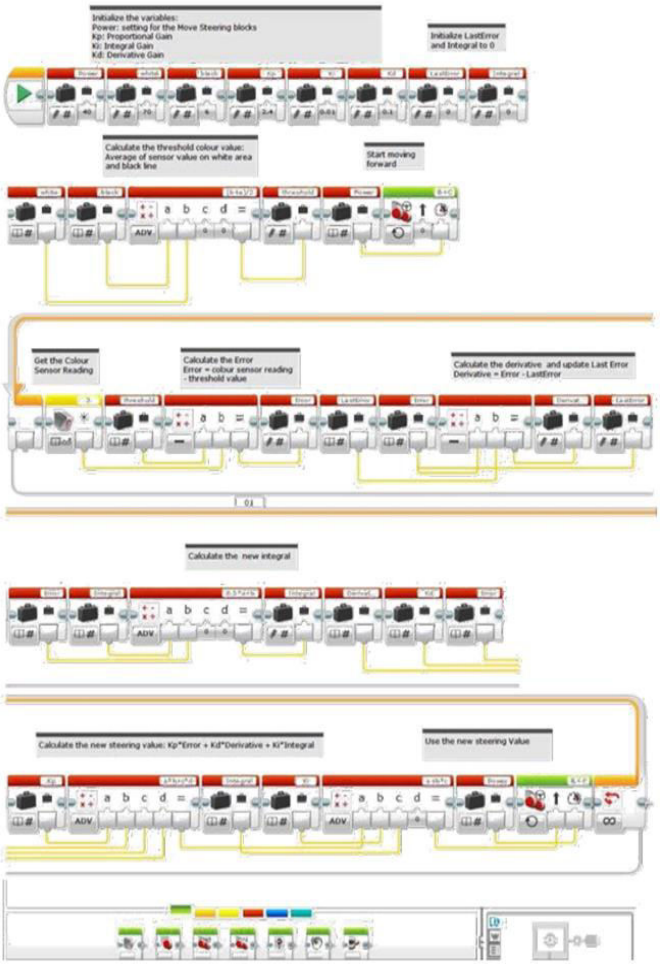

Fig. 5. EV3 Software line following program with PID controller

3. Simulation results

3.1 EV3 large motor characteristics

Table 3 shows the EV3 motor load characteristics, from which the linear relationship between power level and EV3 large motor speed noticeable as shown in Fig.6. Also, from table 3, the rotation speed of the EV3 large motor is proportional to the input voltage.

Table 3: EV3 motor load characteristics

Input Voltage	Torque	Rotation speed	Current	Mechanical power	Electrical power	Efficiency
4.5 V	17.3 N.cm	24 rpm	0.69 A	0.43 W	3.10 W	14 %
6.0 V	17.3 N.cm	51 rpm	0.69 A	0.92 W	4.14 W	22 %
7.5 V	17.3 N.cm	78 rpm	0.69 A	1.41 W	5.17 W	27 %
9.0 V	17.3 N.cm	105 rpm	0.69 A	1.90 W	6.21 W	31 %
10.5 V	17.3 N.cm	132 rpm	0.69 A	2.39 W	7.24 W	33 %
12.0 V	17.3 N.cm	153 rpm	0.69 A	2.77 W	8.28 W	33 %

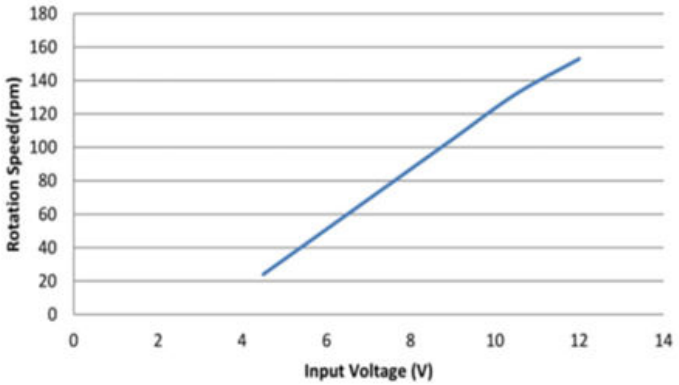

Fig. 6. Graph of rotation speed against applied voltage

3.2 PID parameters tuning

Different values of PID parameters (K_p, K_i, K_d) are chosen in order to get the step response.

1- For K_p=1, $K_{i=}$0, $K_{d=}$0

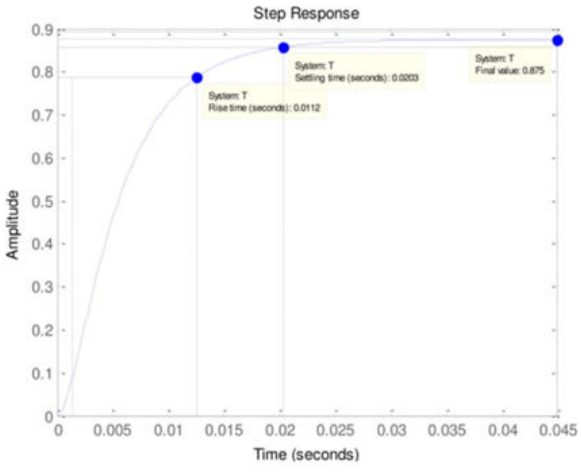

Fig. 7. Step response: K_p=1

Observations:
Rise time = 0.0112 seconds
Settling time = 0.0203 seconds
Final value = 0.875

2- For K_p=5, K_i=0, K_d=0

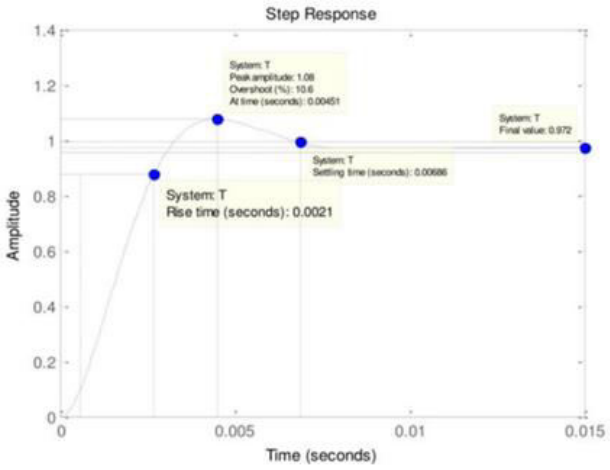

Fig. 8. Step response: K_p=5

Observations:
Rise time = 0.0021 seconds
Settling time = 0.00686 seconds
Final value = 0.972
Overshoot (%) = 10.6
Peak amplitude = 1.08

3- For K_p=2.4, K_i=0, K_d=0

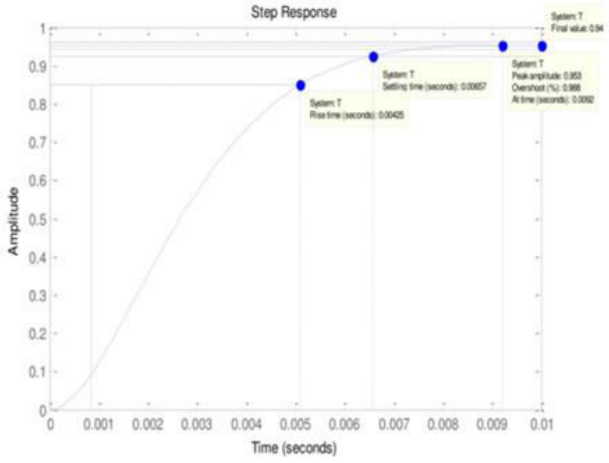

Fig. 9. Step response: K_p=2.4

Observations:
Rise time = 0.00425 seconds
Settling time = 0.00657
Final value = 0.94
Overshoot (%) = 0.988
Peak amplitude = 0.953

4- For K_p=2.4, K_i=0.01, K_d=0

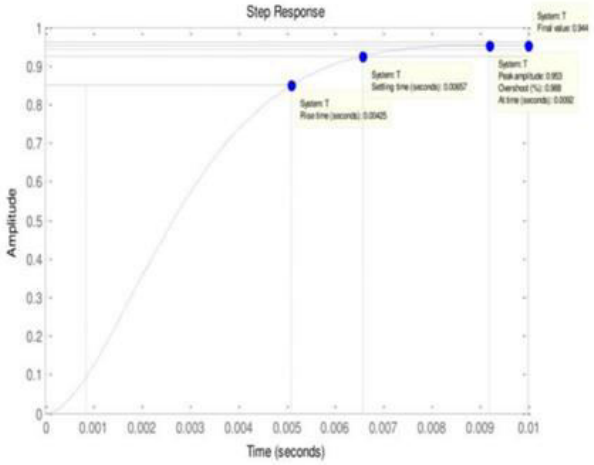

Fig. 10. Step response: K_p=2.4, K_i=0.01, K_d=0

Observations:
Rise time = 0.00425 seconds
Settling time = 0.00657 seconds
Final value = 0.944
Overshoot (%) = 0.988
Peak amplitude = 0.988

5- For K_p=2.4, K_i=0.01, K_d=0.1

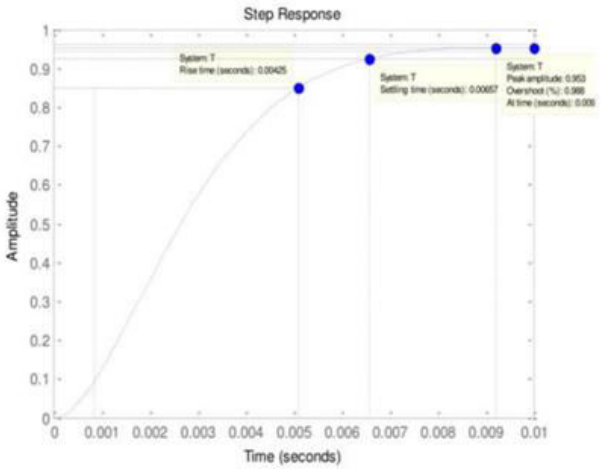

Fig. 11. Step response: K_p=2.4, K_i=0.01, K_d=0

Observations:
Rise time = 0.00425 seconds
Settling time = 0.00657 seconds
Final value = 0.944
Overshoot (%) = 0.988
Peak amplitude = 0.953

3.3 Frequency response

Frequency responses are obtained for different values of PID parameters.

1- For K_p=5, K_i=0, K_d=0

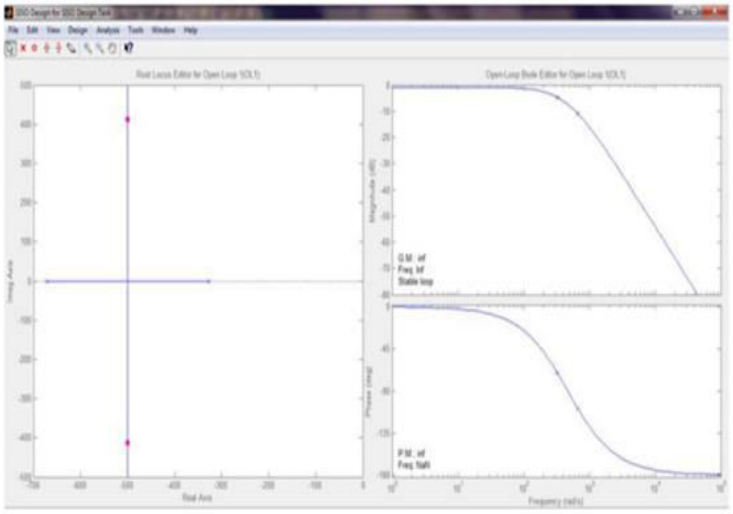

Fig. 12. Various frequency plots for the compensated system during tuning ($K_p = 5$)

Observations
The root locus exhibited complex closed loop poles.
Both the phase and gain margin are infinite.
The system is stable.

2- For K_p=2.4, K_i=0.01, K_d=0.1

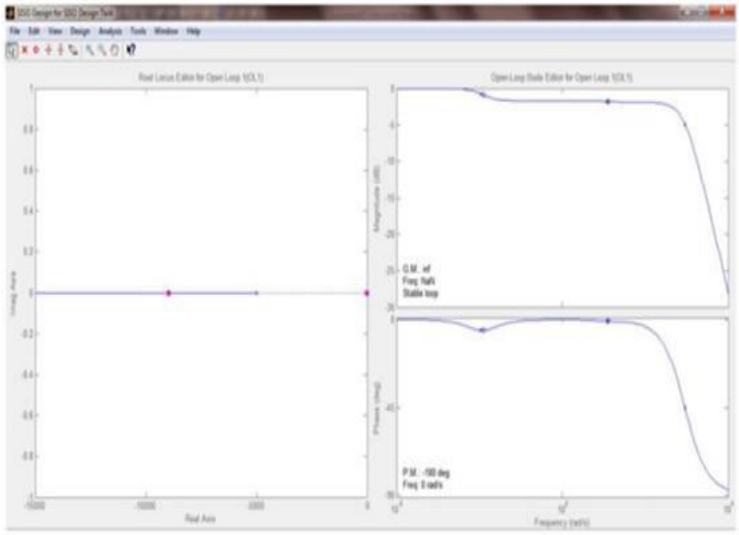

Fig. 13. Various frequency plots for the compensated system (K_p=2.4, K_i=0.01, K_d=0.1)

Observations
The root locus closed-loop poles changed from complex to real.
The system is still stable.
The infinite gain margin showed inherent stability.

4. General analysis

The effects of each of controller parameters, K_p, K_i, and K_d on the line following robot are summarized in the table 4.

Table 4: Effects of increasing PID parameters

Parameter	Rise Time	Overshoot	Settling Time	Steady-state Error
K_p	Decrease	Increase	Small change	Decrease
K_i	Decrease	Increase	Increase	Eliminate
K_d	Small change	Decrease	Increase	No change

The difficulty of tuning increased with the number of parameters that are to be adjusted. To observe the response that resulted from the tuning adjustments, it is necessary to wait for several minutes. This made the tuning by trial-and-error a tedious and time-consuming task.
In practice, the stability of a mathematical model is not sufficient to guarantee acceptable system performance or even to guarantee the stability of the physical system that the model represented. This is because of the approximate nature of mathematical models.
The main problems associated with the implementation of digital control are related to the effects of quantization and sampling. The advantages of digital control outweigh its implementation problems for most of the applications.

5. Conclusions

A line following robot was designed and built using Lego Mindstorms EV3 components. Digital control algorithms were developed. The advantages and limitations of implementing the digital control on different software were studied. The effectiveness of using PID controller for optimum line tracking was demonstrated by inspecting the movement pattern of the robot while following the track. To obtain the desired control response, K_p, K_i and K_d were successfully determined by tuning.

References

[1] Mutheke, Muindi. "Digital control of a line following robot." Graduation Project. University of Nairobi, Kenya, 2015.
[2] Pathak, Abhijit, Refat Khan Pathan, Amaz Uddin Tutul, Nishat Tahsin Tousi, Afsari Sultana Rubaba, and Nahida Yeasmin Bithi. "Line follower robot for industrial manufacturing process." *International Journal of Engineering Inventions* 6, no. 10 (October 2017): 10-17.
[3] Chowdhury, Nakib Hayat, Deloara Khushi, and Md. Mamunur Rashid. "Algorithm for line follower robots to follow critical paths with minimum number of sensors." *International Journal of Computer* 24, no.1 (2017): 13-22.
[4] Kumaresan, P., G Priya., B R Kavitha, G Ramya, and M. LawanyaShri. "Case study: A line following robot for hospital management." *International Journal of Pure and Applied Mathematics* 116, no. 24 (2017): 529-537.
[5] Attar, Aamir, Aadil Ansari, Abhishek Desai, Shahid Khan, and Dipashri Sonawale. "Line follower and obstacle avoidance bot using Arduino." *International Journal of Advanced Computational Engineering and Networking* 5, no. 4 (2017): 18-21.

Precipitation Anomalies Characterization in Papalotla River Basin and Their Implications for Territorial Planning

PhD **Rodrigo ROBLERO-HIDALGO**[1], M.Eng. **Margarita Elizabeth PRECIADO-JIMÉNEZ**[1], PhD **Maritza Liliana ARGANIS-JUÁREZ**[2,*], M.Eng. **Julio SORIANO-MONZALVO**[1], M.Eng. **José Avidan BRAVO JACOME**[2], M.Eng. **Yaridalia RAMÍREZ-ABUNDIS**[2]

[1] Mexican Institute of Water Technology IMTA, Paseo Cuauhnáhuac 8232 Progreso, Morelos, C.P. 62550

[2] National Autonomous University of Mexico UNAM, Institute of Engineering, Av. Universidad 3000. Ciudad Universitaria, Coyoacán, CDMX, C.P. 0451

* MArganisJ@iingen.unam.mx

Abstract: *This paper focuses on calculating the monthly anomaly of precipitation using a straightforward methodology based on average monthly values and drought categorization. The specific case study conducted in this study pertains to the Papalotla River subbasin, which is a part of the Texcoco Lake basin. The research findings reveal that anthropogenic activities, particularly land use change, have had a detrimental impact on the environmental balance of the region. These activities have resulted in several negative consequences such as soil degradation, loss of biodiversity, and environmental pollution. Additionally, the utilization of water resources upstream has led to a reduction in runoff, further exacerbating the environmental challenges faced by the subbasin. Overall, the research highlights the significant disturbances caused by human activities in the Papalotla River subbasin. These disturbances have disrupted the natural area equilibrium, leading to adverse environmental effects.*

Keywords: *Standardized Drought Index, monthly anomaly, Papalotla River, land use*

1. Introduction

Mexico is a country that, due to its geographical characteristics, location, relief and location between two oceans, is impacted by different hydrometeorological phenomena and this increases vulnerability to climate change. Hurricanes, droughts, extreme temperatures and torrential rains have caused serious human losses and high economic and social costs over time. These events limit development opportunities in the short and medium term. These and other consequences of the impacts of climate change have been addressed in various scientific studies and technical papers, which suggest that some of the negative consequences of climate variability are already visible and could worsen over the coming decades. Likewise, the aggregate impact of extreme events, resulting from climate change, can intensify other environmental and social problems, such as land use change, the shape and structure of urban settlements, production processes or the state of ecosystems [1]. As for precipitation, changes in rainfall distribution patterns are observed.
Climate change scenarios present a high level of uncertainty, since in some cases a slight increase is projected in some regions, but in general a decrease in precipitation is appreciated. precipitation anomaly is the main indicator of the behavior of precipitation in a certain period and a certain place, it is a parameter that measures the deviation in percentage of the precipitation of a given period in relation to the historical average value of a period and indicates how far away the rainfall recorded, either below or above what is assumed to be the average or normal value; this indicator is important for assessing weather responses [1]. Droughts, storms and floods, all water-related phenomena, dominate the list of catastrophes of the last 50 years, both in terms of human and economic losses, according to a comprehensive analysis [2] (World Meteorological Organization, 2012).
Desertification is strongly linked to poverty and migration, since unproductive land causes scarcity and migration. In absolute terms, the population below the poverty line increased from 15.9 million to 17.0 million people in the period 2008-2010 and it is estimated that between 300,000 and 400,000 people are displaced each year, leaving behind unproductive land. The international community, including Mexico, has long recognized that land degradation and desertification is a multidimensional economic, social, and environmental problem of concern to more than 167

countries in all regions of the world, affecting some two billion inhabitants and a quarter of the planet's land surface [3]. Desertification risks arise when human interventions modify the natural balance beyond its limits of resistance. Historically, in dry regions, man has often developed social, cultural and economic systems that have allowed him to regulate pressure on basic natural resources (soil, water and vegetation), depending on the availability of those resources. In this way it has achieved a sustainable exploitation in the regime of rainfall variability of the region; the threat that hangs over these environments is, therefore, potential and degradation only appears after the rupture of the balance [4]. This paper presents a methodology with which it is intended to calculate the monthly anomaly of precipitation in a simple way from average monthly values and drought categorization having as a case study the Papalotla River subbasin which is part of the Texcoco Lake basin.

2. Methodology

The Valley of Mexico is closed basin as shown in Figure 1, without natural outlets for rainwater runoff and where there are convective storms of high intensity and short duration, which cause serious problems for the evacuation and control of its waters. In addition to this, the Mexico City metropolitan area (ZMCDMX) has grown in a disorderly manner, and snowing hillsides and old areas, coupled with this the ZMCDMX which is the most populated in the country, with more than 22 million people settled in an area of the order of 7,000 square kilometers, which include Mexico City in whole and in part in the states of Mexico, Hidalgo, Tlaxcala and Puebla.

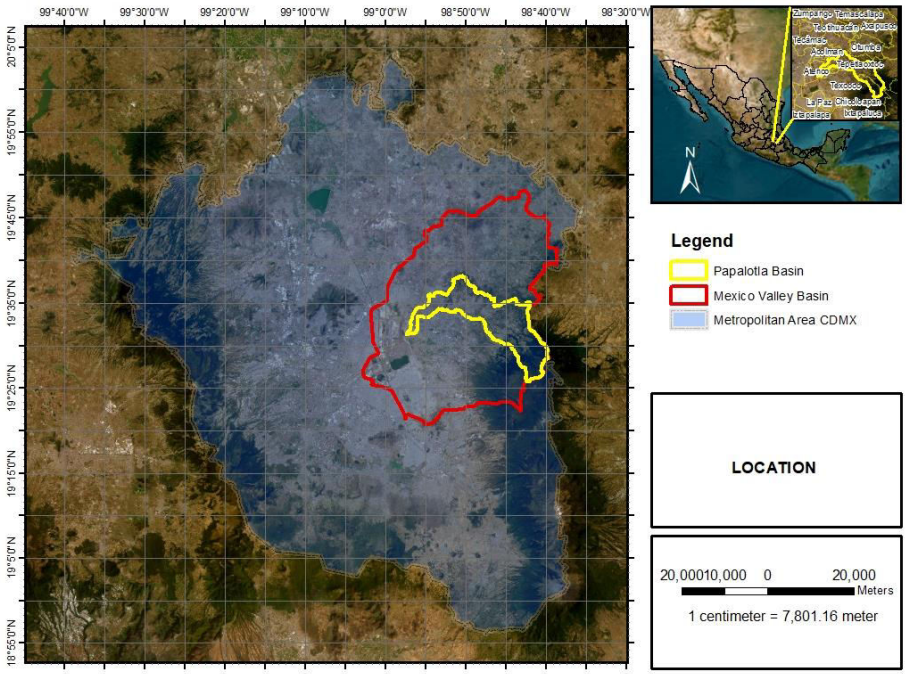

Fig. 1. Location of the Papalotla River Basin

The great difference in unevenness between ravines and subsidence allows runoff to descend unexpectedly, carrying garbage, mud and stones to the drainage systems and silting them. While, in the latter, they are characterized by differential subsidence of land, mainly due to the overexploitation of aquifers. These subsidence's cause slopes and dislocations of drainage networks, causing flooding and waterlogging [5]. Papalotla River basin which will be taken as a study area is located east of the State of Mexico. Its source is located in the Sierra Nevada. It runs through the municipalities of Tepetlaoxtoc, Papalotla, Chiautla, Tezoyuca and Atenco, to finally flow into Texcoco Lake. This river is part of Valley of Mexico basin and like other rivers that make it up presents a high degree of pollution due to the discharge of wastewater, both domestic and the paper and livestock industry since 1985.

As established by the World Meteorological Organization, the Climatological Normal, or normal value, is used to define and compare climate and is generally represented by the average value of a continuous series of measurements of a climatological variable (precipitation, temperature, wind, etc.) over a period of at least 30 years. The difference between the recorded value of the variable and its normal value is known as an anomaly. In general terms, the hydrometeorological data contain both a temporal and spatial structure, therefore, the statistical methodologies used in their analysis should consider this type of structures [6]. It is very important to remember that, of all meteorological parameters, precipitation is one of the most spatial-temporal variability. This fact makes it difficult to determine an interval within which the anomalies that occur most frequently can be grouped, to consider them as common alterations and, therefore, as normal values. We will call this range or interval hereinafter, the Threshold of Normality. The anomalies, in the case of precipitation, are calculated as the quotient between the total recorded in a particular month and its multiannual average value and is expressed as a percentage, so that 100% indicates that a volume of water exactly equal to its historical average was recorded. That both the data move away from 100% up or down, indicates the degree of alteration by excess or default, respectively [7]. There are two very important aspects in the representation of precipitation anomalies on which this proposal of categorization of drought using the standardization of precipitation anomaly is based. Reflecting the situation of the event in relation to the series of past data is as important as the phenomenon itself and converts the numeric value into an index that categorizes the event and it is easily understood. The standardized anomaly is calculated according to the procedure used by Ogallo [2], where:

$$Z_{ij} = \frac{x_{ij} - x_j}{s_j} \quad (1)$$

Where:
Xij is the cumulative total of the analysis period of station j in year i and xj, Sj are the mean and standard deviation of that period, respectively.
Under this premise it is proposed that for the calculation of the proposed anomaly will be monthly by weather station to which the following equation is proposed:

$$Anomaly = \frac{xi - So_i}{So} \quad (2)$$

Where xi is the mean of the value of month i over the period, So_i is the standard deviation of the mean of month i and So is the average deviation of all months.
The standardized drought indices (SI) evaluate the difference between the values of the analyzed variable and the condition considered "normal" in a normalized sample. Thus, the numerical values of the SI index represent anomalies of the variable of interest with respect to the mean [8]. In this work it is proposed that from the results obtained it is categorized according to the range indicated in Table 1 since this allows converting the numerical value into an index that categorizes the event, and this is easily understood.

Table 1: Standardized Drought Index (SI) scale

Value	Category
More than 2	extremely rainy
Between 1.5 and 2	rainy
Between 1 and 1.5	slightly rainy
Between 0.5 and 1	Normal
Between 0 and 0.5	Normal
Between -0.5 and -1	slightly dry
Between -1.5 and -2	dry
Below than -2	extremely dry

Application of the methodology to the Papalotla river basin

Study area is part of the well-known Federal Zone of Texcoco Lake and adjacent lands that are located east of the State of Mexico. In Texcoco Lake nine rivers converge in natural conditions; five in its northern portion (San Juan Teotihuacán, Papalotla, Xalapango, Coxcacoaco, Texcoco) two in the central zone (Chapingo and San Bernardino) and two in the southern portion (Santa Monica and Coatepec). In addition, in the lower zone, through the General del Valle drain, the waters from the Ameca, La Compañía and San Francisco rivers converge. The former lake of Texcoco is fed by the rivers Churubusco, La Compañía, Los Remedios, San Juan Teotihuacán and Papalotla, and reaching the federal zone by two arms, the Santa Rosa and San Bartola, Xalapango, Coxcacoaco, Texcoco (which currently functions as drainage and sanitary drainage of the metropolitan area of Texcoco), San Bernardino, Chapingo, Coatepec and Santa Monica.
Papalotla River basin (Figure 2) is formed by the union of two slopes which join each other in the lower part of the basin, one that collects the runoff from mountainous areas located in the center of the municipality of Tepetlaoxtoc, and another that comes from the mountainous area near the town of Santa Inés (upper part of the basin). The approximate extension of the northern branch is 17.2 km. Papalotla River crosses the municipalities of Papalotla, San Andrés Chiautla, Tezoyuca and Atenco until it reaches the former Texcoco Lake. It has an average annual contribution of 6.42 million cubic meters.

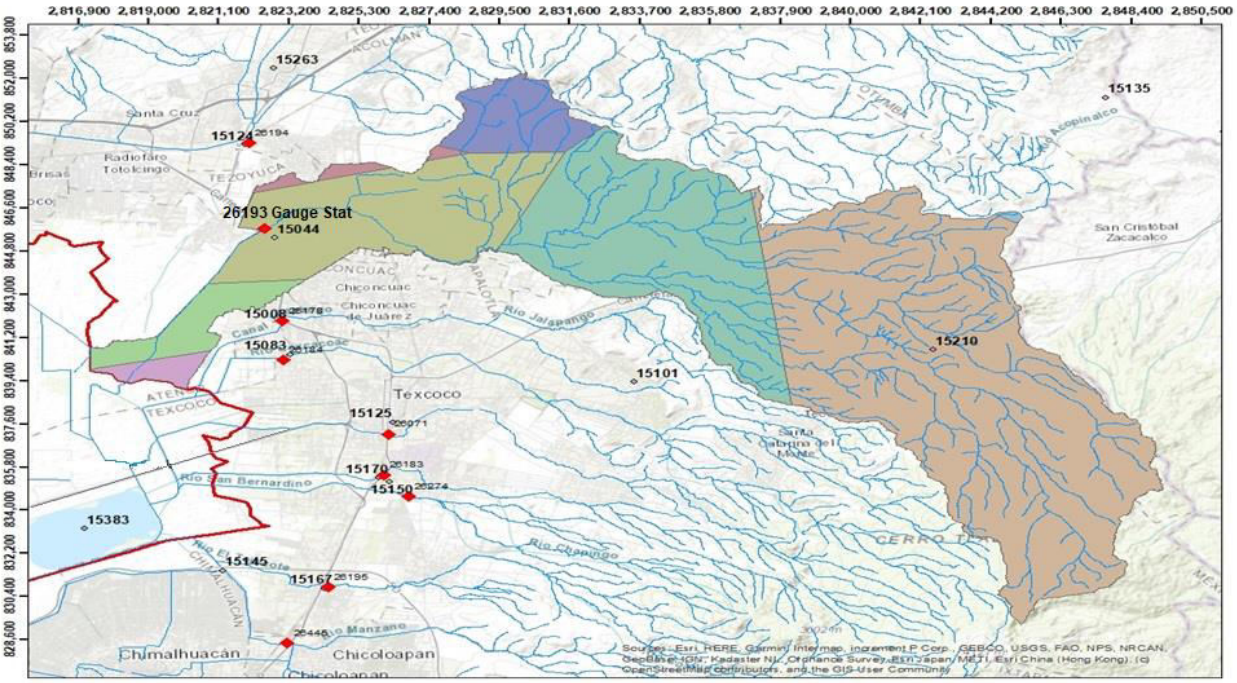

Fig. 2. Papalotla River Basin

3. Results

Based on the climatological data of the Clicom Database, the analysis of accumulated precipitation annual trends records for each of the climatological stations were carried out, which are observed below (Figure 3).

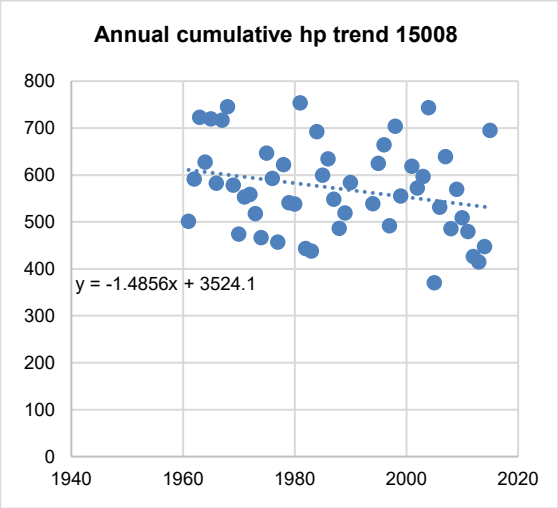
Annual cumulative hp trend 15008
y = -1.4856x + 3524.1

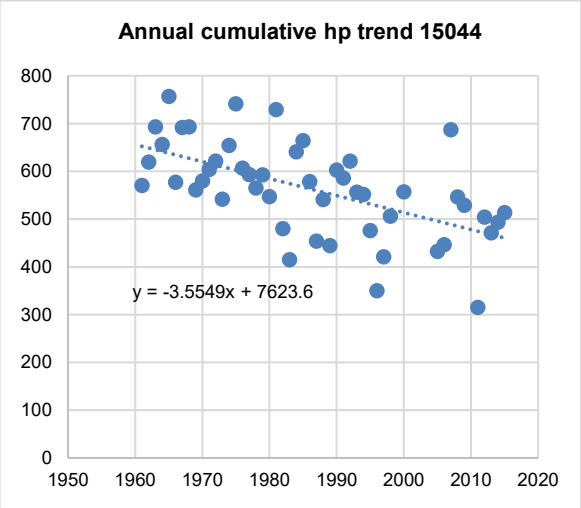
Annual cumulative hp trend 15044
y = -3.5549x + 7623.6

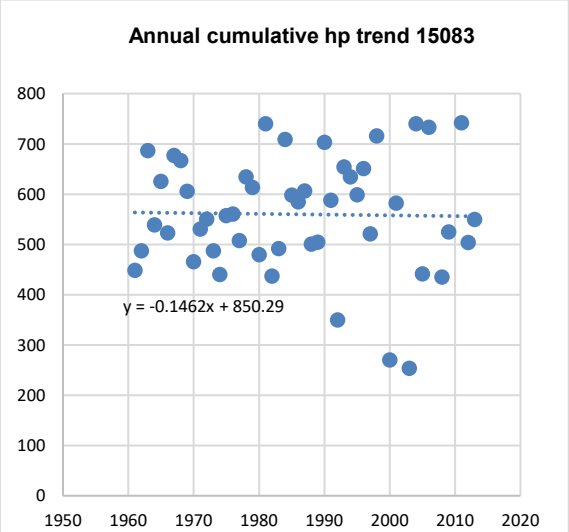
Annual cumulative hp trend 15083
y = -0.1462x + 850.29

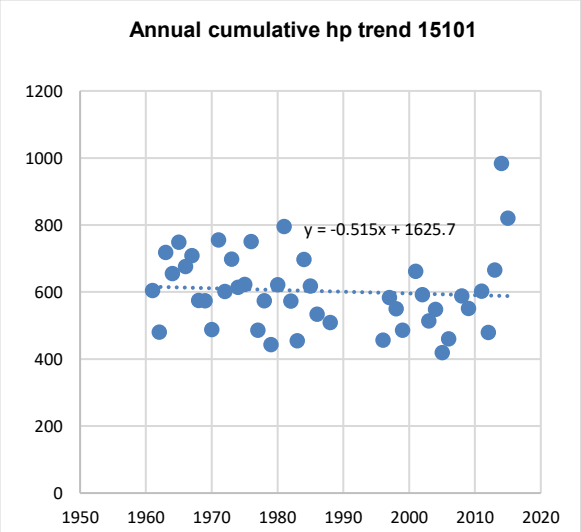
Annual cumulative hp trend 15101
y = -0.515x + 1625.7

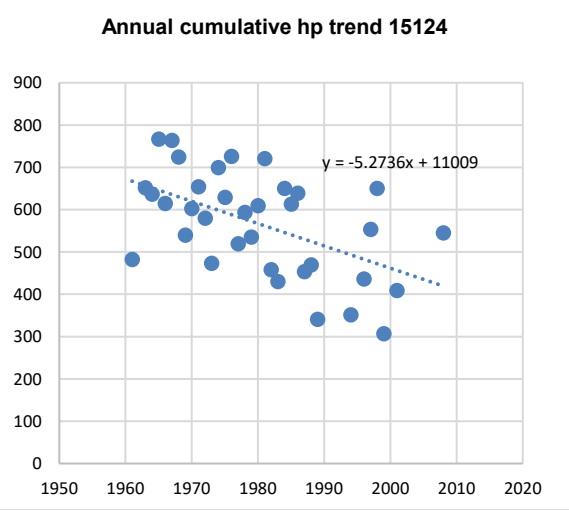
Annual cumulative hp trend 15124
y = -5.2736x + 11009

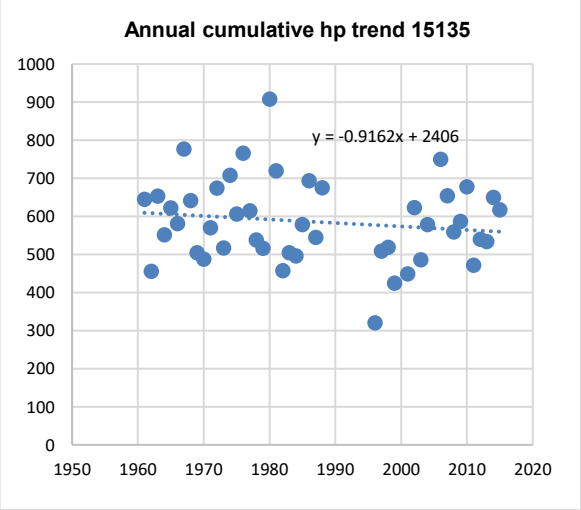
Annual cumulative hp trend 15135
y = -0.9162x + 2406

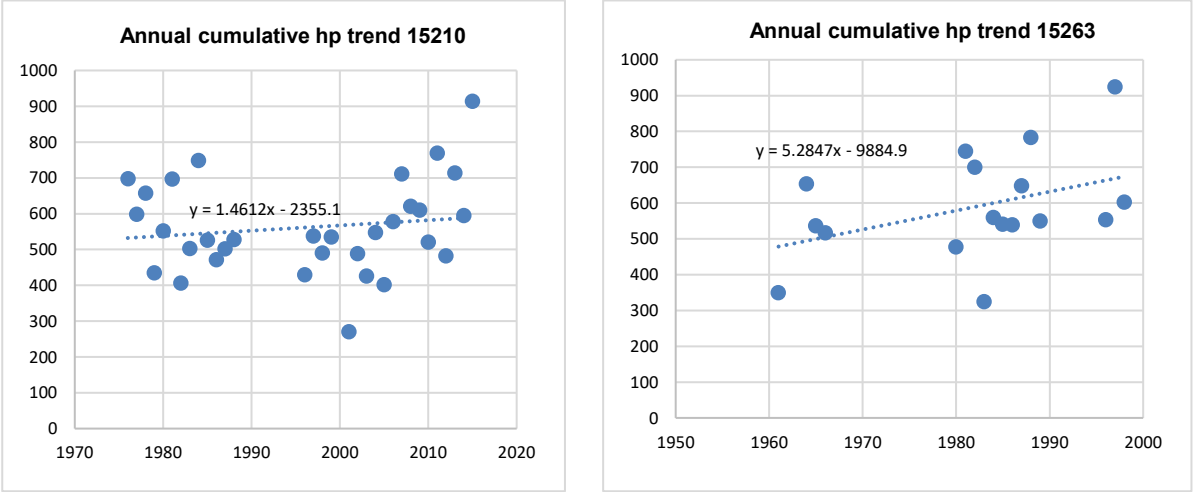

Fig. 3. Annual cumulative hp trend for 15263, 15210, 15135, 15124, 15101, 15083, 15044 and 15008 climatologic Stations

From figure 3 it can be seen that station 15008 shows a downward trend with 26 records above the average of 571.41 and 26 below average. The station has a record of 370 mm per year for 2005. Station 15044 presents a downward trend with an average annual cumulative of 562.98 mm registering 30 data above the average and 20 below the average. The minimum registration was presented in 2011 with 315 mm accumulated annually. Station 15083 presents a very slight downward trend with an average of 559.95 mm accumulated per year being 24 records above the average and 25 below the average with 253.1 mm accumulated in the year 2000.
The station 15101 presents a slight downward trend with 602.83 mm accumulated per year having registered 19 data above the average and 25 below the average, all years accumulated records greater than 400 mm being the lowest in 2005 with 419 mm. The station 15124 presents a marked downward trend with an accumulated annual average of rainfall of 566.28mm with 19 records above the average and 16 below the average the lowest recorded value of accumulated rain was the year of 1999 with 306.5 mm.
Station 15135 presents a downward trend with 21 records above the average that is 585.73 and 25 below the average the lowest value recorded was 320 mm accumulated in 1996. The station 15210 presents a tendency to the high with 26 records above the average that is 561.59mm and 6 below the average the lowest value recorded was 270.6 mm in 2001 it is worth mentioning that this station is the one that occupies more than half of the area of influence of the entire basin, according to the Thiessen polygons shown in Figure 2.
Station 15263 presents a trend to the high with 7 records above the average that is 588.84mm and 10 below the average the lowest value recorded was 324 mm in 1983. Stations 15008, 15044, 15083, 15101, 15124 and 15135 show a downward trend only station 15210 and 15263 have a trend to high.
According to the calculation made using the methodology described above in Table 2, the calculation of the monthly precipitation anomalies for each of the 8 climatological stations is presented.

Table 2: Monthly precipitation anomalies. Climatological Papalotla River basin

Months	15008	15044	15083	15101	15124	15135	15210	15263
January	-0.301	-0.319	-0.267	-0.022	-0.014	-0.014	-0.016	-0.012
February	-0.382	-0.143	-0.164	-0.009	-0.005	-0.013	-0.035	-0.014
March	-0.197	-0.123	-0.183	-0.017	-0.012	-0.011	-0.018	-0.015
April	0.218	0.139	0.298	0.003	-0.006	-0.016	0.003	-0.011
May	0.893	0.581	0.855	0.007	-0.006	0.009	0.013	-0.034
June	2.457	1.886	2.512	0.071	0.036	0.019	0.047	-0.025

Months	15008	15044	15083	15101	15124	15135	15210	15263
July	3.616	2.394	3.235	0.073	0.052	0.013	0.030	-0.037
August	3.152	2.373	2.631	0.053	0.050	-0.002	0.053	-0.014
September	1.706	1.404	1.302	0.051	0.026	-0.001	0.022	-0.047
October	0.814	0.272	0.468	0.016	-0.001	-0.009	0.008	-0.035
November	-0.277	-0.263	-0.143	-0.009	-0.016	-0.020	-0.011	-0.019
December	-0.242	-0.280	-0.237	-0.010	-0.007	-0.013	-0.009	-0.015

Likewise, Figure 4 graphically presents the monthly anomalies for the same weather stations.

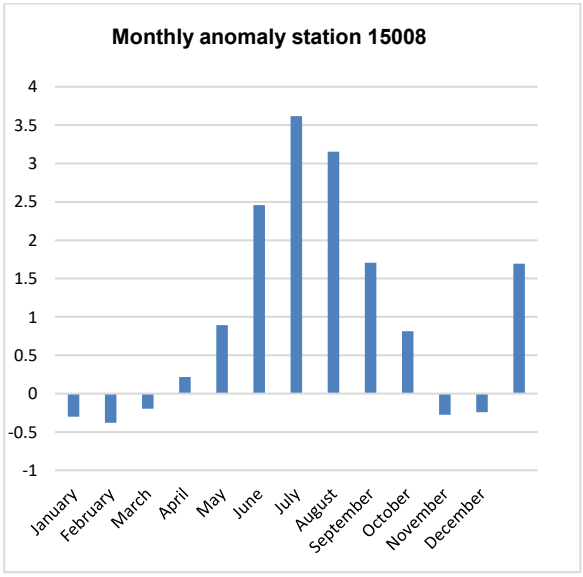

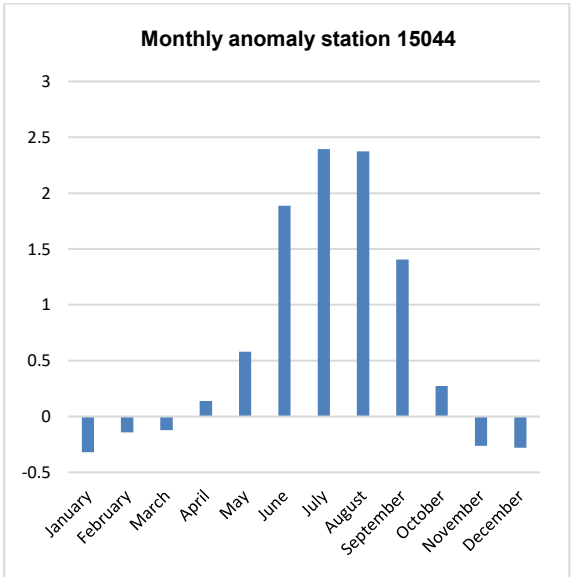

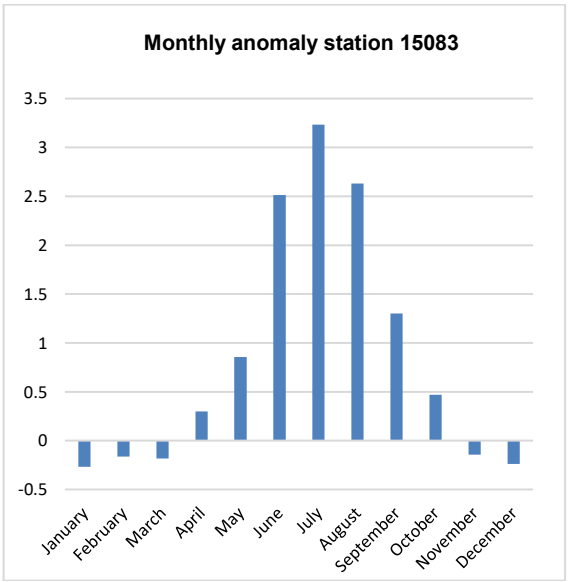

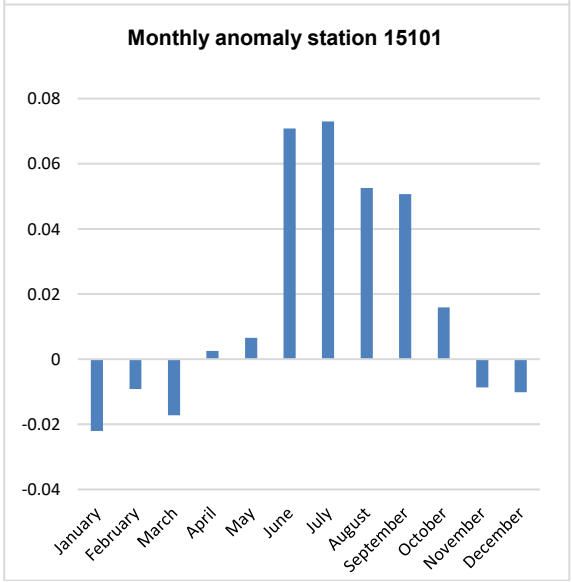

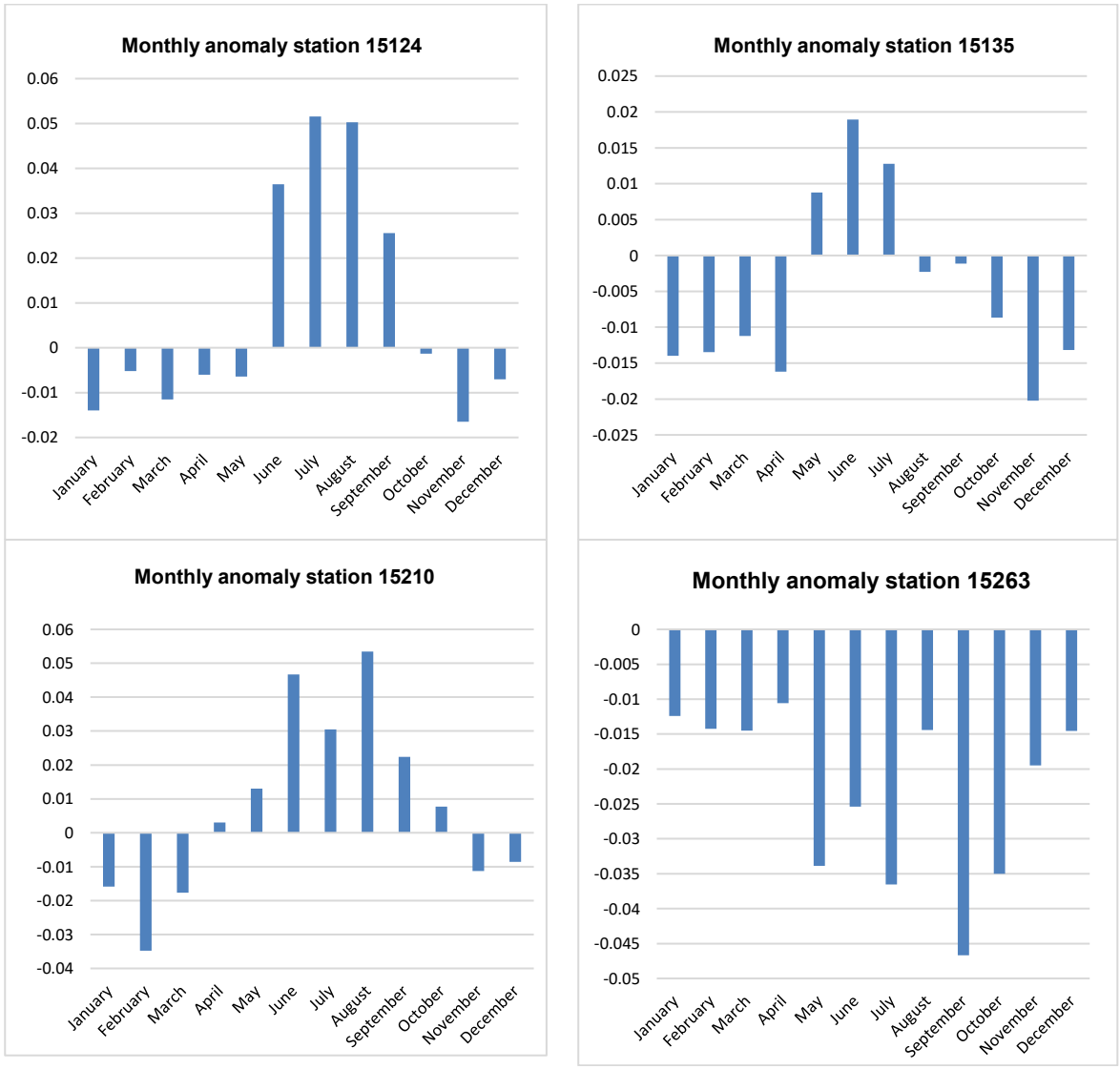

Fig. 4. Monthly anomalies of stations 15263, 15210, 15135, 15124, 15101, 15083, 15044 and 15008

According to the previous categorization it has that for the eight climatological stations of the Papalotla river basin, the slightly dry category is reached in the dry months November to March for seasons 15008 15044, 15083 and 15210 for season 15124 from October to May, for season 15135 from August to April and season 15263 is slightly dry 12 months of the year according to the categorization before described however according to the trend is to present an upward behavior in terms of the amount of precipitation rain is taken as significant data that in 1983 there was an accumulated annual rainfall well below the historical average of the basins that drain towards the Texcoco Lake with 324 mm being the month of September the one that presents the greatest anomaly. But you also have those seasons 15008, 15044 and 15083 reach the extremely rainy category in the months of June to August. Likewise, the historical review of the satellite images from study area for the years 1992 and 2022 was carried out, which can be seen in Figure 5 (year 1992) and Figure 6 (year 2022).

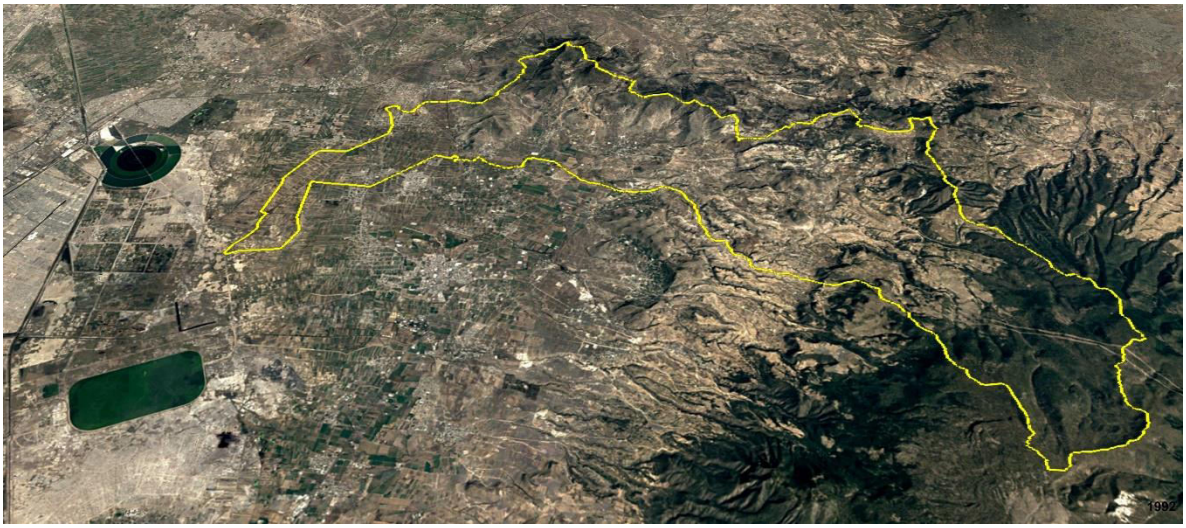

Fig. 5. Satellite image of the Papalotla basin in 1992

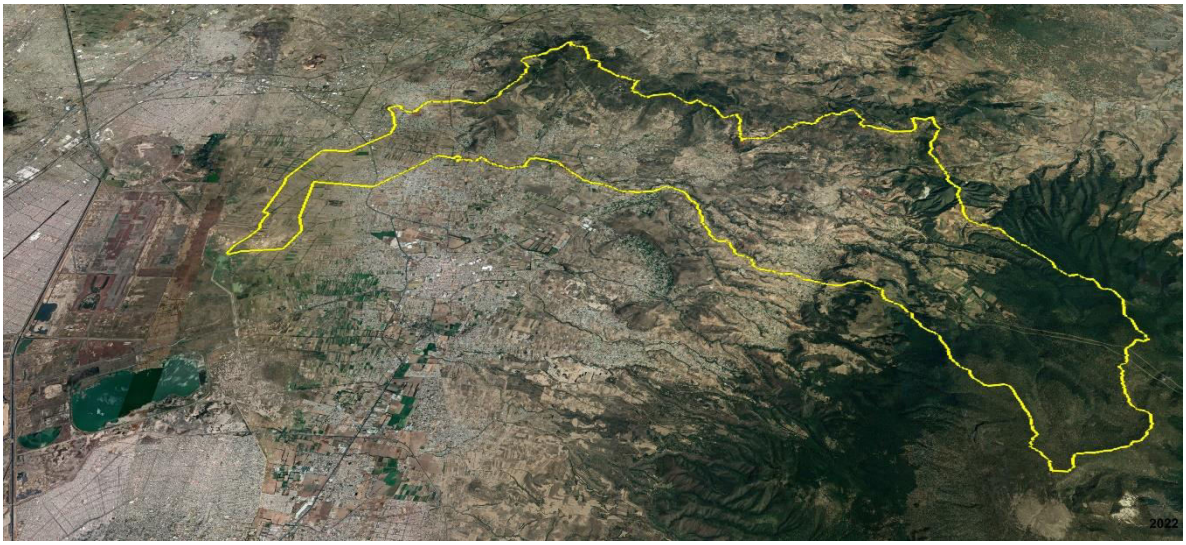

Fig. 6. Satellite image of the Papalotla basin of the year 2022

Figures analysis shows urban areas growth of both downstream basin near to area of the former Texcoco lake and in the middle basin part, and an imminent change of land use from Rainforest to agricultural areas near to upstream part of the basin and mountainous area with great reliefs and rugged terrain. The Papalotla river basin has experienced a process of change in land use, where forest areas have been transformed into agricultural areas and those of agricultural use have been urbanized. These processes of change have affected the functioning of the environments present in this basin, generating a negative impact on hydrological processes, as soil loss increases, as well as the decrease in downstream runoff as shown in Figure 7.

From results obtained there is no clear trend towards droughts in the study basin, which is why it is stated that, due to human activities, such as deforestation and overexploitation of aquifers, among others, the basin is being led towards desertification, induced by anthropogenic action. As can be seen in Figure 7, it can be said that there is a clear downward trend in the runoff at the exit of the Papalotla basin, currently, domestic demand for food and raw materials continues to increase, which generates an increasing pressure on natural resources. Such is the case of fertile soils, which experience a high degree of deterioration, as well as vulnerability to drought and desertification processes. Some international studies mention that due to erosion it is necessary to increase production costs annually by 27% to maintain the same productive level of farmland.

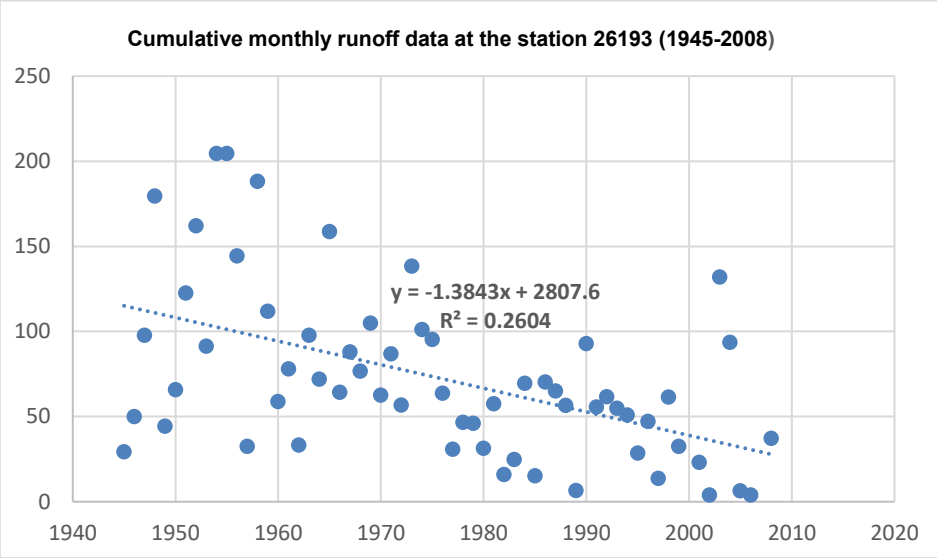

Fig. 7. Monthly accumulated runoff data for hydrometric station 26193 (Bandas-Conagua 2016)

Soil degradation occurs by different processes, the most important being wind and water erosion. When erosion is severe, it hinders the development of vegetation; significantly affects water availability and quality; contributes to the silting of artificial and natural water bodies; causes a decrease in aquifer recharge; human security is sometimes compromised due to landslides, floods and damage to infrastructure works, and eroded soils become a natural source of air pollution due to the emission of particles which can affect human health [9]. Among the Sustainable Development Goals (SDGs) approved by the UN is SDG 15 (Life on Land), which aims to protect, restore and promote the sustainable use of terrestrial ecosystems, sustainably manage forests, halt and reverse land degradation, combat desertification and halt biodiversity loss (United Nation, 2020).

The solution in case of Papalotla river basin to curb desertification is sustainable management of natural resources, especially the conservation of fertile soils and water resources. In this sense, some of the keys found in the literature that can help avoid desertification are:

- ✓ Promote coordinated planning of land uses that includes the management of water resources and livestock and agricultural activities.
- ✓ Preserve vegetation cover, which plays a key role in protecting soil from wind and water erosion, building barriers and stabilizing dunes.
- ✓ Promote climate change education to raise awareness, showing in particular the consequences of desertification and ways to prevent it.
- ✓ Bet on organic farming and certain sustainable practices, such as cover or rotation crops, which prevent soil erosion and prevent drought.
- ✓ Bet on reforestation to regenerate vegetation cover, reactivate moisture circulation and generate biodiversity.
- ✓ Encourage rotational grazing, which limits pressure to a specific area while others regenerate, through their coexistence with crops that allow a more effective nutrient cycling.

4. Conclusions

The statement highlights the increasing visibility and rapid occurrence of adverse effects of climate change, which are having significant impacts on various systems, including social and economic aspects. The Intergovernmental Panel on Climate Change has indicated that there has been a global warming trend since the 1950s. The continuous emission of greenhouse gases (GHGs) contributes to climate change and raises the likelihood of severe, adverse, and irreversible impacts on both people and ecosystems. Environmental degradation is a global issue influenced by multiple factors, including population growth, resource deterioration, and societal perspectives on nature and the environment. In the specific context of the Papalotla River basin, human activities,

particularly land use changes, have seriously disrupted the environmental balance. These activities have led to soil degradation, biodiversity loss, environmental pollution, and a reduction in runoff due to upstream water resource usage. It is crucial to reflect on the territorial planning models implemented in the study area, considering the balance between water demand, unplanned population growth, and the cost associated with ensuring water availability. To avoid an environmental crisis that could disrupt the balance between humans and the environment, it is necessary to evaluate and address these phenomena. With improved understanding of the causes and mechanisms of desertification, as well as the means to prevent and remedy it, it becomes even more important to take proactive measures before the degradation of essential resources such as soil, water, and vegetation reaches irreversible thresholds. In summary, the statement emphasizes the urgency of promoting evaluation, awareness, and action to prevent an environmental crisis and maintain the equilibrium between humans and the environment.

References

[1] National Institute of Ecology and Climate Change / Instituto Nacional de Ecología y Cambio Climático (INECC). *National Atlas of Vulnerability to Climate Change Mexico / Atlas Nacional de Vulnerabilidad al Cambio Climático México*. 1st ed., Vol. 1, 2019. Accessed May 31, 2023. https://atlasvulnerabilidad.inecc.gob.mx/page/fichas/ANVCC_LibroDigital.pdf.

[2] World Meteorological Organization / Organización Meteorológica Mundial. *User's Guide on the Standardized Precipitation Index / Índice normalizado de precipitación. Guía del usuario. OMM-No 1090.* 2012. Accessed May 30, 2023. https://www.droughtmanagement.info/literature/WMO_standardized_precipitation_index_user_guide_es_2012.pdf.

[3] Morales, César, and Soledad Parada (Eds.). *Poverty, desertification and degradation of natural resources / Pobreza, desertificación y degradación de los recursos naturales*. Vol. 1. Santiago de Chile, Comisión Económica para América Latina y el Caribe (CEPAL), 2005.

[4] López Bermúdez, F., and M.C. Sánchez Fuster. "The droughts and its impact in the desertification on Segura basin. Notes to management and water sustainability areas." *International Journal of Social Sciences* 17 (2012): 155–168.

[5] Comisión Nacional de Áreas Naturales Protegidas. Albores González, M.L., R. Aviña Carlin, C. Sánchez Ibarra, and G. F. Tavera Alonso. "Preliminary supportive study for the establishment of the natural protected area. Lake Texcoco natural resources protection area." / "Estudio previo justificativo para el establecimiento del área natural protegida. Área de protección de recursos naturales Lago de Texcoco." December 2021. Accessed May 25, 2023. https://www.conanp.gob.mx/pdf/separata/EPJ-APRN-LagodeTexcoco.pdf.

[6] Mormeneo, Ines, and Raúl Díaz. "A method of classifying rainfall anomalies." / "Método para clasificar la anomalía de las lluvias." *Revista Brasileira de Agrometeorologia, Santa Maria* 11, no. 1 (2003): 159–167.

[7] Institute of Hydrology, Meteorology and Environmental Studies / Instituto de Hidrología, Meteorología y Estudios Ambientales (IDEAM). *Determination of a normal range for precipitation - Comparative analysis between normal thresholds (80-120%) and (90-110%)* / *Determinación de un rango normal de precipitación - Análisis comparativo entre umbrales normales (80-120%) y (90-110%)*. Santa Fe de Bogotá, April 2014. Accessed May 30, 2023. http://www.ideam.gov.co/documents/21021/21789/Nota+T%C3%A9cnica+-+Umbrales+de+Normalidad.pdf/2909eb15-ccd1-4c30-a20f-a50922a3514e.

[8] Government of Mexico. *Tzolkin: Mesoamerican Drought Monitor.* / *Tzolkin: Monitor Mesoamericano de Sequía.* Accessed May 31, 2023. http://galileo.imta.mx/Sequias/moseq/marcoteoricoGob.html.

[9] Martínez Sifuentes, Aldo Rafael, José Villanueva Díaz, Juan Estrada Ávalos, Cirilo Vázquez Vázquez, and Ignacio Orona Castillo. "Soil loss and runoff modification caused by land use change in the Conchos river basin, Chihuahua." *Nova Scientia* 12, no. 25 (October 2020): 1 - 26. Accessed June 1, 2023. http://nova_scientia.delasalle.edu.mx/ojs/index.php/Nova/article/view/2321.

[10] United Nation. "Goal 15: Sustainably manage forests, fight desertification, halt and reverse land degradation, halt biodiversity loss." / "Objetivo 15: Gestionar sosteniblemente los bosques, luchar contra la desertificación, detener e invertir la degradación de las tierras, detener la pérdida de biodiversidad." *Sustainable Development Goals*. 2020. Accessed June 1, 2023. https://www.un.org/sustainabledevelopment/es/biodiversity/.

[11] Intergovernmental Panel on Climate Change (IPCC). *Climate Change 2014: Synthesis Report*. 2014. Accessed May 30, 2023. https://www.ipcc.ch/site/assets/uploads/2018/05/SYR_AR5_FINAL_full_wcover.pdf.

FLUIDAS

NATIONAL PROFESSIONAL ASSOCIATION OF HYDRAULICS AND PNEUMATICS IN ROMANIA

fluidas@fluidas.ro